Structure Property Relations in Complex Copolymer Systems

Dissertation

zur Erlangung des Grades
‚Doktor der Naturwissenschaften'

am Fachbereich Chemie
der Johannes Gutenberg-Universität
in Mainz

Ahmad Azhar Juhari

Mainz, 2010

Datum der mündlichen Prüfung: 26. Juli 2010

Abstract

A thorough investigation was made of the structure-property relation of well-defined statistical, gradient and block copolymers of various compositions. Among the copolymers studied were those which were synthesized using isobornyl acrylate (IBA) and *n*-butyl acrylate (*n*BA) monomer units. The copolymers exhibited several unique properties that make them suitable materials for a range of applications. The thermomechanical properties of these new materials were compared to acrylate homopolymers. By the proper choice of the IBA/*n*BA monomer ratio, it was possible to tune the glass transition temperature of the statistical P(IBA-*co*-*n*BA) copolymers. The measured T_g's of the copolymers with different IBA/*n*BA monomer ratios followed a trend that fitted well with the Fox equation prediction. While statistical copolymers showed a single glass transition (T_g between -50 and 90 ºC depending on composition), DSC block copolymers showed two T_g's and the gradient copolymer showed a single, but very broad, glass transition. PMBL-PBA-PMBL triblock copolymers of different composition ratios were also studied and revealed a microphase separated morphology of mostly cylindrical PMBL domains hexagonally arranged in the PBA matrix. DMA studies confirmed the phase separated morphology of the copolymers. Tensile studies showed the linear PMBL-PBA-PMBL triblock copolymers having a relatively low elongation at break that was increased by replacing the PMBL hard blocks with the less brittle random PMBL-*r*-PMMA blocks. The 10- and 20-arm PBA-PMBL copolymers which were studied revealed even more unique properties. SAXS results showed a mixture of cylindrical PMBL domains hexagonally arranged in the PBA matrix, as well as lamellar. Despite PMBL's brittleness, the triblock and multi-arm PBA-PMBL copolymers could become suitable materials for high temperature applications due to PMBL's high glass transition temperature and high thermal stability. The structure-property relation of multi-arm star PBA-PMMA block copolymers was also investigated. Small-angle X-ray scattering revealed a phase separated morphology

of cylindrical PMMA domains hexagonally arranged in the PBA matrix. DMA studies found that these materials possess typical elastomeric behavior in a broad range of service temperatures up to at least 250°C. The ultimate tensile strength and the elastic modulus of the 10- and 20-arm star PBA-PMMA block copolymers are significantly higher than those of their 3-arm or linear ABA type counterparts with similar composition, indicating a strong effect of the number of arms on the tensile properties. Siloxane-based copolymers were also studied and one of the main objectives here was to examine the possibility to synthesize trifluoropropyl-containing siloxane copolymers of gradient distribution of trifluoropropyl groups along the chain. DMA results of the PDMS-PMTFPS siloxane copolymers synthesized via simultaneous copolymerization showed that due to the large difference in reactivity rates of 2,4,6-tris(3,3,3-trifluoropropyl)-2,4,6-trimethylcyclotrisiloxane (F) and hexamethylcyclotrisiloxane (D), a copolymer of almost block structure containing only a narrow intermediate fragment with gradient distribution of the component units was obtained. A more dispersed distribution of the trifluoropropyl groups was obtained by the semi-batch copolymerization process, as the DMA results revealed more ‘‘pure gradient type’’ features for the siloxane copolymers which were synthesized by adding F at a controlled rate to the polymerization of the less reactive D. As with trifluoropropyl-containing siloxane copolymers, vinyl-containing polysiloxanes may be converted to a variety of useful polysiloxane materials by chemical modification. But much like the trifluoropropyl-containing siloxane copolymers, as a result of so much difference in the reactivities between the component units 2,4,6-trivinyl-2,4,6-trimethylcyclotrisiloxane (V) and hexamethylcyclotrisiloxane (D), thermal and mechanical properties of the PDMS-PMVS copolymers obtained by simultaneous copolymerization was similar to those of block copolymers. Only the copolymers obtained by semi-batch method showed properties typical for gradient copolymers.

Table of Contents

Overview

The Introduction and Motivation section discusses briefly the development of the study of copolymers from its infancy to the modern day discoveries and techniques, as well as its motivation for this particular study. The methodological systems used will then be discussed in Chapter 1, which covers dynamic mechanical analysis and small angle X-ray scattering. In Chapter 2, each of the studied materials as well as the devices involved (rheometer, tensiometer, calorimeter etc.) are described in detail, with an explanation of the methods used. Finally, all the findings of this work are discussed in three subchapters in Chapter 3, and are compared with available literature.

Introduction & Motivation

A polymer is a large molecule composed of many fundamental units, called monomers, connected by chemical bonds. If these monomers are identical, the result is a "homopolymer." If the monomers are of two or more different types, then the product is a hetero- or copolymer that can either be random or have a well-defined sequence. Polymers are the most commonly encountered complex material in the world. With the exception of metals and inorganic compounds, most of the materials that we come into contact with everyday are polymeric. These include elastomers in our automobile tires, paints, plastic wall and floor coverings, foam insulation, and so forth, in our house.

Although there are many varieties of polymers, they all have some common features. The rapid growth of polymer science over the past few decades has been due in large part to a deeper understanding of the relationship between the physical characteristics of polymers and the structure of the polymer molecules. It has become apparent that molecular properties such as chain length, chain stiffness, degree of branching, molecular architecture, and the number of charge groups are more significant than the detailed chemical make-up of polymers in determining their physical characteristics [1]. An understanding of the relationship between such molecular properties and the physical characteristics can help efficiently direct the synthesis of new materials with useful properties, as constantly advancing technologies demand new, high performance and more specialized materials with highly specialized functions [2-9].

What also has become apparent is that such materials are now rarely one-component systems. And the investigation on systems built with two or more components is in demand, especially for structure property correlations. Figure 0.1 shows a few examples of the two-component systems that are rapidly gaining interest.

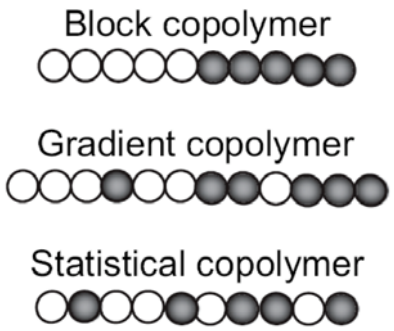

Figure 0.1. Two component polymer systems, or copolymers.

Multi-component polymer systems can offer a huge potential because they can be tailor-made for a vast number of applications. However, among the main challenges in polymer technology today is the exact control of the polymer architecture, as well as understanding the correlations between chemical structure or architecture and a material's characteristics. The pursuit of the design of these new more specialized, and high performance materials require more precise control over the polymerization process and over the structure of resulting polymers. Among the factors to be controlled are: the molecular weight and its distribution, structural topology of macromolecules, and the type and distribution of functional groups in the chain.

One example of a two-component system is the block copolymer, in which the instantaneous composition changes discontinuously and abruptly along the chain. A block copolymer is composed of two or more sequences of monomers joined together by chemical bonds. Several commonly encountered block copolymers are depicted in Figure 0.2. Block copolymers are fascinating materials with unique mechanical, optical, and structural properties. They can be used as surfactants, as compatibilizing agents in polymer blends, as adhesives etc.

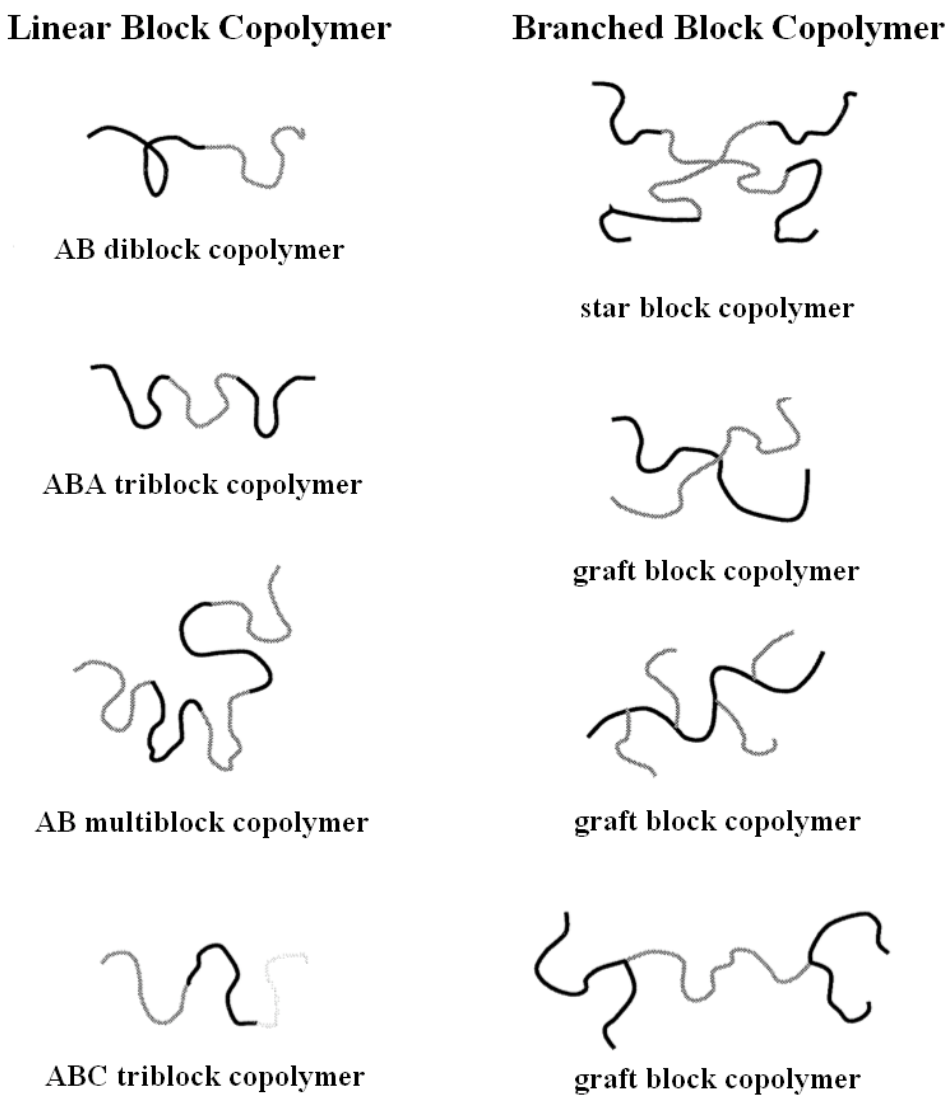

Figure 0.2. Commonly encountered block copolymers.

The most important property of block copolymers is their ability to self-assemble. Due to the possible incompatibility between different polymer species in a block copolymer, the very low value of entropy of mixing for macromolecules, and the fact that the different polymer blocks are connected by chemical bonds, block copolymers can undergo a microphase separation and assemble into various ordered structures [10-18]. Recently, self-assembled ordered polymer structures with periodicities on the nanometer scale have become an important area of study because of their potential applications in nanotechnology. For instance, it has been suggested that block copolymers can be used in the development of new classes of electronic devices [19] and in the synthesis of mesoporous solids that can be used as catalysts and sorption media [20]. An important factor contributing to the block copolymers' widespread popularity is the controllability of the size and morphology of the microstructure, and hence the material properties, by varying the molecular weight, molecular architecture, and composition of the copolymers.

Another example of a two-component system, which has gained considerable interest, is the gradient copolymer, in which instantaneous composition varies continuously along the chain contour. Latest reports, both theoretical [21-24] and experimental [25-28] show that the physical properties of gradient copolymers differ considerably from those of the corresponding block and random copolymers. The main effects observed were related to differences in local dynamics, which in the case of the gradient copolymers with their broad range of local compositions manifests itself in a very broad spectrum of relaxation times of segmental motions. Qualitatively, in gradient polymers the temperature dependencies of their dynamic properties and of their microphase separation morphologies remain the same as compared to diblock copolymers, but changes in the composition gradients will alter the microphase separation transition temperature continuously along the temperature scale. The experimental data also suggest a strong dependence of the morphological and dynamic states of the gradient copolymer materials on their thermal history.

In contrast to block and gradient copolymers, one other example is the statistical copolymer, which has a constant composition along the copolymer chain. All three types of these copolymers that have just been mentioned, even if built with the same type and number of units, may have completely different properties as a result of their architecture alone. And it is this relationship that has become the main motivation for this study. Despite early mechanical and thermodynamic investigations of statistical, gradient, and block copolymers, there are still many systems of great industrial and technological interest which can still further explain the relationship between copolymer architecture and its effects on the thermomechanical behavior. And it is the focus of this study to explore these specific systems which have not been studied before.

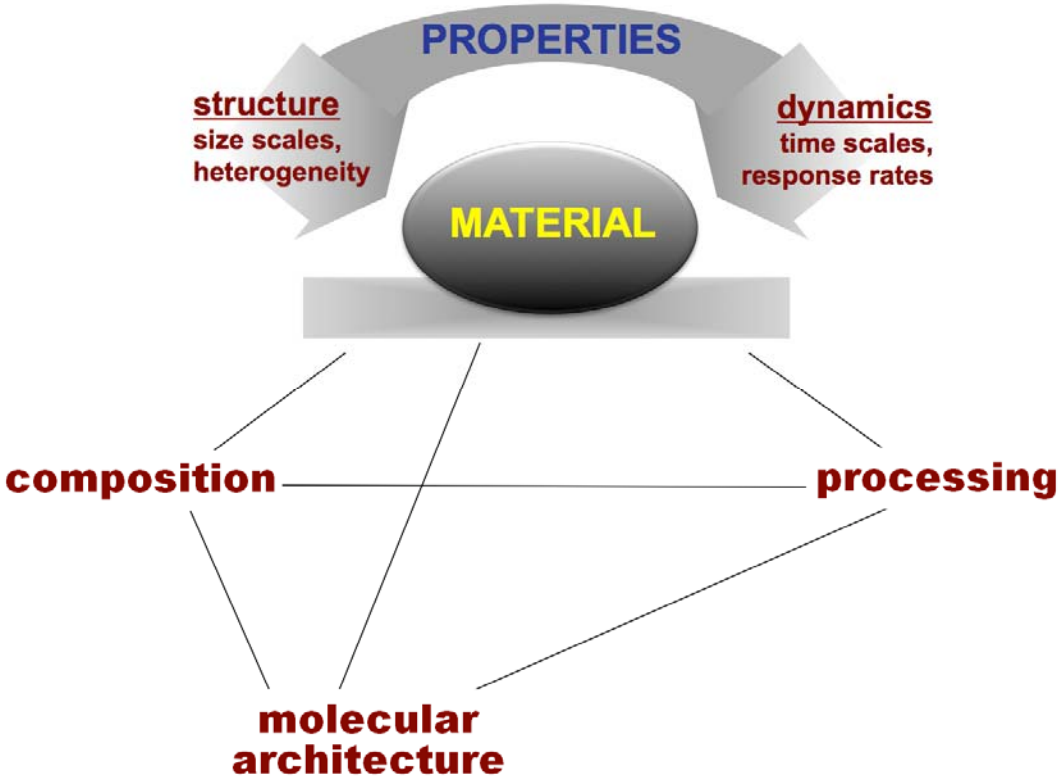

Figure 0.3. Characterization of the properties of copolymer materials.

1 Methodological Systems

A significant portion of the studies reported in this volume involved dynamic mechanical analysis and X-ray diffraction. This chapter discusses the theory, as well as the basic underlying concepts behind these two methodological systems.

1.1 Dynamic Mechanical Analysis

Dynamic mechanical analysis (DMA) is a technique used to characterize a material by analyzing its flow and deformation. A material's reactions to periodic variations or oscillations of an applied external mechanical field are recorded. The possible resulting responses to such a field (stress or strain) are either dissipation of the input energy in a viscous flow (non-reversible response), or storage of the energy elastically (reversible response), or a combination of both of these two extreme cases. Through the use of DMA it is possible to detect variations in both contributions as a function of temperature or of the frequency of the oscillatory deformation. The relaxation processes, which govern the behavior of a given material, can therefore then be determined.

1.1.1 Definitions

- Hooke's and Newton's law

Polymers are viscoelastic, exhibiting properties of both elastic solids as well as viscous liquids. It is necessary to derive expressions that relate stress and strain in order to better understand the mechanical behavior of polymers. For an ideal elastic solid, Hooke's law states that

$$\sigma = E\varepsilon \tag{1.1}$$

where tensile stress σ is the force applied per unit cross-sectional area, and linear strain ε is the change in length divided by the original length of the material. E is the material's Young's modulus.

A given force, F when applied to an ideal elastic solid or a spring, is proportional to x which is the displacement of the spring from its equilibrium position, and can be expressed as

$$F = -kx \tag{1.2}$$

where k is the material specific spring constant.

For cases involving shearing, a shear stress σ is related to the corresponding shear strain γ by the relationship

$$\sigma = G\gamma \tag{1.3}$$

where G is the *shear* modulus.

As with ideal elastic solids, an ideal viscous liquid can also be defined. A viscous liquid obeys Newton's law of viscosity

$$\tau = \eta \frac{\partial V}{\partial y} \tag{1.4}$$

where V is the velocity and y is the direction of the velocity gradient in the liquid.

In cases of velocity gradients in single xy plane we can express the following

$$\sigma = \eta \frac{\partial \gamma}{\partial t} \tag{1.5}$$

where the shear stress σ is directly proportional to the rate of change of shear strain γ in time t. η is the liquid's viscosity.

With the assumption that the shear stresses related to stress and strain rate are additives, a linear viscoelastic behavior can be formulated by combining equations (1.3) and (1.5) to form the following

$$\sigma = G\gamma + \eta \frac{\partial \gamma}{\partial t} \tag{1.6}$$

which represents one of the simple models for linear viscoelastic behavior known as the Voigt model, which is discussed in detail in Section 1.1.3.

- Stress and strain in DMA

Through the use of DMA the relationship between strain (deformation) and the resulting stress is investigated. In the case where the sample being examined is confined between two parallel plates (Figure 1.1), where the upper plate moves at a constant velocity while the lower plate is stationary, the force F needed to move the upper plate of contact area A can be expressed as

$$F = \sigma A \tag{1.7}$$

where σ is the shear stress, which is constant through the gap. The shear strain (deformation) is defined as the ratio of the horizontal displacement of the moving plate Δx, to the distance between the two plates H

$$\gamma = \frac{\Delta x}{H} \tag{1.8}$$

In a dynamic mechanical experiment, the applied strain is a time- and frequency-dependent sinusoidal shear strain of given amplitude γ_0

$$\gamma(t) = \gamma_0 \sin(\omega t) \tag{1.9}$$

Such a deformation results in a response (shear stress) which remains sinusoidal and can differ only by phase shift and amplitude

$$\sigma(t) = \sigma_0 \sin(\omega t + \delta) \tag{1.10}$$

The dynamic mechanical measurement follows this basic principle. A sinusoidal strain is applied, and the resulting response (stress), is simultaneously measured. The resulting response will depend on the nature of the material, for example, in the case of an ideal elastic system, the stress signal is in phase with the applied strain, whereas for an ideal viscous system, the stress is 90° out of phase with the strain. Real polymers exhibit viscoelastic behavior and the input and output signals are shifted at a phase angle $0^o < \delta < 90^o$.

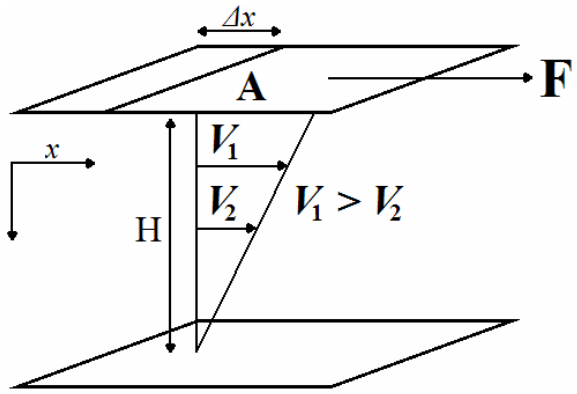

Figure 1.1. Illustration of shear strain and stress in the dynamic mechanical measurement. A sample is placed between two plates, a fixed lower plate and a moving upper plate which moves at constant velocity. The force is denoted by F, and the contact area by A.

The Boltzmann superposition principle states that the response of a material to a given load is independent of the response to any load which is already on the material. Materials which behave in this manner are described as linear viscoelastic.

If the incremental strains $\Delta\gamma_1$, $\Delta\gamma_2$, $\Delta\gamma_3$ etc. are applied to the material at times τ_1, τ_2, τ_3, respectively, then the total stress at time t can be written as

$$\sigma(t) = \Delta\gamma_1 G(t-\tau_1) + \Delta\gamma_2 G(t-\tau_2) + \Delta\gamma_3 G(t-\tau_3) + \ldots \qquad (1.11)$$

where the stress relaxation modulus $G(t-\tau_1)$ is a decreasing function of time. The summation of (1.11) can generally be expressed in integral form as

$$\sigma(t) = \int_{-\infty}^{t} G(t-\tau) d\gamma(\tau) \qquad (1.12)$$

- Different test geometries in DMA

Oscillatory shear experiments allow four possible sample geometries, depending on the physical state of material. The different geometries are illustrated in Figure 1.2. For melts, Plate-plate and cone-plate are typically used, while rectangular bars are more suited for solids, and couette for liquids or polymer solutions.

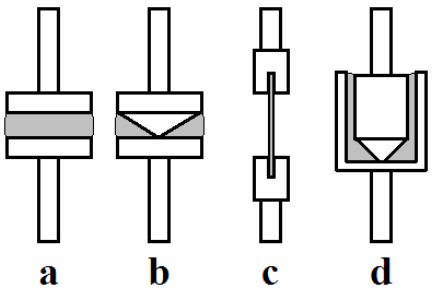

Figure 1.2. Types of test geometries used for different materials; (a) plate-plate and (b) cone-plate for the melt, (c) rectangular bars for solids and (d) couette for polymer solutions or liquids. Geometry (a) was used for this present investigation.

- *G'* and *G"*, storage and loss moduli

Properties of linear viscoelastic materials can be described by the storage *G'* and loss *G"* moduli, which correspond to the elastic and viscous components respectively. The units of both these moduli are Pa.

For isotropic materials, the dynamic mechanical experiment would involve measuring the applied sinusoidal shear strain $\gamma(t)$ of amplitude γ_0 and angular frequency ω as shown in equation (1.9). The resulting stress $\sigma(t)$ of amplitude σ_0 and phase lag δ is simultaneously measured (Figure 1.3).

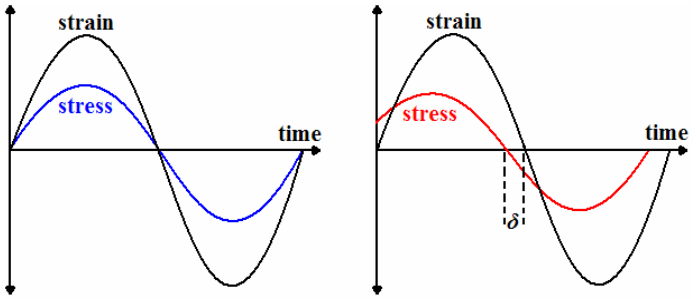

Figure 1.3. Time profile of a simple shear experiment (see Figure 1.1) with and without phase lag δ.

Equation (1.10) can be expanded to

$$\sigma(t) = (\sigma_0 \cos\delta)\sin(\omega t) + (\sigma_0 \sin\delta)\cos(\omega t) \tag{1.13}$$

and it then becomes evident that the stress could consist of two components: one of magnitude $(\sigma_0 \cos\delta)$ in phase with the strain; and another one of magnitude $(\sigma_0 \sin\delta)$ being 90° out of phase with the strain. The stress-strain relationship can therefore be defined by a quantity *G'*, which is in phase with the strain, and by a quantity *G"*, which is 90° out of phase with the strain, i.e.

$$\sigma = \gamma_0 [G'(\omega)\sin(\omega t) + G''(\omega)\cos(\omega t)] \tag{1.14}$$

where

$$G'(\omega) = \frac{\sigma_0}{\gamma_0}\cos\delta \text{ and } G''(\omega) = \frac{\sigma_0}{\gamma_0}\sin\delta \tag{1.15}$$

- Complex shear modulus

It is convenient to expresse the shear stress and shear strain by using complex notation due to the phase lag δ

$$\gamma^* = \gamma_0(\cos\omega t + i\sin\omega t) = \gamma' + i\gamma'' \tag{1.16}$$

$$\sigma^* = \sigma_0[\cos(\omega t + \delta) + i\sin(\omega t + \delta)] = \sigma_0 \exp[i(\omega t + \delta)] \tag{1.17}$$

Hence, the complex shear modulus (Figure 1.4) is defined as

$$G^* = \frac{\sigma^*}{\gamma^*} = \frac{\sigma_0}{\gamma_0}\exp(i\delta) = \frac{\sigma_0}{\gamma_0}\cos\delta + i\frac{\sigma_0}{\gamma_0}\sin\delta = G' + G'' \tag{1.18}$$

$$\text{and } |G^*| = \frac{\sigma_0}{\gamma_0} = \sqrt{G'^2 + G''^2} \tag{1.19}$$

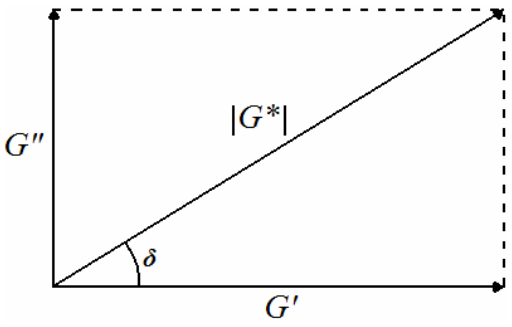

Figure 1.4. Diagram showing the complex modulus $G^* = G' + iG''$. *G'* corresponds to the storage modulus (elastically stored energy) and *G"* to the loss modulus (dissipated energy).

The compliance J^* is also sometimes used instead of the shear modulus G^*, and is defined by

$$J^* = J' - iJ'' \tag{1.20}$$

Therefore we obtain that

$$J' = \frac{G'}{G'^2 + G''^2} \text{ and } J'' = \frac{G''}{G'^2 + G''^2} \tag{1.21}$$

The loss tangent is also a useful parameter. It is a measure of the ratio of energy lost (as heat) to energy stored in a material in one cyclic deformation, and is expressed as

$$\tan\delta = \frac{G''}{G'} \tag{1.22}$$

The particular temperature dependence of tan δ will make useful as a test of thermorheological simplicity. The tan δ is sometimes referred to as damping.

1.1.2 Oscillatory response of real systems

The "master curve," a typical illustration of the $G'(\omega)$ and $G''(\omega)$ behavior for a homopolymer is illustrated in Figure 1.5, where the frequency dependence for *n*-butyl acrylate is shown. The *G'* and *G"* values are in the range of 1 to 10^9 Pa. Compare this to the situation in crystalline solids where typically a constant, frequency independent modulus of about 10^{11} Pa is obtained. The range of values of the moduli, which change with temperature and frequency, is characteristic of polymers and other soft viscoelastic materials. A number of specific regions of the master curve can be identified, as follows:

a) the glassy state, where an elastic response at the higher frequencies is observed and the storage modulus *G'* predominates and reaches the value of about 10^9 Pa. In this region, the polymer lacks molecular mobility since no motion longer than a segment exists, so it maintains the disordered nature of a melt. However, limited localized segmental movements are still possible giving rise to weak sub-glass relaxations. These relaxations are characteristic of all amorphous polymers and glass-forming liquids in general. The existence of the segmental flow region indicates a transitional phase between the glassy and the rubbery (viscoelastic) state. This transition however, is not a real thermodynamic transition, meaning that there is no heat of fusion associated, but only a change in the specific heat. The loss modulus (*G"*) predominates in this region and decreases slower than *G'*. This is due to the energy dissipation in the form of heat, caused by friction in the main chain segments, which consist of a few repeating units that become mobile and as a result begin to move. As the temperature continues to increase, an increasing fraction of chain segments acquire enough energy to overcome the intra- and inter-molecular forces.

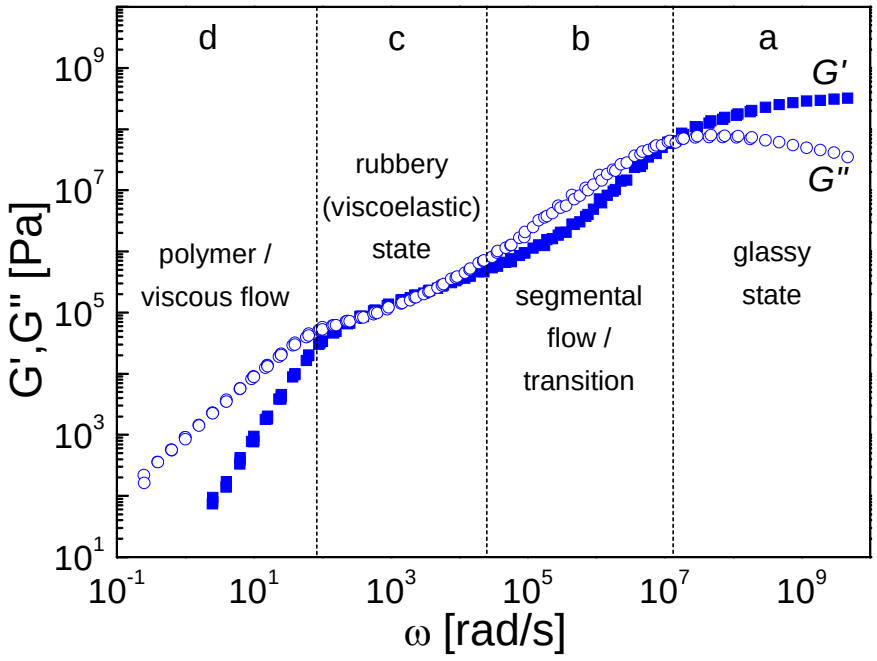

Figure 1.5. The various regions in the viscoelastic spectrum of the homopolymer *n*-butyl acrylate.

b) the rubbery (viscoelastic) state, where the shear modulus decreases around three decades compared to the glassy state to approximately 10^6 Pa and elastic behavior dominates (*G'*>*G"*). This "rubbery plateau" is never perfectly flat as there is always a slight increase of *G'* with frequency, as can be seen in Figure 1.5. In this region, the slope of *G'* is small, and the change in *G"* with increase in frequency is also small or in some case decreases to a minimum, before rising again at higher frequencies. The lower the slope of the *G'* curve, the deeper the minimum of *G"*. This is due to the increasing separation of the segmental and chain modes. However, this rubbery plateau exists only if the molecular weight of the polymer is greater than the so-called entanglement molecular weight M_e, which corresponds to the molecular weight contained between two physically entangled points. The onset of entanglement is

believed to occur at a critical molecular weight $M_c \approx 2.4M_e$ [29-30]. The extension of the plateau is proportional to the polymer molecular weight and the height of the plateau is inversely proportional to M_e.

c) the viscous state or the polymer flow region, where dissipation of energy prevails and *G"* predominates. At this low frequency, motion of entire chains takes place. When frequencies are low enough, *G"* increases linearly with frequency and *G'* is proportional to quadratic frequency. The behavior can be derived from simple models of viscoelastic systems such as the Maxwell model, which is discussed later.

Two relaxation processes taking place at specific relaxation times can also separate the different regions discussed above:

1) At the border between the glassy state and segmental region, the *G'* and *G"* cross (Figure 1.5). This crossover point is a guide used to determine what is known as the segmental relaxation time τ_s, which is given by the inverse of the frequency at that point $(\omega\tau_s = 1)$. For narrow dispersions, the crossover frequency is identical to the frequency where *G"* develops a maximum.

2) The chain relaxation time is determined from the crossover point of *G'* and *G"* at the border between the rubber region and the viscous state, using $\omega\tau_c = 1$.

These two crossover points and its correspondence to the relaxation times in the polymer systems are mere approximations. A more accurate measure of the characteristic relaxation times is the maximum in *G"*, which is located in the approximate vicinity of the crossover points for narrow molecular weight distributions. For broad distributions the crossing of the moduli and the maximum

in *G"* are shifted away from each other, making the crossing point a less accurate indication of the relaxation times.

Both the segmental and chain relaxation times as functions of temperature can be determined from the following equation

$$\log \tau(T) = \log \tau(T_{ref}) + \log(a_T) \tag{1.23}$$

where T_{ref} is the reference temperature and a_T is the shift factor. Equation (1.23) is applicable only for systems that are thermorheologically simple, which is discussed later.

- Entanglement molecular weight

The entanglement of a polymer chain is a type of intermolecular interaction, which does not involve an energetic change and is purely an entropic and topological phenomenon. Chain entanglement affects mainly polymer chain motions. The molecular weight between two adjacent temporary entanglement points, which is defined as the entanglement molecular weight M_e, can be calculated from the plateau modulus G_N as

$$M_e = \frac{\rho_N R T_N}{G_N} \tag{1.24}$$

where ρ_N is the density of the polymer at temperature T_N, at which the plateau modulus G_N is measured and R is the ideal gas constant (R=8.314 $Jmol^{-1}K^{-1}$). The value of the plateau modulus, G_N can be obtained from the frequency where the minimum of the loss tangent tan δ is located, shown in the following equation

$$G_N = G'(\omega)_{\tan \delta_{\min}} \tag{1.25}$$

1.1.3 Mechanical models of linear viscoelasticity

A simple representation of linear viscoelastic behavior can be demonstrated using models consisting of Hookean springs that obey Hooke's law, as well as Newton's dashspots, which are represented as oil-filled cylinders in which a loosely fitting piston moves at a rate proportional to the viscosity of the oil and to the applied stress. In the simplest case consisting of a spring and a dashpot, two models can be constructed. These elements are either coupled in series (the Maxwell model), or in parallel (the Voigt model) as illustrated in Figure 1.6. The viscoelastic functions which are exhibited in each of these models are summarized in Table 1.1.

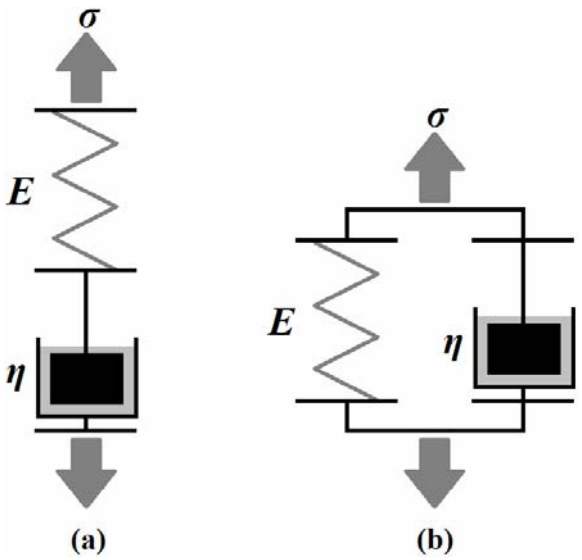

Figure 1.6. (a) Maxwell, and (b) Voigt mechanical models for viscoelastic behavior.

Table 1.1

Viscoelastic functions of the Maxwell and the Voigt model.

The Maxwell model	The Voigt model
$J(t) = J_0 + t/\eta$	$J(t) = J_0\left(1 - e^{-t/\tau}\right)$
$E(t) = E_0 e^{-t/\tau}$	$E(t) = E_0$
$E'(\omega) = E_0\omega^2\tau^2\left(1 + \omega^2\tau^2\right)$	$E'(\omega) = E_0$
$E''(\omega) = E_0\omega\tau\left(1 + \omega^2\tau^2\right)$	$E''(\omega) = E_0\omega\tau = \omega\eta$
$\eta'(\omega) = \eta/\left(1 + \omega^2 t^2\right)$	$\eta'(\omega) = \eta$
$J'(\omega) = J_0$	$J'(\omega) = J_0/\left(1 + \omega^2\tau^2\right)$
$J''(\omega) = J_0/\omega\tau = 1/\omega\eta$	$J''(\omega) = J_0\omega\tau/\left(1 + \omega^2\tau^2\right)$
$\tan\delta = 1/\omega\tau$	$\tan\delta = \omega\tau$

- The Maxwell model

Stress-strain relation for the spring (see equation (1.1)) is written as

$$\sigma = E\varepsilon_1 \tag{1.26}$$

and for the dashpot

$$\sigma = \eta\frac{d\varepsilon_2}{dt} \tag{1.27}$$

Both the spring and the dashpot have the same stress, and the sum of the strain in the spring and the dashpot makes up the total strain ($\varepsilon = \varepsilon_1 = \varepsilon_2$).

Therefore, the equation of motion in this model is

$$\frac{d\varepsilon}{dt} = \frac{d\varepsilon_1}{dt} = \frac{d\varepsilon_2}{dt} = \frac{1}{E}\frac{d\sigma}{dt} + \frac{\sigma}{\eta} \tag{1.28}$$

Two cases could be considered:

a) stress relaxation for a constant strain ($d\varepsilon/dt = 0$)
In this first case,

$$\frac{1}{E}\frac{d\sigma}{dt} + \frac{\sigma}{\eta} = 0 \tag{1.29}$$

and with the solution

$$\frac{d\sigma}{\sigma} = -\frac{E}{\eta}dt \tag{1.30}$$

integration would then lead to

$$\sigma = \sigma_0 \exp\left(-\frac{Et}{\eta}\right) = \sigma_0 \exp\left(-\frac{t}{\tau}\right) \tag{1.31}$$

where σ_0 is the initial stress at time $t = 0$, and $\tau = \eta/E$ is the relaxation time in this model. Equation (1.31) shows that in the Maxwell model, the stress decays exponentially with the time t. It is obvious that the stress relaxation behavior cannot usually be represented by a single exponential decay term for real polymers, nor does it necessarily decay to zero at infinite time.

b) constant stress ($d\sigma/dt = 0$).
In this case, from equation (1.28) we obtain that $d\varepsilon/dt = \sigma/\eta$, which is a constant value. This would imply that the Maxwell model cannot describe creep. The time dependence of stress is written as

$$\sigma = \sigma_0 \exp(i\omega t) \tag{1.32}$$

and can be inserted into equation (1.28) as the Maxwell model yields the frequency dependence of storage and loss moduli (Figure 1.7)

$$E' = \frac{E_0 \omega^2 \tau^2}{1+\omega^2\tau^2} \text{ and } E'' = \frac{E_0 \omega \tau}{1+\omega^2\tau^2} \tag{1.33}$$

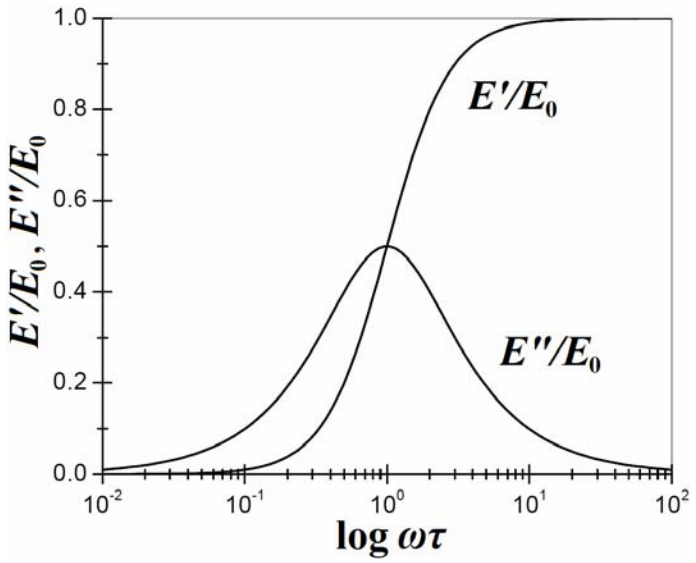

Figure 1.7. The Maxwell model's representation of the frequency dependence of *E'* and *E''*.

The plateau of *E'* prevails over *E''* in the high frequency range, which is characteristic for elastic behavior. The elastic modulus of a material in this frequency range is given by

$$E_0 = \lim_{\omega \to \infty} E'(\omega) \tag{1.34}$$

E'' would be higher than the *E'* in the low frequency region, which is typical for Newtonian flow. In this range *E'* and *E''* are proportional to ω^2 and ω. On a logarithmic scale *E'* and *E''* have slopes of 2 and 1, respectively (Figure 1.5).

The zero shear viscosity can be obtained in this range according to

$$\eta_0 = \lim_{\infty \to 0} \frac{E''(\omega)}{\omega} \tag{1.35}$$

- The Voigt model

This model consists of a spring and dashpot in parallel. The displacements of the spring and the dashpot are equal, whereas the total stress σ comes from both of these elements

$$\varepsilon = \varepsilon_1 = \varepsilon_2 \text{ and } \sigma = \sigma_1 + \sigma_2 \tag{1.36}$$

And from equations (1.26) and (1.27), we derive the equation of motion

$$\sigma = E\varepsilon + \eta \frac{d\varepsilon}{dt} \tag{1.37}$$

which, after integration, gives

$$\varepsilon = \frac{\sigma_0}{E}\left[1 - \exp\left(-\frac{E}{\eta}t\right)\right] \tag{1.38}$$

where σ_0 is the constant stress. The strain ε rises exponentially to the value of σ_0/E with retardation time $\tau' = \eta/E$. Equation (1.38) and hence the Voigt model can describe time dependence of creep. However, stress relaxation cannot be predicted by this model.

It is important to point out that the Maxwell and the Voigt models are simplifications and cannot properly describe the viscoelastic behavior in a wide frequency range and would fail completely at creep and stress relaxation

prediction respectively. If we wanted to describe the real behavior of polymer systems more precisely, we could couple several Maxwell units in parallel or, for instance, combine the Voigt and Maxwell units in series as has been done with Burger's model (Figure 1.8).

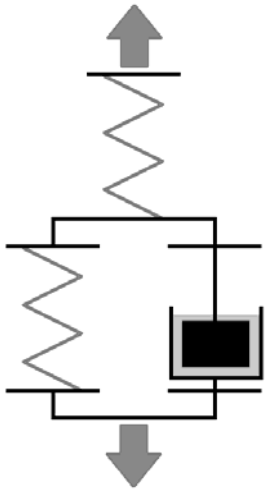

Figure 1.8. Three-element model (Burger's model) of viscoelasticity.

1.1.4 Thermorheological simplicity and time-Temperature superposition

Dynamic mechanical spectrometers have a typical frequency range between 10^{-2} and 500 rad/s. It can be seen from Figure 1.5 that the frequency range of the "master curve" covers many decades, which are not possible to be measured directly by the available apparatus. To overcome these limits, master curves are constructed by combining results of measurements performed at various temperatures within the same frequency window, typically 10^{-1} to 10^{2} rad/s, as illustrated in Figure 1.9. One of these dependences located above the glass transition is taken as a reference, meaning it is not shifted, and all other curves are shifted along the frequency scale to overlap with dependences measured at adjacent temperatures. The responses of *G'* and *G"* obtained at higher and lower temperatures than the reference temperature, are shifted to lower and higher frequencies respectively. The end result is a continuous master curve corresponding to the chosen reference temperature T_{ref}.

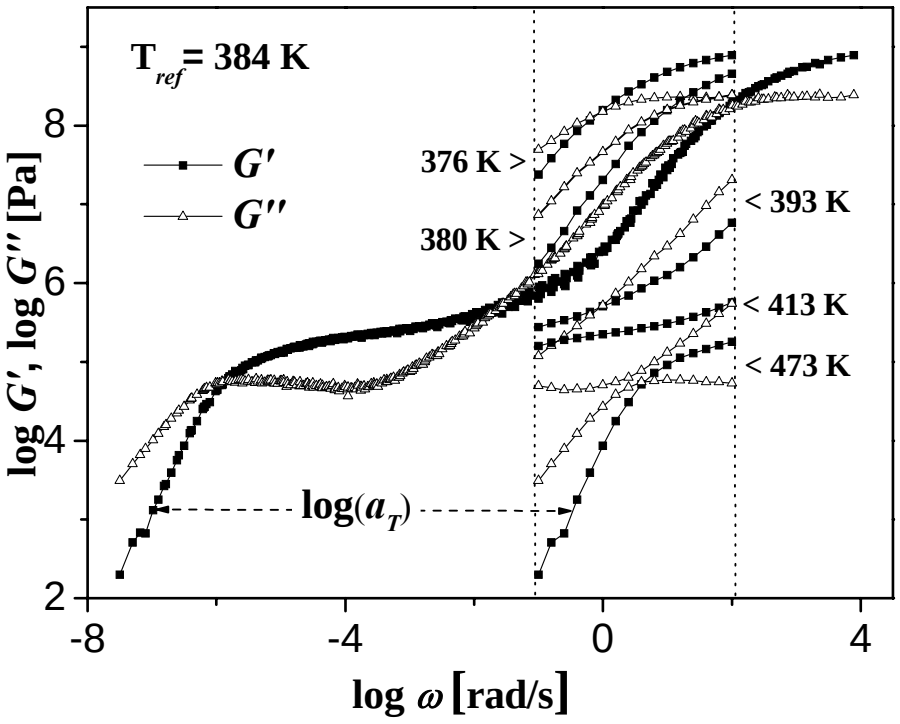

Figure 1.9. Master curve constructed for a polystyrene test sample (M_w=200 kg/mol). Frequency dependences of *G'* and *G''* are measured at various temperatures with a fixed frequency window (between the two vertical dotted lines). One of these dependencies is taken as a reference and is not shifted. All the other curves are shifted horizontally by log a_T to overlap with dependencies measured at adjacent temperatures. Dependencies measured at higher and lower temperatures are moved to lower and higher frequencies, respectively.

The procedure used to determine the storage and loss moduli over a very broad frequency range is based on what is known as the time-temperature or frequency-temperature equivalence principle. It states that the viscoelastic behavior at one temperature can be related to that at another temperature by a change in the time-scale only. In other words, the temperature change is equivalent to the change of the deformation frequency of a given material. The equivalence principle is valid

only for thermorheologically simple materials, that is, materials where the distribution of relaxation times does not change with temperature. Therefore, obviously it does not work in the temperature/frequency range where relaxation processes with different temperature dependencies of relaxation times overlap. The principle holds true only for amorphous homopolymers, and does not hold for semicrystalline polymers, for polymer blends or block copolymers. In the case of semicrystalline polymers and block copolymers, the reason for the failure of tTs is the existence of molecular and supramolecular organization that change as a function of temperature. In the case of immiscible polymer blends, tTs also fails as a result of the different shift factors for the different components in the blend. And in the case of miscible polymers, tTs fails again provided that the difference in the glass transition temperatures (T_g) of the two components is above 40 K.

- The Williams-Landel-Ferry (WLF) equation

The *G'*, *G''* dependencies obtained at various temperatures and their horizontal shifts provide directly the temperature dependence of shift factor, $\log a_T (T,T_{ref})$, as illustrated in Figure 1.10. This relationship between the shift factor and the temperature can be expressed using the WLF equation, which was postulated by Williams, Landel and Ferry [31], and written as

$$\log a_T = \frac{C_1^{T_{ref}} \left(T - T_{ref}\right)}{C_2^{T_{ref}} + T - T_{ref}} \tag{1.39}$$

where $C_1^{T_{ref}}$ and $C_2^{T_{ref}}$ are material dependent constants that depend on the reference temperature T_{ref}. For comparison purposes, it may be useful to express these constants in correspondence to another reference temperature, particularly the glass transition temperature T_g.

The new constants then, $C_1^{T_g}$ and $C_2^{T_g}$ with T_g as a reference temperature, can be determined using the following conversion relations

$$C_1^{T_g} = \frac{C_1^{T_{ref}} C_2^{T_{ref}}}{C_2^{T_{ref}} + T_g - T_{ref}} \tag{1.40}$$

$$C_2^{T_g} = C_2^{T_{ref}} + T_g - T_{ref} \tag{1.41}$$

Earlier assumptions based on analysis of limited data postulated that $C_1^{T_g}$ and $C_2^{T_g}$ were universal constants. However, these assumptions was not supported when the results for a wider variety of viscoelastic materials were considered. From (1.40) and (1.41), we derive that

$$C_1^{T_g} C_2^{T_g} = C_1^{T_{ref}} C_2^{T_{ref}} \tag{1.42}$$

$$T_g - C_2^{T_g} = T_{ref} - C_2^{T_{ref}} \equiv T_\infty \tag{1.43}$$

where T_∞ is the Vogel temperature or the "ideal" glass temperature at which, regardless of the T_{ref}, log a_T becomes infinite in accordance with equation (1.39).

The WLF equation holds true above the glass temperature until T_g + 100 K. Although the equation was originally based purely on empirical observations, it can also be derived directly from free volume theories.

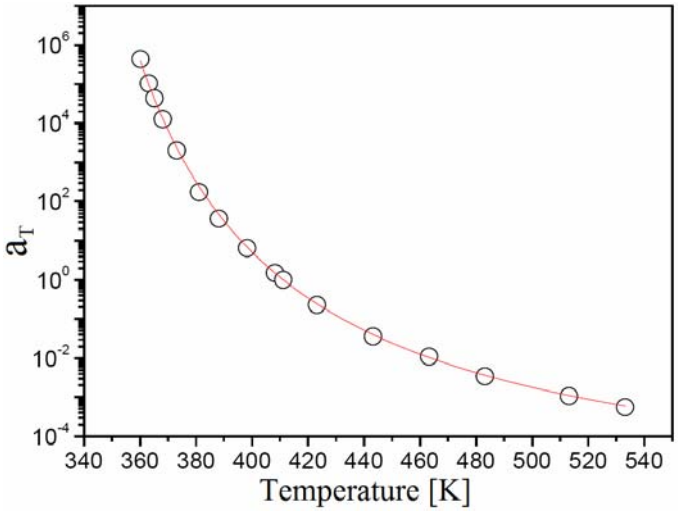

Figure 1.10. An example of the temperature dependence of a shift factor a_T. The line is a fit of the WLF equation (2.39).

1.1.5 Origin of the liquid-to-glass "transition"

The theory behind liquid-to-glass "transition" has not yet been fully understood. The origin of the slowing-down process of the relaxation times of a system as it approaches glass transition is one of the most fundamental problems in polymer physics of liquids, in general, with several technologically important aspects such as physical aging and refractive index stabilization [32-34]. Identifying the main thermodynamic parameter that controls the slow dynamics in glass-forming liquids, which gives rise to the dynamic arrest at T_g is still a topic of debate. Theoretical predictions consider two extreme cases:

- Free-volume theories [35-36]
- Thermally activated processes on a constant density "energy landscape" (Arrhenius model) [32-33]

In the first case, the controlling parameter is volume (V) or density (ρ) and the slowing-down results from the decrease of the available volume or free volume. In the second case, the controlling parameter is temperature (T), the landscape is considered as fixed and the super-Arrhenius dependence of relaxation times on

$T(\tau(T))$ is attributed to changes in the barriers and the minima encountered in the exploration of the landscape. Clearly these cases should be considered as extreme, since molecular transport in general, is driven by thermal activation processes with potential energy barriers, which depend on local density [37]. Both approaches are described below.

A. Free volume theories of the glass "transition"

The theories imply that if conformational changes in the polymer chains are to take place, there must be space available for the newly rearranged molecular segments to exist in. The total amount of free space per unit volume of the polymer is called the fractional free volume V_f. As the temperature of the polymer system decreases towards the glass temperature, the polymer chains rearrange themselves to reduce the free volume, to certain point until the polymer chains are moving so slowly that they cannot rearrange within the time-scale of the experiment and the volume of the material contracts like that of a solid. If V_g is the fractional free volume at T_g. So ideally, above this temperature, the fractional free volume can be written as

$$V_f = V_g + \alpha_f \left(T - T_g\right) \tag{1.44}$$

where α_f is the expansion coefficient of free volume.

Based on experimental data for monomeric liquids, Doolittle's equation [38] finds a relationship between the viscosity and the free volume via

$$\eta = A \exp\left(\frac{B}{V_f}\right) \tag{1.45}$$

where A and B are constants.

Taking into account the relationship between zero shear viscosity and the shift factor

$$\frac{\eta_0(T)}{\eta_0(T_{ref})} = a_T \tag{1.46}$$

we obtain that

$$a_T = \frac{\exp\left(\frac{B}{V_f}\right)}{\exp\left(\frac{B}{V_f^r}\right)} = \exp\left(B\left(\frac{1}{V_f} - \frac{1}{V_f^r}\right)\right) \tag{1.47}$$

where V_f is the fractional free volume at T and V_f^r is the fractional free volume at the reference temperature. If the glass transition temperature is set as the reference temperature and the fractional free volume at this temperature is V_f^g, then it would result in the following equation

$$a_T = \exp\left(B\left(\frac{1}{V_f} - \frac{1}{V_f^g}\right)\right) \tag{1.48}$$

If we insert equation (1.44) into equation (1.48), it would give

$$a_T = \exp\left(\frac{\left(-\frac{B}{V_f^g}\right)(T - T_g)}{\left(\frac{V_f^g}{\alpha_f}\right) + T - T_g}\right) \tag{1.49}$$

And by taking the logarithm of equation (1.49), the following can be obtained

$$\log a_T = -\left(\frac{\left(\frac{B}{2.303 V_f^g} \right)\left(T - T_g\right)}{\left(\frac{V_f^g}{\alpha_f} \right) + T - T_g} \right) \tag{1.50}$$

which is the WLF equation (1.39) with $C_1 = B/2.303 V_f^g$ and $C_2 = V_f^g / \alpha_f$. It is shown later that the WLF equation is equivalent to the Vogel Fulcher Tammann (VFT) equation, and that the latter can also be derived from the free volume theory.

- Vogel-Fulcher-Tammann (VFT) relation

The Vogel-Fulcher-Tammann equation was introduced by Fulcher [39-41] and Tammann and Hesse [41] and successfully relates viscosity to temperature.

$$\eta_0(T) = A \exp\left(\frac{B}{T - T_\infty} \right) \tag{1.51}$$

Taking the logarithm of equation (1.51) would give

$$\log \eta_0(T) = \log A + \left(\frac{B^*}{T - T_\infty} \right) \tag{1.52}$$

where η_0 is the zero shear viscosity, $A = \eta_0\left(T_{ref}\right)$, B is the "activation parameter", $B^* = B \log e$ and T_∞ is a temperature at which the viscosity becomes infinite.

By taking into account the relationship between zero shear viscosity and relaxation time

$$\frac{\eta_0(T)}{\eta_0(T_{ref})} = \frac{\tau(T)}{\tau(T_{ref})} = a_T \tag{1.53}$$

we can obtain that

$$\tau(T) = A\exp\left(\frac{B}{T - T_\infty}\right) \tag{1.54}$$

$$\log\tau(T) = \log A + \left(\frac{B^*}{T - T_\infty}\right) \tag{1.55}$$

Both pairs of equations, (1.51, 1.52) as well as (1.54, 1.55), are known as the Vogel-Fulcher-Tammann (VLF) equation.

- Interchangeability of VFT and WLF equations

Using the equation for the temperature dependence of the viscosity (1.52), we may also formulate the shift factor $\log a_T$. Equations (1.53) and (1.52) can give

$$\begin{aligned}\log a_T &= \log\frac{\eta_0(T)}{\eta_0(T_{ref})} = \log\eta_0(T) - \log\eta_0(T_{ref}) \\ &= \log A + \frac{B^*}{T - T_\infty} - \left(\log A + \frac{B^*}{T_{ref} - T_\infty}\right) \\ &= B^*\left(\frac{T_{ref} - T}{(T - T_\infty)(T_{ref} - T_\infty)}\right) \\ &= \frac{B^*}{T_{ref} - T_\infty}\cdot\frac{T - T_{ref}}{T - T_{ref} + (T_{ref} - T_\infty)}\end{aligned} \tag{1.56}$$

The last part of this equation can be expressed as

$$\log a_T = \frac{C_1\left(T - T_{ref}\right)}{C_2 + T - T_{ref}} \tag{1.57}$$

where

$$C_1 = \frac{B^*}{T_{ref} - T_\infty} \text{ and } C_2 = T_{ref} - T_\infty \tag{1.58}$$

This illustrates that WLF and VFT equations are in fact the same. A comprehensive conversion list of VFT into WLF parameters and vice versa can be written

$$\begin{array}{l|l} A = \log\tau\left(T_{ref}\right) - C_1 & \log\tau\left(T_{ref}\right) = A + \dfrac{B^*}{T_{ref} - T_\infty} \\ B^* = C_1 C_2 & C_1 = \dfrac{B^*}{T_{ref} - T_\infty} \\ T_\infty = T_{ref} - C_2 & C_2 = T_{ref} - T_\infty \end{array} \tag{1.59}$$

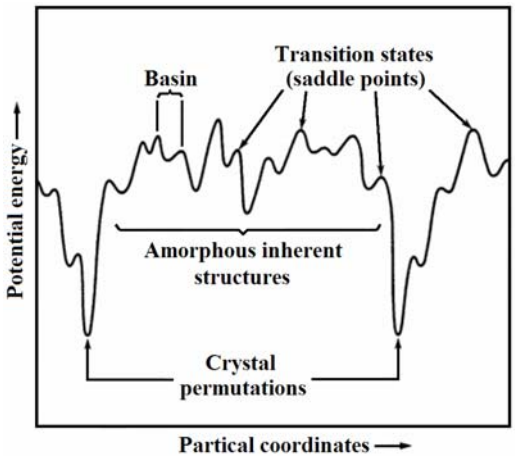

Figure 1.11. A representation of potential energy ("energy landscape") in the multidimensional configuration space for a many-particle system (taken from F.H. Stillinger, Science 1995).

B. Thermally activated processes

Another approach to the liquid-to-glass transition is related to the thermally activated processes on a constant "energy landscape" which is considered as fixed for the entire system, meaning that it does not change upon cooling. A schematic diagram of such an energy landscape is illustrated in Figure 1.11. Potential energy depends on the spatial location of all the particles in system, and includes contributions from various intermolecular as well as intramolecular forces such as electrostatic polarization effects, covalency, hydrogen bonding, electron-cloud-overlap repulsions and intermolecular force fields among other things [33]. In Figure 1.11, the minima correspond to mechanically stable arrangements of all particles. The smallest displacement from such an arrangement would restore forces to the non-displaced particles arrangement. Equivalent minima can be achieved by permutations of identical. Lower lying minima are occupied by the system provided which is cooled to absolute zero slowly enough to maintain thermal equilibrium. Pure substances then become virtually perfect crystals [33]. Higher lying minima correspond to less ordered systems with some or completely amorphous regions.

C. Relative contribution of density and temperature on the segmental dynamics

Liquid-to-glass transition is a contentious issue and the domination of either density or temperature in controlling the slowing-down process is still an open question. However, it is possible to determine which of the two parameters plays the more important role with respect to the dynamics. This can be accomplished by calculating the ratio of the activation energy at constant volume to enthalpy of activation E_v^* / H^*. This dynamic quantity provides a quantitative measure of the relative importance of density and temperature on the dynamics [42] of the α-process. By defining the enthalpy of activation as

$$H^* = R\left(\frac{\partial \ln \tau}{\partial (1/T)}\right)_p \tag{1.60}$$

and the activation energy at constant volume as

$$E_V^* = R\left(\frac{\partial \ln \tau}{\partial(1/T)}\right) \tag{1.61}$$

it can be shown that the ratio E_V^*/H^* can be expressed as

$$\frac{E_V^*}{H^*} = 1 - \left(\frac{\partial P}{\partial T}\right)_V \left(\frac{\partial T}{\partial P}\right)_\tau \tag{1.62}$$

$$\frac{E_V^*}{H^*} = 1 - \frac{\left(\frac{\partial \rho}{\partial T}\right)_P \left(\frac{\partial \ln \tau}{\partial P}\right)_T}{\left(\frac{\partial \rho}{\partial P}\right)_T \left(\frac{\partial \ln \tau}{\partial T}\right)_P} \tag{1.63}$$

$$\frac{E_V^*}{H^*} = 1 - \frac{\left(\frac{\partial \ln \tau}{\partial \rho}\right)_T}{\left(\frac{\partial \ln \tau}{\partial \rho}\right)_P} \tag{1.64}$$

Because a change in temperature (T) would affect both the thermal energy (k_BT) and the density (ρ), it is impossible to separate the two effects by T alone. To disentangle the effects of T and ρ on the dynamics, pressure-dependent measurements have been invaluable [43-44] since pressure (P) can be applied isothermally, therefore affecting only ρ, and have been used to provide a quantitative assessment of their relative importance. Not only do the pressure-dependent experiments provide the $T_g(P)$ dependence, but it also provides the origin of the freezing of the segmental relaxation times (τ_S) at the liquid-to-glass transition. Measuring the relaxation times, for example, as a function of the thermodynamic variables T and P, coupled with the equation of state would allow quantifying the role of temperature and density on the segmental dynamics [42,

45-46]. The E_v^*/H^* ratio can vary from 0, for volume dominated dynamics, to 1, where thermal energy dominates. The monomeric volume plays a key role in controlling the actual value [47]. In principle, this ratio can be calculated for any substance provided that it is possible to measure the $\tau_S(T)$ and $\tau_S(P)$ dependencies normally through dielectric spectroscopy measurements and the equation of state from *PVT* measurements.

It has been shown that the same ratio of activation energies can be obtained from the ratio of the isobaric $\alpha_P = (\partial \ln V/\partial T)_P$ to the isochronic $\alpha_\tau = (\partial \ln V/\partial T)_\tau$ thermal expansion coefficients as

$$\frac{E_V^*}{H^*} = \frac{1}{1-\frac{\alpha_p}{\alpha_\tau}} \tag{1.65}$$

- Thermodynamic scaling of the glass transition dynamics

A number of different methods have been proposed to account for the scaling of the relaxation time and the different E_v^*/H^* values of different polymers and glass-forming liquids. The variables that have been proposed include:

- $\log\tau \propto T^{-1}V^{-\gamma}$ [44, 48-49], where γ is a material constant that provides a measure of the relative importance of ρ as opposed to T. The γ=4 is of particular interest since it can be linked to the soft-sphere repulsive forces ($\sim r^{-3\gamma}$) that constitute the first (repulsive) part of the more general distance-dependent potential $U(r) \propto 4\varepsilon\left[(\sigma/r^{-12}) - (\sigma/r)^{-6}\right]$, where ε and σ have the units of energy and length, respectively [44, 49].

- $\ln\tau \propto (\rho - \rho^*)T^{-1}$, where ρ is an adjustable parameter. In many cases, this thermodynamic scaling gives equally good results [50-52] the T and ρ ranges are extremely large [52].

- monomer volume V_m and its correlation to the dynamic quantity E_v^*/H^*. It has been shown that $E_v^*/H^* \sim 0.72 - 0.77V_m$ for a series of glass-forming liquids. This would suggest that the reason for the low E_v^*/H^* values in a number of glass-forming liquids and polymers is their large monomer size. This proposed method suggests that monomer volume and local packing play an important role in controlling the dynamics.

D. Parameters beyond free volume and thermal activation

Molecular transport is generally driven by thermal activation processes with potential energy barriers E that depend on local density [37]. The probabilities for local rearrangements can by given by

$$P(V,T) = \exp\left(-\frac{E(V)}{kT}\right) \tag{1.66}$$

It then becomes apparent that the free volume and Arrhenius models are two extreme cases of the E vs. V dependence, shown in Figures 1.12(a) and 1.12(b). In the Arrhenius model, a volume independent activation energy is assumed, whereas in the case of the free volume model, the assumptions made can be interpreted as a discontinuous change of the activation energy at certain V_c, from an infinite value below V_c to 0 above V_c [37]. In Figure 1.13, the temperature dependencies of relaxation times for the considered models for $E(v)$ are shown in the form of what is known as the Angel plot. This is an indication of the varying behavior of the model system, which approximately corresponds to the variation of properties observed for real systems. The different activation energies and relaxation time dependencies should be regarded only as examples illustrating the

possibilities to describe a class of behaviors ranging between the Arrhenius model on one hand, and the typical non-Arrhenius case described by the traditional free volume model, on the other.

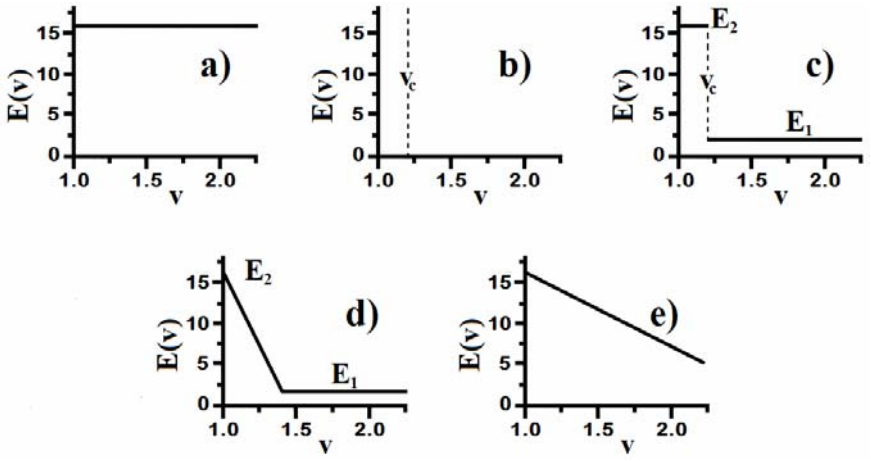

Figure 1.12. Different types of dependencies of the activation energy for local molecular rearrangements vs. local volume: (a) corresponding to the Arrhenius model, (b) corresponding to the free volume model and, (c) to (e) some other possible dependencies (taken from T. Pakula, J. Mol. Liq. 86, 2000, 109-121).

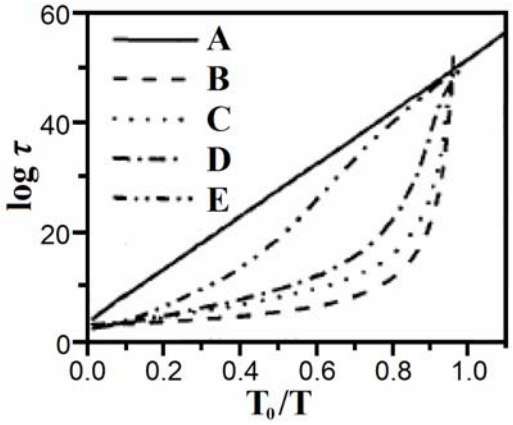

Figure 1.13. Temperature dependencies of relaxation times calculated using $E(v)$ dependencies shown in Figure 1.12 (lines A-E correspond to cases (a)-(e) of Figure 1.12, respectively) (taken from T. Pakula, J. Mol. Liq. 86, 2000, 109-121).

1.1.6 Proposed fit function for the master curve

To describe more completely the frequency dependence of storage and loss moduli, all the master curves were successfully fitted to the following function

$$y = \log\left(\frac{A_1}{10^{-b_1(x-lt_1)}+10^{-b_2(x-lt_1)}} + \frac{A_2}{10^{-b_3(x-lt_2)}+10^{-b_4(x-lt_2)}}\right) \tag{1.67}$$

$$z = \log\left(\frac{A_1}{10^{-c_1(x-lt_1)}+10^{-c_2(x-lt_1)}} + \frac{A_2}{10^{-c_3(x-lt_2)}+10^{-c_4(x-lt_2)}}\right) \tag{1.68}$$

where A_1 and A_2 are related to the height of the plateaus of the real part of the modulus (storage modulus) above the frequency corresponding to the reciprocal relaxation time $lt_1 = -\log\tau_s$, $lt_2 = \log\tau_c$, where τ_s and τ_c are the segmental and chain relaxation times, respectively. The parameters b_1 to b_4, and c_1 to c_4 describe the slopes on both sides of the characteristic frequency related to the reciprocal relaxation. These fit parameters are illustrated in Figure 1.14.

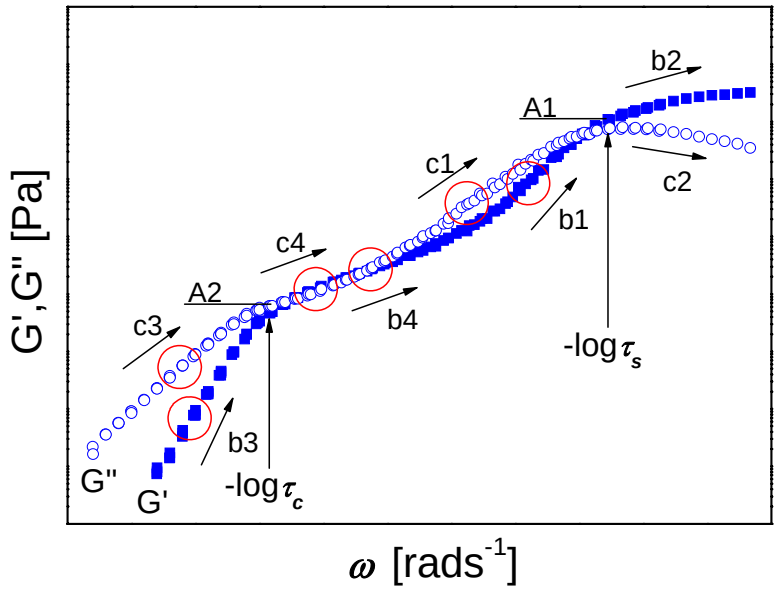

Figure 1.14. Fit parameters of the empirical function (equation (1.67)).

1.2 Small Angle X-Ray Scattering

Small-angle X-ray scattering (SAXS), which involves X-rays of wavelength 0.1 to 0.2 nm, is capable of delivering structural information of macromolecules between 5 and 25 nm, of repeat distances in partially ordered systems of up to 150 nm [53].

X-ray scattering occurs as a result of the interaction of X-rays with electrons in the material. The X-rays scattered from different electrons interfere with each other and produce a diffractive pattern that varies, if the material is not homogeneous, with scattering angle. The variation of the scattered intensity with angle provides information on the electron density distribution, and hence the atomic positions in the material.

As shown in Figure 1.15, a sample is irradiated with a collimated beam of X-rays and the scattered intensity is measured as a function of the scattering angle 2θ (the angle between the scattered and incident beam).

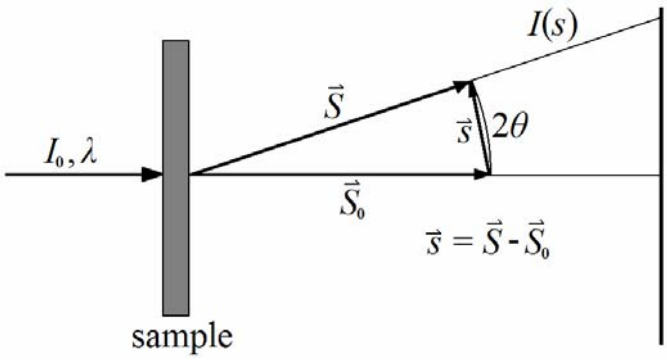

Figure 1.15. Definition of the scattering vector $\vec{s}$ of the scattering of the X-ray beam of the intensity I_0 and the wavelength λ.

The incident beam is described by the unit vector $\vec{S}_0$, while the scattered beam by $\vec{S}$. The scattering vector $\vec{s}$ is defined as

$$\vec{s} = \frac{\vec{S} - \vec{S}_0}{\lambda} \tag{1.76}$$

where λ is the wavelength of the X-rays. The length of the scattering vector $\vec{s}$ can then be written as

$$s = \frac{2\sin\theta}{\lambda} \tag{1.77}$$

SAXS patterns are typically represented as scattered intensity as a function of the magnitude of the scattering vector

$$q = \frac{4\pi\sin\theta}{\lambda} \tag{1.78}$$

where 2θ is the angle between the incident X-ray beam and the detector measuring the scattered intensity.

1.2.1 Bragg's law

Bragg's law states that when X-rays hit an atom, they make the electronic cloud move, as does any electromagnetic wave. The movement of these charges re-radiates waves with the same frequency, and this phenomenon is known as Rayleigh scattering, or elastic scattering. The scattered waves can themselves be scattered but this secondary scattering is assumed to be negligible. These re-emitted wave fields interfere with each other either constructively or destructively, producing a diffraction pattern on a detector. This resulting wave

interference pattern is the basis of diffraction analysis. X-ray wavelengths are comparable with inter-atomic distances (~150 pm) and thus are an excellent probe for this length scale.

When phase shift is a multiple of 2π, then the interference is constructive, and this condition can be expressed by Bragg's law [53]. Suppose that a single monochromatic wave is incident on aligned planes of lattice points, with separation d, at angle θ, as shown in Figure 1.16.

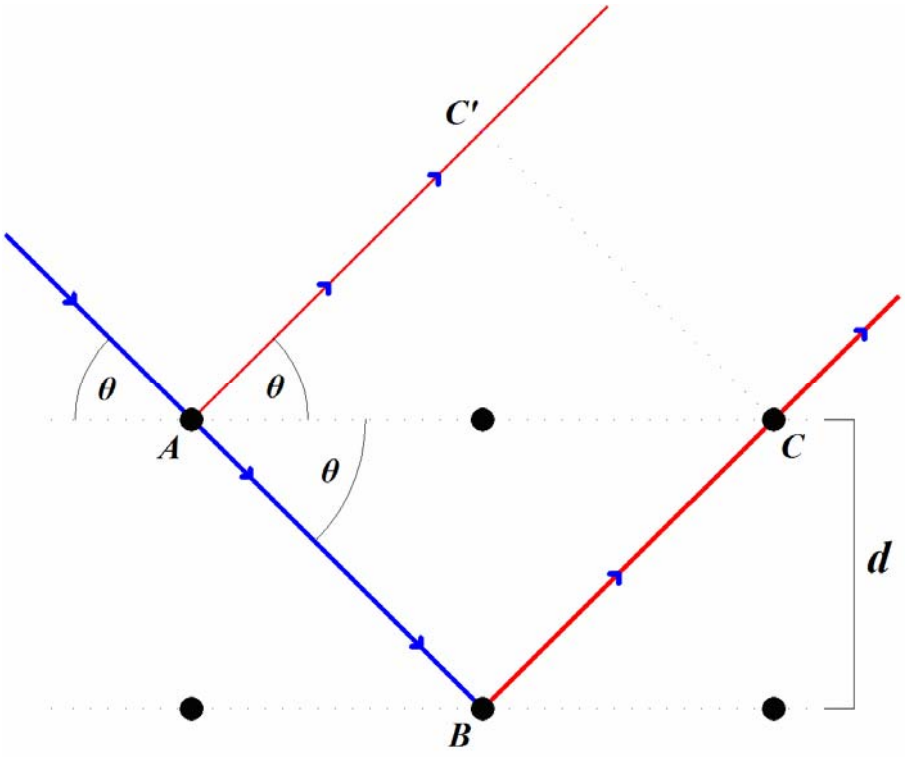

Figure 1.16. An illustration of the Bragg's law.

If we observe the figure, we see that there is a path difference between the ray that gets reflected along AC' and the ray that gets transmitted, and then reflected, along AB and BC respectively. This path difference is

$$(AB + BC) - (AC')$$

The two separate waves will arrive at a point with the same phase, and hence undergo constructive interference, only if this path difference is equal to any integer value of the wavelength

$$(AB + BC) - (AC') = n\lambda$$

where n is an integer determined by the order given, λ is the wavelength of the X-rays, d, as shown in Figure 1.16, is the spacing between the planes in the lattice, and θ is the angle between the incident ray and the scattering planes, both incorporated into the equation

$$AB = BC = \frac{d}{\sin\theta} \text{ and } AC = \frac{2d}{\tan\theta}$$

from which it follows that

$$AC' = AC\cos\theta = \frac{2d}{\tan\theta}\cos\theta = \left(\frac{2d}{\sin\theta}\cos\theta\right)\cos\theta = \frac{2d}{\sin\theta}\cos^2\theta$$

When the equations are put together

$$n\lambda = \frac{2d}{\sin\theta}(1 - \cos^2\theta) = \frac{2d}{\sin\theta}\sin^2\theta$$

which can be simplified to the Bragg's law equation

$$n\lambda = 2d\sin\theta \tag{1.79}$$

2 Materials & Their Characterization

The studies documented in this volume was made possible through close collaboration with highly established synthesis groups, most notably the group of xxxxxxxxx xxxxxxxxx xxxxxxxxxxxxx at the xxxxxxxxxx xx xxxxxxxxx, xxxxxxxx xxxxxx xxxxxxxxxx in xxxxxxxxxx, xxxxxxxxxxxx, as well as the group of xxx xxxxx xxxxxx of the xxxxxx xx xxxxxxxxx xxx xxxxxxxxxxxxxx xxxxxxx, xxxxxx xxxxxxx xx xxxxxxxx in xxxx, xxxxxx, all of whom were invaluable in their contributions to the design and innovation of the broad range of materials studied and reported here. Various techniques were used for the preparation of these materials, most noteworthy being that of atom transfer radical polymerization (ATRP).

ATRP is a type of controlled/living radical polymerization which was developed in the mid-1990s and can be applied to the preparation of many different (co)polymers [54]. The technique allows for the preparation of polymers with predetermined molecular weights, low polydispersity and controlled functionality, composition and topology. Radical polymerization techniques including that of ATRP are also known to be very tolerant of functional groups, allowing for the polymerization of a broad range of unsaturated molecules [55]. This provides an opportunity to form well-defined block, gradient and statistical copolymers with a wide-ranging spectrum of properties [56-57].

2.1 Acrylate-based Linear Copolymers

For this first study, isobornyl acrylate (IBA) and *n*-butyl acrylate (*n*BA) were used as component monomers to synthesize linear statistical, gradient and block copolymers (Figure 2.1) via ATRP.

The PIBA- and P*n*BA-based copolymers were prepared with systematically varied molecular weights and compositions. Their copolymerization with specific predetermined ratios was accomplished by carefully changing the monomer feed during the polymerization process. Table 2.1 contains a complete list of the synthesized homopolymers as well as the linear statistical, gradient and block copolymers which were prepared for this study.

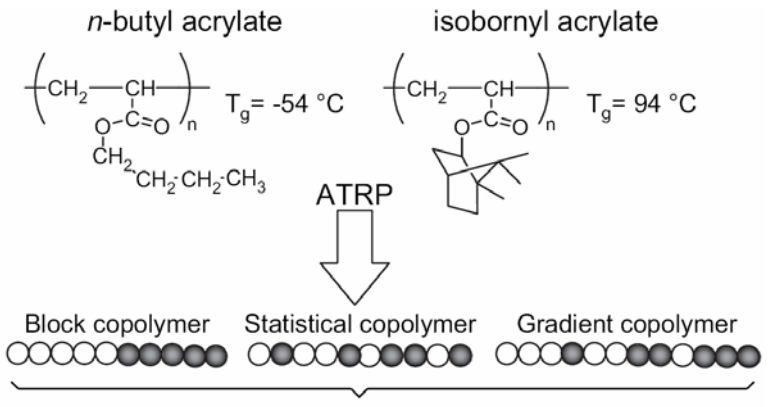

Polymer	Repeating unit	T_g (° C)
poly(*n*-propyl acrylate) PPA	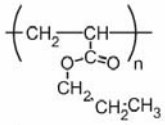	-40
poly(ethyl acrylate) PEA	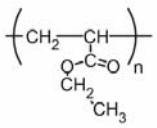	-24
poly(methyl acrylate) PMA	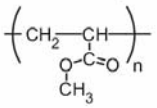	10
poly(*t*-butyl acrylate) P*t*BA	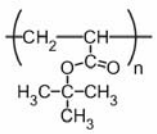	43

Figure 2.1. Copolymerization of isobornyl acrylate and *n*-butyl acrylate in different fashion and comparison of properties of resulting copolymers with acrylate-based homopolymers such as P*t*BA, PMA, PEA and PPA.

Table 2.1

Properties of different types of (co)polymers prepared by ATRP.

Sample	Type of copolymer	Unit M1	Unit M2	M1 wt% (GC)	T_g predicted[a]	M1 wt% (NMR)	GPC results		$M_{n,\text{theo}}$[b]
							PDI	M_n	
WJ-02-09	homopoly.	IBA (DP=290)	-	100	94.0	-	1.06	28500	35400
WJ-02-11	homopoly.	*t*BA (DP=470)	-	100	43.0	-	1.07	48900	43800
WJ 135	homopoly.	MA (DP=630)	-	100	10.0	-	1.16	42200	40000
WJ-02-07	homopoly.	EA (DP=900)	-	100	-24.0	-	1.06	96900	70200
WJ-02-29	homopoly.	*n*PA (DP=700)	-	100	-40.0	-	1.06	86000	58800
WJ-02-10	homopoly.	nBA (DP=460)	-	100	-54.0	-	1.07	47900	40800
WJ-02-13	random	IBA (DP=240)	*n*BA (DP=100)	80	46.5	79	1.06	34000	48000
WJ-02-19	random	IBA (DP=480)	*n*BA (DP=200)	80	46.5	78	1.08	63700	66000
WJ-02-14	random	IBA (DP=150)	*n*BA (DP=245)	50	7.0	53	1.05	43500	51600
WJ-02-20	random	IBA (DP=300)	*n*BA (DP=490)	50	7.0	54	1.06	69000	67000
WJ-02-35	random	IBA (DP=41)	*n*BA (DP=90)	43	-10.6	41	1.08	26300	18400
WJ-02-36	random	IBA (DP=82)	*n*BA (DP=180)	43	-10.6	39	1.07	39700	31600
WJ-02-28	random	IBA (DP=165)	*n*BA (DP=360)	43	-10.6	44	1.07	53000	48800
WJ-02-24	random	IBA (DP=245)	*n*BA (DP=540)	43	-10.6	42	1.10	100500	92400
WJ-02-16	random	IBA (DP=110)	*n*BA (DP=315)	35	-20.4	38	1.06	44300	45000
WJ-02-22	random	IBA (DP=220)	*n*BA (DP=630)	35	-20.4	33	1.12	107500	92400
WJ-02-15	random	IBA (DP=60)	*n*BA (DP=390)	20	-32.7	19	1.05	44700	44400
WJ-02-21	random	IBA (DP=120)	*n*BA (DP=780)	20	-32.7	22	1.07	81900	76800
WJ-02-17	random	IBA (DP=30)	*n*BA (DP=440)	10	-41.9	13	1.06	55600	45000
WJ-02-23	random	IBA (DP=60)	*n*BA (DP=880)	10	-41.9	16	1.13	94000	76900
WJ-02-30	block	WJ-02-09	*n*BA (DP=470)	50	94, -54	54	1.12	54600	46300
WJ-02-45	gradient	IBA (DP=192)	*n*BA (DP=307)	47	-	47	1.13	74800	62300

[a] predicted using Fox equation;
[b] $M_{n,\text{theo}}=([M]_0/[In]_0) \times \text{conversion} \times M_{monomer}$

2.2 Acrylate-based Triblock and Multi-arm Block Copolymers

The preparation of well-defined homopolymers as well as diblock and triblock copolymers of methylene-γ-butyrolactone (MBL) using ATRP has been previously reported. MBL, found in tulips, is the simplest member of butyrolactones found and isolated from various plants [58-61]. Such natural products are renewable, environmentally friendly, biocompatible, and biodegradable. Also, they may possess some special physical and biomedical properties. Recently, the possibility of using natural products to replace petroleum-based raw materials in large commodity markets, such as plastics, fibers, and fuels has been reviewed [61]. MBL consists of a five-membered ring with an ester group and possesses structural features similar to those of methyl methacrylate and polymerizes in a similar manner. Poly(α-methylene-γ-butyrolactone) (PMBL) has good durability, a high refractive index of 1.540, and high T_g (195 ºC) [62]. Various copolymers and blends containing MBL units have good optical properties and resistance to heat, weathering, scratches and solvents.

In this section, block copolymers based on poly(*n*-butyl acrylate) (PBA), poly(α-methylene-γ-butyrolactone) (PMBL) and poly(methyl methacrylate) (PMMA) were synthesized. The copolymers were systematically prepared with different composition ratios as well as different types of architecture, from linear A-B-A-type triblock copolymers to multi-arm star-like block copolymers.

2.2.1 PMBL-PBA-PMBL triblock copolymers

For this study, a series of well-defined triblock copolymers containing a middle block of PBA and outer blocks of PMBL or random PMBL-PMMA were synthesized via ATRP. The basic reaction taking place in the preparation of these materials is illustrated in Figure 2.2.

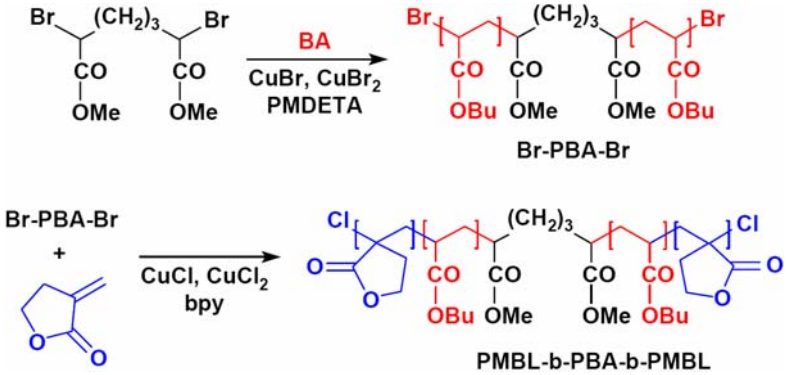

Figure 2.2. Preparation of PMBL-*b*-PBA-*b*-PMBL triblock copolymers.

These linear triblock copolymers with hard PMBL outer segments and soft PBA control segments were prepared with varied composition ratios between the soft and hard components, as listed in detail in Table 2.2.

Table 2.2

Compositions of prepared PMBL-PBA-PMBL triblock copolymers with PMBL outer hard blocks, and of prepared (PMBL-*r*-PMMA)-PBA-(PMBL-*r*-PMMA) triblock copolymers with random copolymer outer hard blocks.

Sample	Triblock composition	Hard block (mol%)[a]	Hard block (wt%)[a]	MBL/MMA (mol%)[a]
B215-L40	$PBA_{215}(\text{-}b\text{-}PMBL_{20})_2$	15.8	12.6	100/0
B215-L68	$PBA_{215}(\text{-}b\text{-}PMBL_{34})_2$	23.7	19.3	100/0
B215-L120	$PBA_{215}(\text{-}b\text{-}PMBL_{60})_2$	36.3	30.3	100/0
B375-L32	$PBA_{375}(\text{-}b\text{-}PMBL_{16})_2$	7.9	6.1	100/0
B375-L60	$PBA_{375}(\text{-}b\text{-}PMBL_{30})_2$	13.8	10.9	100/0
B375-L144	$PBA_{375}(\text{-}b\text{-}PMBL_{72})_2$	27.6	22.7	100/0
B375-L106M26	$PBA_{375}(\text{-}b\text{-}PMBL_{53}\text{-}r\text{-}PMMA_{13})_2$	26.0	21.3	80/20
B375-L82M50	$PBA_{375}(\text{-}b\text{-}PMBL_{41}\text{-}r\text{-}PMMA_{25})_2$	26.0	21.4	62/38
B375-M132	$PBA_{375}(\text{-}b\text{-}PMMA_{66})_2$	26.0	21.6	0/100

[a]based on ^{1}H NMR spectra

2.2.2 PBA-PMBL multi-arm block copolymers

While linear A-B-A-type triblock copolymers have been commonplace, the synthesis of polymers with hyperbranched, brush and star-shaped molecular architecture has only in recent years attracted much interest due to their different properties from those of linear polymers. And the expansion in the synthesis of these polymers has been possible due to the emergence of various new controlled polymerization techniques, which includes that of ATRP.

All of the star-like copolymers studied here were prepared by grafting polymer chains onto very short linear multifunctional initiators. It should be noted that this is a completely new approach, as in the past, similar but much longer macro initiators were used for the synthesis of polymer brushes, with a much higher aspect ratio of length of backbone vs length of side chains [63-67]. For the synthesis of the star-like copolymers, the side chains are much longer than the backbone, resulting in the rather star-like structures.

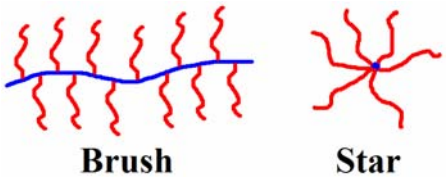

Figure 2.3. Schematic representation of the brush and star architectures.

The relative asymmetry of these stars should depend on the aspect ratio (Figure 2.3). ATRP was used for both preparation of the multifunctional initiator and the consecutive arm growth. The arm extension of living arm-ends was performed to form star-like block copolymers.

In this study, a series of 10- and 20-arm star-like block copolymers containing middle soft PBA block and outer hard PMBL block were synthesized by ATRP. A list of the prepared samples is shown in Table 2.3.

As an initiator, a poly(2-bromoisobutyryloxyethyl acrylate) (PBiBEA) with degree of polymerization (DP) of 10 and 20, prepared by ATRP of trimethylsilyloxyethyl acrylate (HEATMS) and its subsequent esterification, was used.

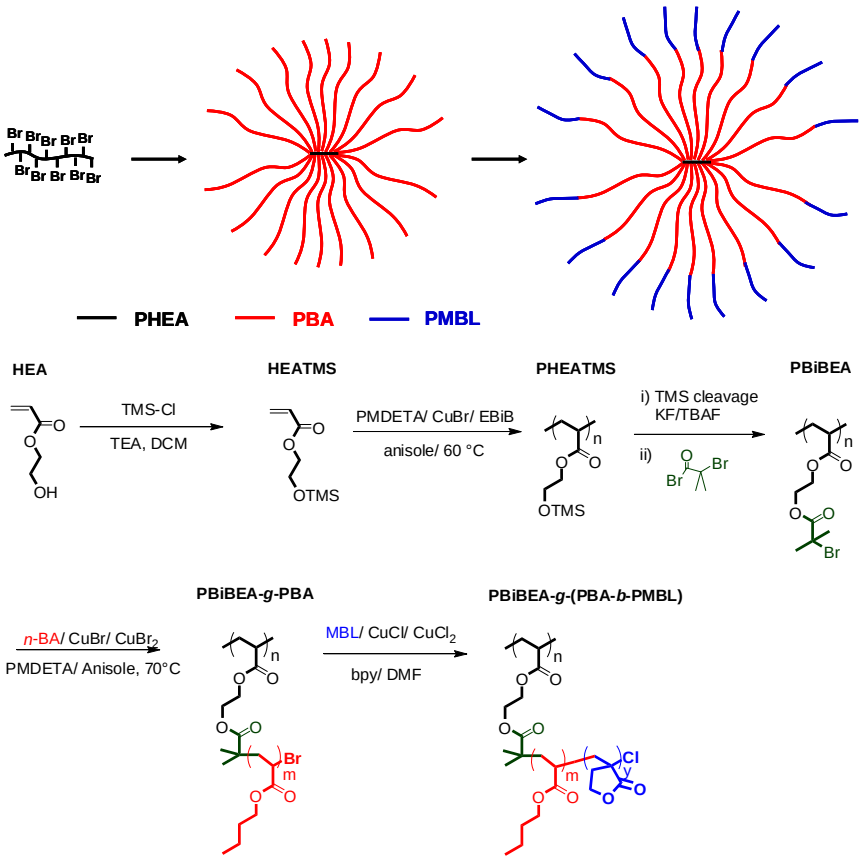

Figure 2.4. Synthesis of PBiBEA-*g*-(PBA-*b*-PMBL) star copolymers.

Table 2.3

Compositions of the prepared PBiBEA-g-(PBA-b-PMBL) star-like block copolymers.

Sample	Triblock composition	PMBL (mol %)[#]	PMBL (wt %)[#]
10B115-A30	$PBiBEA_{10}$-(PBA_{115}-$PMBL_{30}$)$_{10}$	20.7	16.5
10B115-A47	$PBiBEA_{10}$-(PBA_{115}-$PMBL_{47}$)$_{10}$	29.0	24.2
10B240-A46	$PBiBEA_{10}$-(PBA_{240}-$PMBL_{46}$)$_{10}$	16.1	12.7
10B240-A86	$PBiBEA_{10}$-(PBA_{240}-$PMBL_{86}$)$_{10}$	26.4	21.6
20B115-A47	$PBiBEA_{20}$-(PBA_{115}-$PMBL_{47}$)$_{20}$	29.0	24.2
20B115-A57	$PBiBEA_{20}$-(PBA_{115}-$PMBL_{57}$)$_{20}$	33.1	27.6
20B230-A96	$PBiBEA_{20}$-(PBA_{230}-$PMBL_{96}$)$_{20}$	29.4	24.2
20B750-A156	$PBiBEA_{20}$-(PBA_{750}-$PMBL_{156}$)$_{20}$	17.2	13.7

[#]based on ^{1}H NMR spectra

2.2.3 PBA-PMMA multi-arm block copolymers

In our second study of star-like copolymers, a series of 10- and 20-arm block copolymers containing middle soft PBA block and outer hard PMMA block were synthesized via ATRP. The same PBiBEA initiator was used.

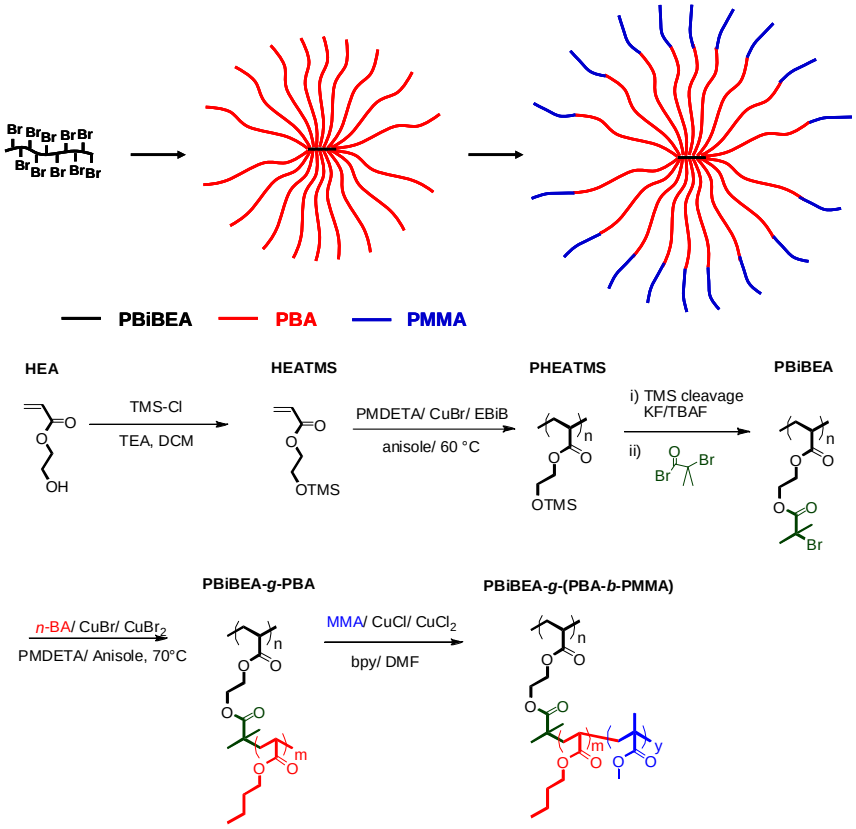

Figure 2.5. Synthesis of PBiBEA-*g*-(PBA-*b*-PMMA) star copolymers.

Table 2.4

Compositions of PBiBEA-*g*-(PBA-*b*-PMMA) star-like block copolymers.

Sample	Triblock composition	PMMA (mol %)*	PMMA (wt %)*
10B115-M29	$PBiBEA_{10}$-$(PBA_{115}$-$PMMA_{29})_{10}$	20.1	16.4
10B115-M51	$PBiBEA_{10}$-$(PBA_{115}$-$PMMA_{51})_{10}$	30.7	25.7
10B240-M54	$PBiBEA_{10}$-$(PBA_{240}$-$PMMA_{54})_{10}$	18.4	14.9
10B240-M117	$PBiBEA_{10}$-$(PBA_{240}$-$PMMA_{117})_{10}$	32.8	27.6
20B115-M38	$PBiBEA_{20}$-$(PBA_{115}$-$PMMA_{38})_{20}$	24.8	20.5
20B115-M60	$PBiBEA_{20}$-$(PBA_{115}$-$PMMA_{60})_{20}$	34.3	28.9
20B230-M59	$PBiBEA_{20}$-$(PBA_{230}$-$PMMA_{59})_{20}$	20.4	16.7
20B230-M107	$PBiBEA_{20}$-$(PBA_{230}$-$PMMA_{107})_{20}$	31.8	26.6
20B750-M180	$PBiBEA_{20}$-$(PBA_{750}$-$PMMA_{180})_{20}$	19.4	15.8
20B750-M300	$PBiBEA_{20}$-$(PBA_{750}$-$PMMA_{300})_{20}$	28.6	23.8

*based on ^{1}H NMR spectra

2.3 Siloxane-based Linear Gradient Copolymers

In this section, siloxane-based linear gradient copolymers were synthesized mainly via anionic ring-opening copolymerization of cyclotrisiloxanes. Gradient organic copolymers have commonly been synthesized using mostly controlled radical polymerization (CRP) techniques [21, 25, 27, 68-72]. However, there are only a few examples of gradient copolymers obtained by anionic [21, 73-74] and cationic [75] polymerizations. And reports on the synthesis of gradient polysiloxanes are very scarce [76-77]. Nevertheless, gradient functionalized polysiloxanes of well-defined structure may be of interest due to the unique surface properties of polysiloxanes [78] and the advantageous features related to the gradient copolymer backbone structure.

2.3.1 Fluorosiloxane-based copolymers

Copolymers based on fluorosilicones are studied here for the very first time, as previously, only the synthesis of vinylmethyl polysiloxanes of gradient structure has been published [78]. For this study, gradient and block copolymers which are composed of 2,4,6-tris(3,3,3-trifluoropropyl)-2,4,6-trimethylcyclotrisiloxane (F) with hexamethylcyclotrisiloxane (D) were synthesized. A detailed list of the synthesized copolymers and homopolymers is shown in Table 2.5.

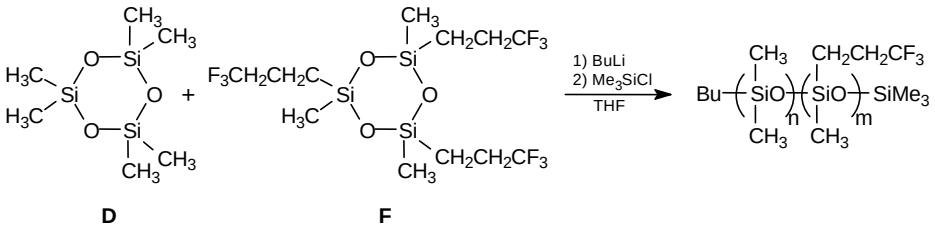

Figure 2.6. Synthesis of PMTFS-PDMS copolymers.

Table 2.5

List of prepared block, spontaneous gradient and forced gradient D-F copolymers.

Polymer	D-F	M_n (theoretical)	M_n NMR	M_n-SEC[a] in CH_2Cl_2 (M_w/M_n)
Block copolymer	1:1	15,000	14,600	13,500 (1.13)
Gradient spontaneous	1:1	11,000	14,700	10,000 (1.13)
Gradient spontaneous	2:1	10,000	13,600	11,000 (1.12)
Gradient spontaneous	1:2	11,000	16,700	13,000 (1.20)
Gradient spontaneous	1:1	11,000	15,400	11,000 (1.15)
Forced Gradient	1:1	15,000	-	16,700 (1.17)
Gradient spontaneous DFD[b]	1:1	40,000		44,000 (1.15)
Forced Gradient DFD[b]	1:1	40,000	39,300	45,800 (1.15)
Homopoly. PDMS	-	15,000	-	-
Homopoly. PMTFPS	-	20,000	-	18,000 (1.07)

[a]Relative to PS standards
[b]DFD copolymers (initiator $Pb_2Si(OLi)_2$)

2.3.2 Vinylsiloxane-based copolymers

In this study, vinyl functionalized copolysiloxanes were synthesized by equilibrium copolymerization of cyclotetrasiloxanes [79-81] or by non-equilibrium polymerization of cyclotrisiloxanes with cyclotetrasiloxanes [82-83] (Figure 2.7), the vinyl-containing gradient polysiloxanes obtained by the anionic ring-opening copolymerization of 2-vinyl-2,4,4,6,6-pentamethylcyclotrisiloxane (D_2V) [76] or 2,4,6-trivinyl-2,4,6-trimethylcyclotrisiloxane (V) with hexamethylcyclotrisiloxane (D) [77].

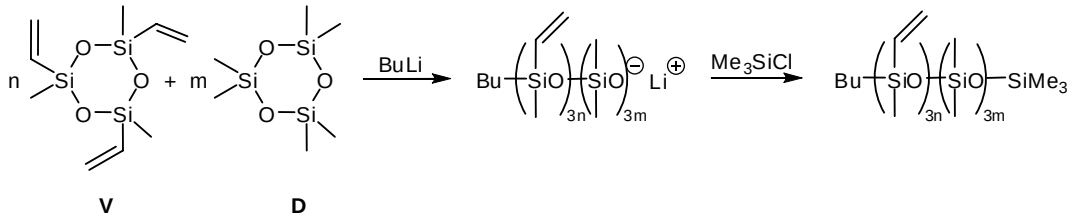

Figure 2.7. Synthesis of PDMS-PMVS copolymers.

Table 2.6

List of prepared block, spontaneous gradient and forced gradient D-V copolymers.

Polymer	D-V	M_n (theoretical)	M_n (NMR)	M_n (SEC)[a] in CH_2Cl_2 (M_w/M_n)
Block Copolymer	1:1	22000	20000	24000 (1.47)
Forced Gradient	1:1	21000	-	25700 (1.32)
Gradient Spontaneous	1:1	32000	-	35500 (1.40)
Gradient Spontaneous	1:2	13000	15700	15300 (1.25)
Gradient Spontaneous	2:1	14000		18500 (1.28)
Homopolymer PDMS	-	14500		17400 (1.56)
Homopolymer PMVS	-	14500		

[a]Relative to PS standards.

2.4 Material Characterization

Characterization of the synthesized materials was done via differential scanning calorimetry (DSC), dynamic mechanical analyses (DMA), tensile strength measurements, and small-angle X-ray scattering (SAXS). This section outlines the technical specifications of these characterization methods.

2.4.1 Dynamic mechanical analyses (DMA)

DMA was performed using the Advanced Rheometric Expansion System (ARES) equipped with a force-rebalanced transducer, as well as the Rheometrics RMS 800 mechanical spectrometer, which is schematically illustrated in Figure 2.8. The studied materials (pellets of 6 mm diameter and around 1 mm thickness) were placed between two parallel plates. When required, the specimens were first heated above T_g to become soft, therefore establishing better contact to the plates.

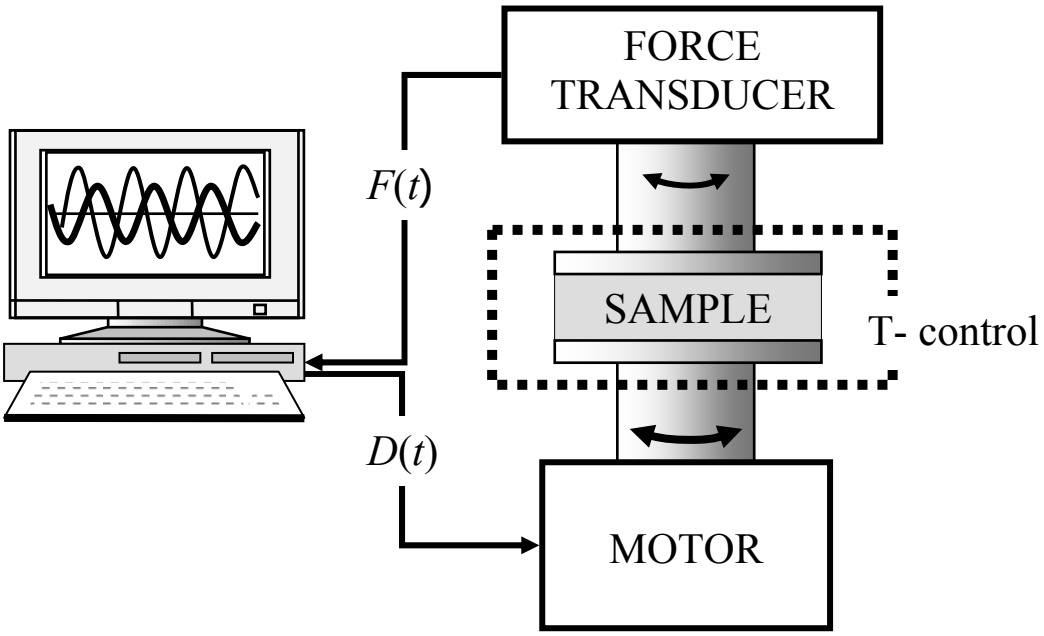

Figure 2.8. A schematic diagram of the dynamic mechanical analyzer. The deformation (shear strain) input signal $D(t)$ is applied by the motor and the resulting torque $F(t)$ is measured by the force transducer.

Before obtaining temperature dependence of storage *G'* and loss *G"* moduli, isothermal strain sweeps at different temperatures are performed in order to separate the linear from the non-linear viscoelastic regimes. The strain dependent torque was measured and compared with the strain dependence of storage (*G'*) and loss (*G"*) moduli (Figure 2.9).

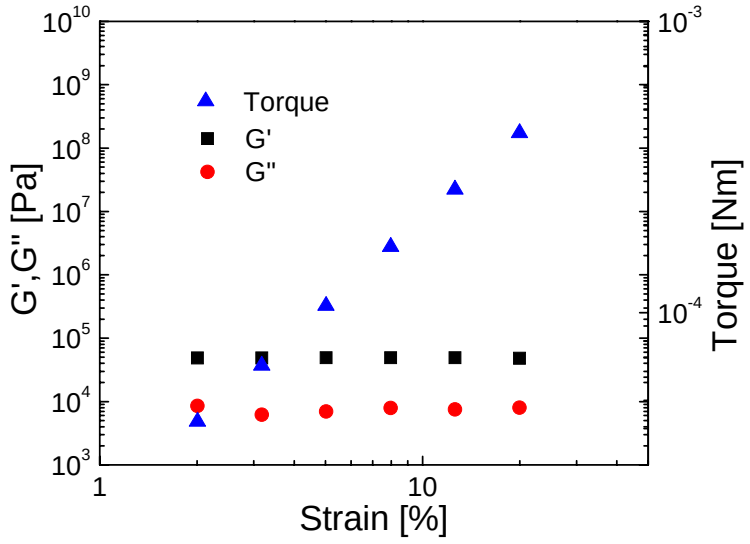

Figure 2.9. Isothermal strain sweep for an multi-arm PBA-PMMA block copolymer taken as an example. The sample is sheared between two plates (see Figure 1.2) and the resulting torque is recorded. Notice the insensitivity of the shear moduli to the applied strain (linear viscoelastic regime).

For analyses of thermomechanical properties of the materials, shear deformation was applied under conditions of controlled deformation amplitude, which was kept in the range of the linear viscoelastic response of the studied samples. Plate-plate geometry has been used with plate diameters of 6 mm. The gap between plates (sample thickness) was about 1 mm. Experiments have been performed under a dry nitrogen atmosphere. Frequency dependencies of the storage (*G'*) and the loss (*G"*) parts of the shear modulus have been determined from frequency sweeps measured within the frequency range 10^{-2}-10^{2} rad/s at various temperatures. Master curves for *G'* and *G"* at a reference temperature have been

obtained using the time-temperature superposition, i.e., shifting the data recorded at various temperatures only along the frequency coordinate.

2.4.2 Differential scanning calorimetry (DSC)

Thermal characterization of polymers was performed using a Mettler DSC-30 calorimeter as well as a DuPont 2000 thermal analysis system. Experiments were conducted with cooling and heating rates of 10 K/min. The transition temperatures were taken as corresponding to the maximum of the enthalpic peak and determined from the second heating run at the inflection point.

2.4.3 Small-angle X-ray scattering (SAXS) analyses

Small-angle X-ray scattering measurements were conducted using a rotating anode (Rigaku RA-Micro 7) X-ray beam with a pinhole collimation and a two-dimensional detector (Bruker Highstar) with 1024 x 1024 pixels. A double graphite monochromator for the Cu Kα radiation (λ = 0.154 nm) was used. The beam diameter was about 0.8 mm, and the sample to detector distance was 1.8 m. The recorded scattered intensity distributions were integrated over the azimuthal angle and are presented as functions of the scattering vector q ($s = 2\sin(\theta)/\lambda$, where 2θ is the scattering angle).

2.4.4 Tensile tests

Tensile tests were performed using a mechanical testing machine Instron 6000. Samples with thickness in the order of 0.2– 0.5 mm were drawn with the rate of 5 mm/min at room or at elevated temperature. Dependencies of stress vs draw ratio were recorded. Elastic modulus, elongation at break and stress at break were determined by the averaging of 3–5 independent drawing experiments performed at the same conditions.

3 Results & Discussion

This chapter extensively documents the findings of our investigations on the various complex copolymer systems. The morphology and thermomechanical properties of all of the synthesized materials were analyzed mainly via DSC, DMA, tensile strength measurements, and SAXS.

3.1 Comparing Acrylate-based Copolymers to Homopolymers

The primary goal of this work was to compare thermomechanical properties of block, gradient and statistical copolymers of *n*BA and IBA with various acrylate homopolymers. As shown in the last chapter in Figure 2.1, the copolymers were prepared with systematically varied molecular weights and compositions to assist in the investigation of structure property correlation. The choice of *n*BA and IBA was dictated by the very different thermal properties of its homopolymers. The glass transition temperature (T_g) of P*n*BA is -54 ºC whereas T_g of PIBA is 94 ºC. Thus, their copolymerization with carefully selected ratios could result in polymers with thermal properties similar to various acrylate homopolymers such as poly(*t*-butyl acrylate) (P*t*BA), poly(methyl acrylate) (PMA), poly(ethyl acrylate) (PEA) and poly(*n*-propyl acrylate) (PPA). For example, the glass transition temperature (T_g) of the resulting statistical poly(isobornyl acrylate-*co*-*n*-butyl acrylate) (P(IBA-*co*-*n*BA)) copolymers could be tuned by changing the monomer feed during the polymerization process. This way, it may be possible to generate materials which could hopefully mimic thermal behavior of the homopolymers mentioned above.

3.1.1 Statistical P(IBA-*co*-*n*BA) copolymers

When comparing the thermomechanical properties of acrylate homopolymers and P(IBA-*co*-*n*BA) copolymers, the first important question is whether the copolymer system is isotropic in the bulk state or rather exhibits a micro-phase

separation. To answer this question the DSC thermographs for all samples described in Table 2.1 were measured. Some typical results obtained from statistical copolymers with different compositions (the green line) together with the respective curves for PIBA and P*n*BA homopolymers are shown in Figure 3.1. Clearly, all the copolymers are completely amorphous and exhibit only a single glass transition at a temperature increasing with the increase of the IBA content. This indicates that there is no micro-phase separation in the statistical P(IBA-*co*-*n*BA) copolymers, a finding further confirmed by DMA and SAXS experiments, which will be discussed below.

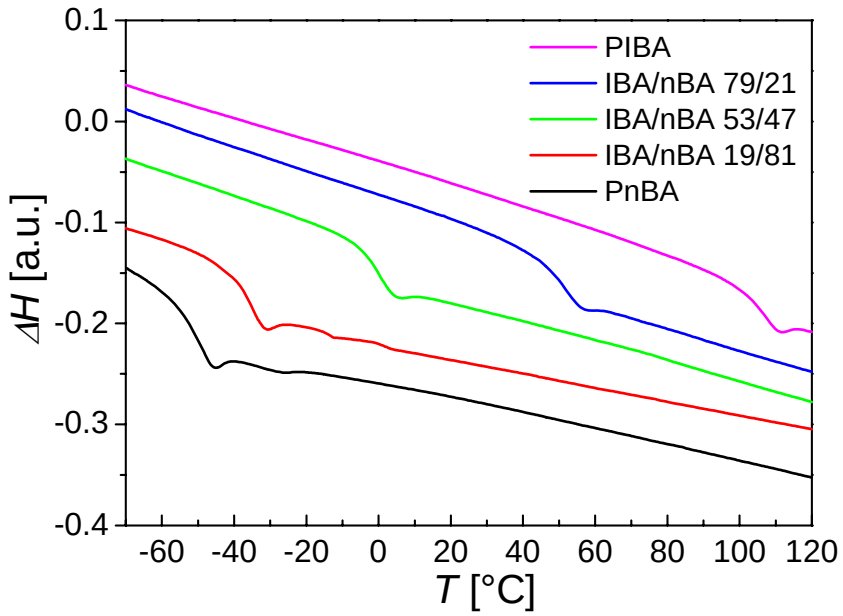

Figure 3.1. DSC thermograms of statistical P(IBA-*co*-*n*BA) copolymers with different monomer compositions: IBA(19%)-*n*BA(81%) copolymer (red, WJ-02-15), IBA(53%)-*n*BA(47%) copolymer (green, WJ-02-14), IBA(79%)-*n*BA(21%) copolymer (blue, WJ-02-13) of IBA and *n*BA. The thermographs of the respective homopolymers are also shown for comparison (black for *n*BA and pink for IBA, respectively).

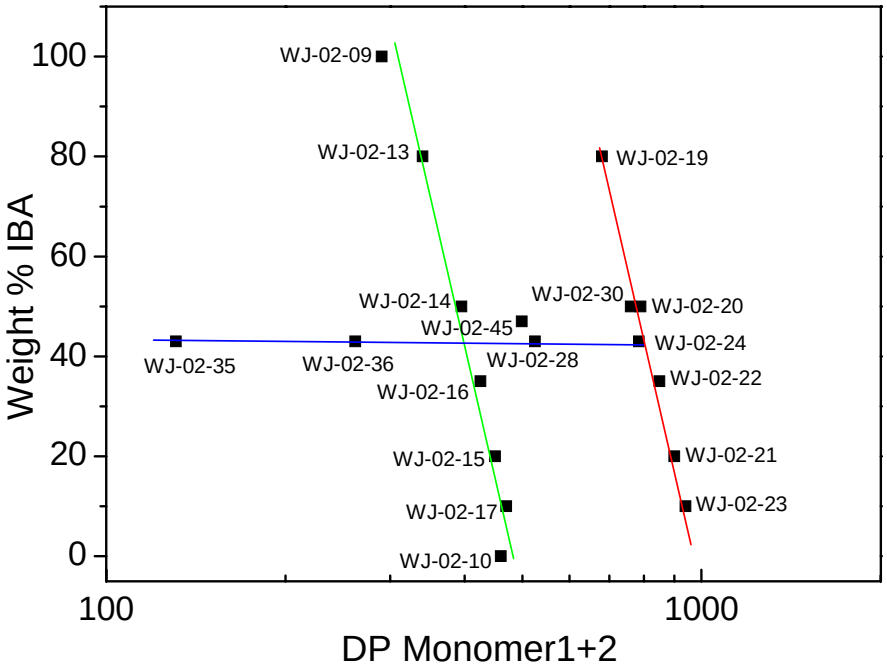

Scheme 3.1. Schematic representation of prepared copolymer samples of P(IBA-*co*- *n*BA) with different molecular weights and compositions (Table 2.1 presents detailed characterization of all copolymers).

The T_g's of all statistical copolymers (from the green and red lines in Scheme 3.1) are plotted vs. their IBA content in Figure 3.2. The T_g varies continuously with composition in both low and high molecular weight samples. To describe such type of composition dependence of the T_g of copolymers or miscible polymer blends, the Fox equation was used

$$\frac{1}{T_g} = \frac{w_1}{T_{g1}} + \frac{w_2}{T_{g2}}$$

where T_g is the glass transition temperature of the copolymer, T_{g1} and T_{g2} are the glass transition temperatures of the two homopolymers, and w_1 and w_2 are the

weight fractions of the two repeat units in the copolymer. As can be seen in Figure 3.2, the experimentally measured T_g values closely follow the predictions of the Fox equation, which is represented by the line linking the two homopolymers' T_g's.

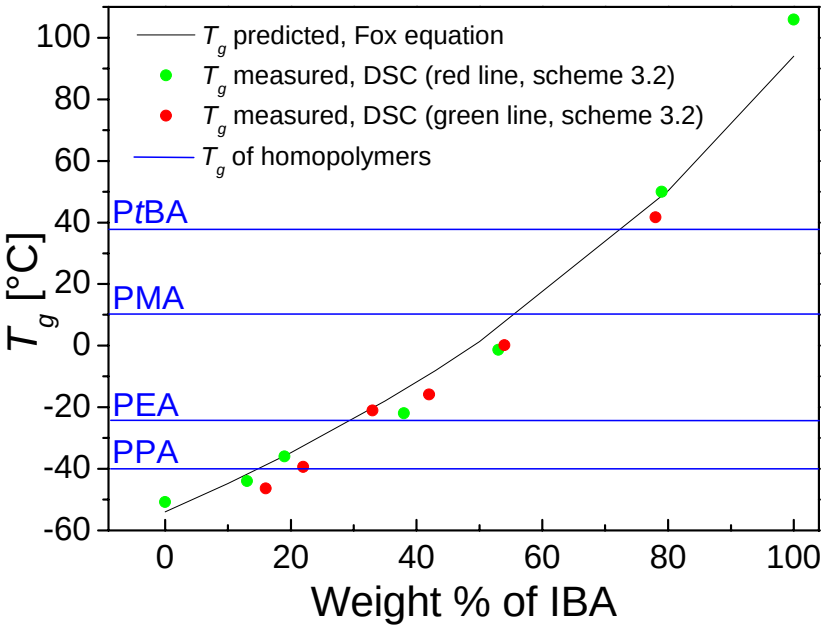

Figure 3.2. Tuning T_g in statistical copolymers of P(IBA-*co*-*n*BA) with different IBA/*n*BA ratios and two different degrees of polymerization.

DMA was used to study the influence of the composition on the dynamics of the P(IBA-*co*-*n*BA) copolymers. In Figure 3.3 the frequency dependence of the real (*G'*) and imaginary (*G''*) parts of the shear modulus (master curves) are presented for a series of statistical copolymers with similar (low) degree of polymerization and an increasing amount of the IBA content (the green line in Scheme 3.1). It is important to emphasize that all statistical copolymers studied here, allowed for a construction of a smooth master curves and the shift factors conform to the WLF equation. This confirms that the statistical P(IBA-*co*-*n*BA) copolymers obey the principle of time-temperature superposition, i.e., they can be considered as

thermorheologically simple. This subject can be addressed more quantitatively by analyzing the temperature dependence of the minimum of tan(δ), as recently shown for a series of cycloolefin copolymers with different norbornene content [84]. Such analyses, however, are beyond the scope of this study.

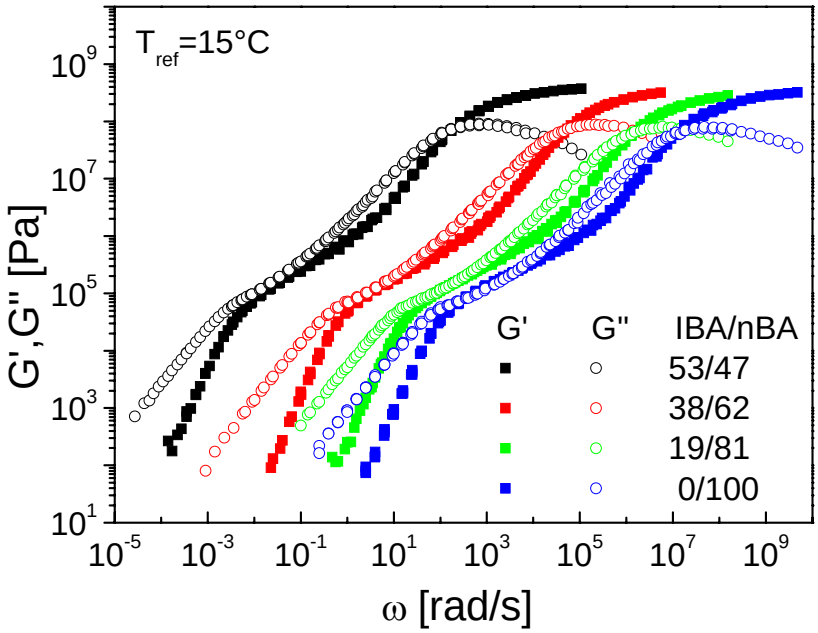

Figure 3.3. Typical examples of G' and G'' dependencies (master curves) on frequency for a linear P*n*BA homopolymer and statistical P(IBA-*co*-*n*BA) copolymers with similar degrees of polymerization and different IBA/*n*BA ratios (Scheme 3.1, the green line).

Let us first consider the pure P*n*BA. As can be seen in Figure 3.3, the relaxation spectrum of this homopolymer shows the two distinct characteristic regions which was discussed in Chapter 1. The one at high frequencies is related to segmental (local) motions of the polymer chains and the lower frequency, or terminal one, is related to relaxation of entangled chains. These two parts of the spectra are characterized with their respective relaxation times, τ_s and τ_c [23]. These relaxation times determine the time range within which the characteristic rubbery

plateau is observed for linear polymers. For most of the linear flexible polymers, as well as for P*n*BA, the plateau height is between 10^5 and 10^6 Pa. Outside the rubbery plateau range the linear polymer melts become glassy at high frequencies and flow within longer time periods, i.e., at low frequencies.

As can be seen from Figure 3.3, the increased amount of IBA in the copolymer composition leads to a systematic shift of the master curves to lower frequencies. This effect is related to the strong increase of the glass transition temperatures of the respective copolymers. However, the shape of the master curves does not change significantly and there is no evidence of any new relaxation processes in the copolymers as compared to a P*n*BA homopolymer. This is an additional indication that the statistical P(IBA-*co*-*n*BA) copolymers do not exhibit a phase separation. In order to better understand the influence of the composition on the dynamics of the statistical copolymers, we have determined the characteristic times τ_c related to the terminal relaxation process by the crossing points of the *G'* and *G''* curves observed at the transition to the flow range at low frequency. Results are shown in Figure 3.4(a) as a function of the IBA content for the copolymers from the green and the red line in Scheme 3.1. As in earlier study [85], the terminal relaxation times are normalized to the relaxation times of the segmental motion, which makes the results nearly independent of the reference temperature and free of effects related to the chain length dependence of the segmental motion, usually observed for short chains.

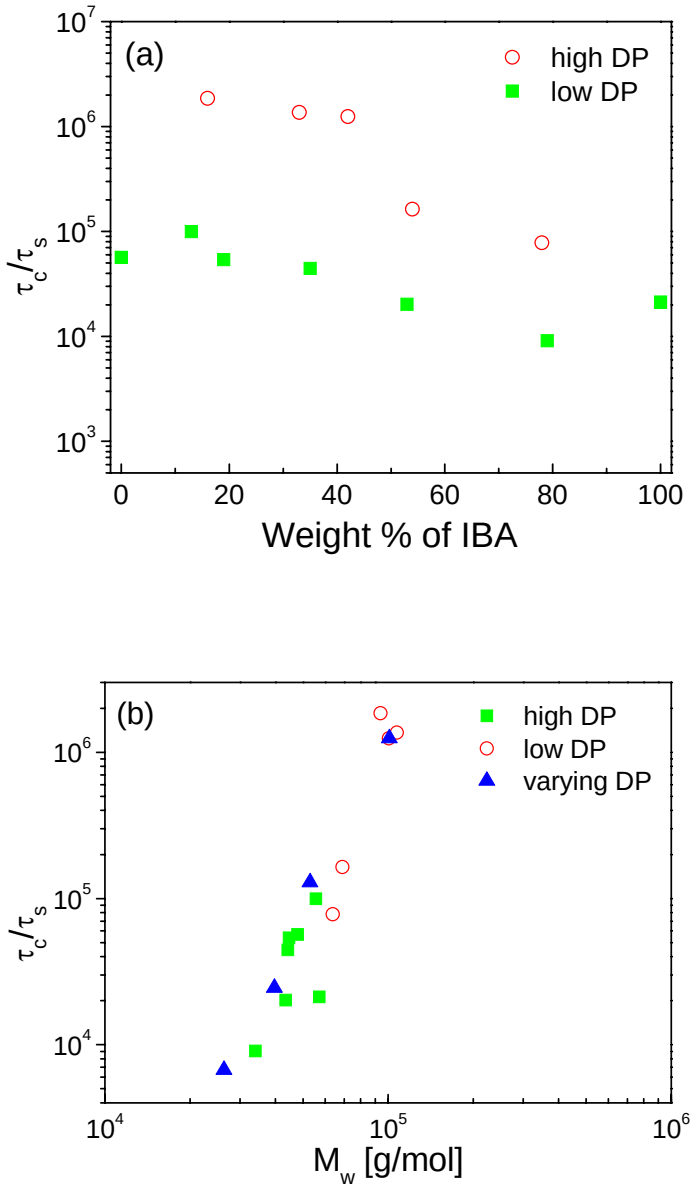

Figure 3.4. Effect of (a) the composition, and (b) the molecular weight, of statistical copolymers P(IBA-*co*-*n*BA) on the chain relaxation times.

As can be seen in Figure 3.4(a), the terminal relaxation times of the copolymers depend weakly on the IBA content and much stronger on the degree of polymerization. Furthermore even this weak dependence is most likely related to the slight decrease of the copolymers molecular weight with the decrease of IBA

content (see Table 2.1). This is further illustrated in Figure 3.4(b) where the same data are plotted versus the molecular weight of the copolymers. For comparison, the data for statistical copolymers with similar composition but different degree of polymerization (the blue line on Scheme 3.1) are also shown. All statistical copolymers show similar molecular weight dependence of the terminal relaxation times independent of their composition. The slope of this dependence is approximately 4, a value slightly higher than that typically found for homopolymer melts in the entangled regime, i.e., ~3.4.

3.1.2 Statistical copolymers mimicking homopolymers.

As shown in a previous section, the glass transition of the statistical P(IBA-*co*-*n*BA) copolymers can be tuned to any value between the T_g's of the two homopolymers (i.e., between -54 and 94 ºC) by proper choice of the comonomer ratio. It is possible therefore, to synthesize copolymers with glass transition temperatures matching the T_g of other acrylate homopolymers. This is illustrated in Figure 3.2, where the glass transition temperatures of the PPA, PEA, PMA and P*t*BA are shown as horizontal lines. It is interesting to verify if the statistical P(IBA-*co*-*n*BA) copolymers can mimic not only the T_g's of the acrylate homopolymers, but also their mechanical properties. In order to do this, we plotted in Figure 3.5(a) the DMA master curves measured for PPA homopolymer and IBA(16%)-*n*BA(84%) copolymer with similar molecular weight. The two master curves overlap very well both in the high frequency region (due to the similar T_g's) and in the low frequency region (due to the similar M_n). Nevertheless, a closer look at Figure 3.5(a) reveals also some differences.

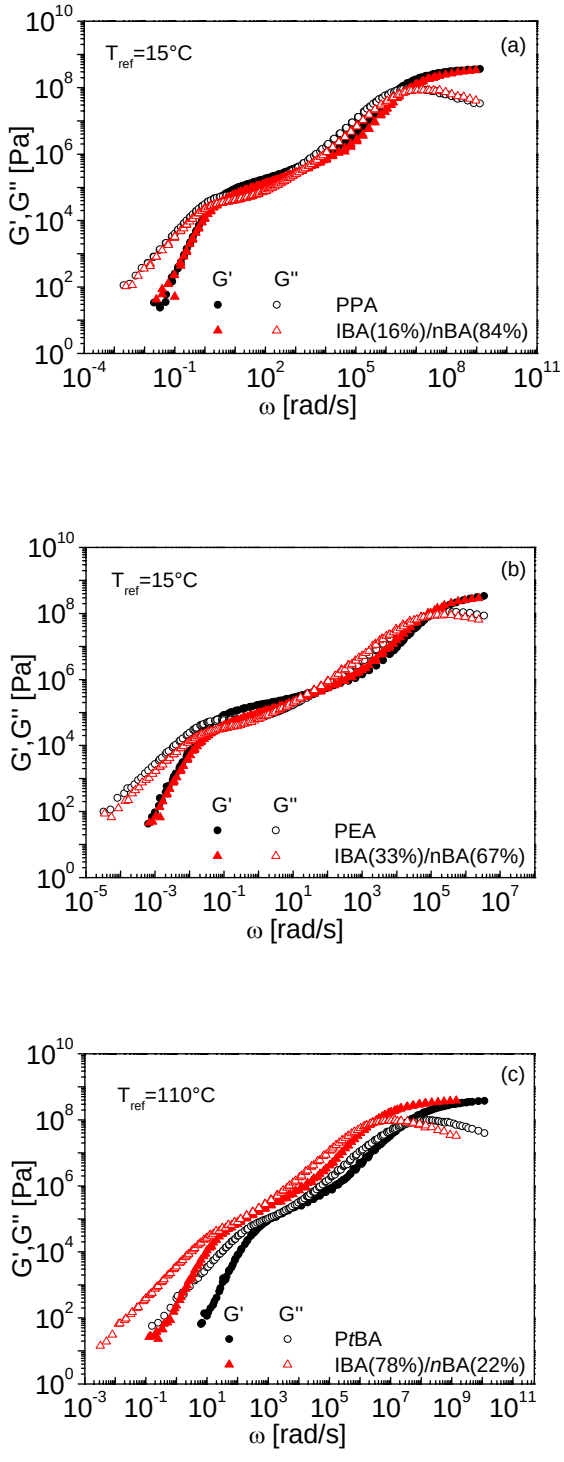

Figure 3.5. Comparison of the shear moduli spectra of (a) PPA (T_g = -40 ºC, M_n = 86 000 g/mol; WJ-02-29) and IBA(16%)-*n*BA(84%) copolymer (T_g = -39 ºC, M_n = 94 000 g/mol; WJ-02-23); (b) PEA (T_g = -24 ºC, M_n = 96 900 g/mol; WJ-02-07)

and IBA(33%)-*n*BA(67%) copolymer (T_g = -20 ºC, M_n = 107 500 g/mol; WJ-02-22); (c) P*t*BA (T_g = 37 ºC, M_n = 48 900 g/mol; WJ-02-11) and IBA(78%)-*n*BA(22%) copolymer (T_g = 42 ºC, M_n = 63 700 g/mol; WJ-02-19).

Most importantly, in the characteristic rubbery plateau region, the storage modulus (*G'*) of the P(IBA-*co*-*n*BA) copolymer is significantly lower than the corresponding value for the PPA homopolymer. This effect is even more evident in Figure 3.5(b), which compares the master curve of statistical copolymer with IBA(33%)/*n*BA(67%) with that of the PEA homopolymer of similar molecular weight. Again, the overlap of the two spectra is remarkably good at high and low frequencies, but the significant difference in the storage modulus is observed in the plateau region. This means that while mimicking perfectly the glass transition temperatures of the PEA and PPA, the P(IBA-*co*-*n*BA) copolymers are significantly softer than their homopolymer counterparts. It is interesting to verify if similar observations can be made also when comparing the copolymers with higher IBA content, i.e., higher glass transition temperature with the PMA and PtBA homopolymers. Unfortunately, as can be seen from Figure 3.2, none of the synthesized copolymers had the appropriate composition in order to match the T_g of the PMA. Nevertheless, the IBA(78%)-*n*BA(22%) copolymer (WJ-02-19) has a glass transition temperature very similar to that of the P*t*BA. The DMA master curves of these two materials are shown in Figure 3.5(c). The spectra are very similar although slightly shifted due to the small difference in the glass transition temperatures. More importantly, the copolymer is again softer than the homopolymer, i.e., has a lower *G'* value in the rubbery plateau region.

The data for the *G'* in this region for all materials presented in Figure 3.5 are summarized in Table 2. For comparison the values for *n*BA and IBA homopolymers are also shown. As can be seen from the table in all cases, the P(IBA-*co*-*n*BA) copolymers are significantly softer than the respective homopolymers having same glass transition temperatures. The lower plateau modulus of the copolymers indicates that they should have higher entanglement

M_w. The effect is most likely related to the rather big and rigid side group of IBA, which prevents the copolymer chains from a denser packing and therefore results in a less dense and softer IBA containing copolymers. This conclusion is further confirmed by the very low plateau modulus of the IBA homopolymer itself.

Table 3.1

Glass transition temperature and rubbery plateau storage modulus for the polymers shown in Figure 3.5

Polymer	Sample name	T_g [°C]	plateau *G'* [kPa]
PPA	WJ-02-29	-40	140
IBA(16%)-*n*BA(84%)	WJ-02-23	-39	95
PEA	WJ-02-07	-24	170
IBA(33%)-*n*BA(67%)	WJ-02-22	-20	70
PtBA	WJ-02-11	37	135
IBA(78%)-*n*BA(22%)	WJ-02-19	42	85
***n*BA**	WJ-02-10	-54	130
IBA	WJ-02-09	105	80

3.1.3 Gradient P(IBA-*grad*-*n*BA) and block PIBA-*b*-P*n*BA copolymers

As discussed above, the statistical P(IBA-*co*-*n*BA) copolymers exhibit homopolymer-like thermomechanical properties, with no evidence for a two phase behavior. However, the situations are remarkably different in the case of gradient and especially block copolymers. In order to illustrate this, Figure 3.6(a) compares the DSC thermographs of a statistical copolymer and a gradient copolymer, with similar IBA/*n*BA composition and comparable molecular weight. As expected, the statistical copolymer shows a clear glass transition at a temperature between the T_g's of the two homopolymers in agreement with the Fox equation. The gradient copolymer, however, reveals a broad glass transition region with no obvious glass transition temperature [21, 86-87]. Such behavior is probably caused by the broad distribution of IBA and *n*BA segments with different lengths along the gradient copolymer chains.

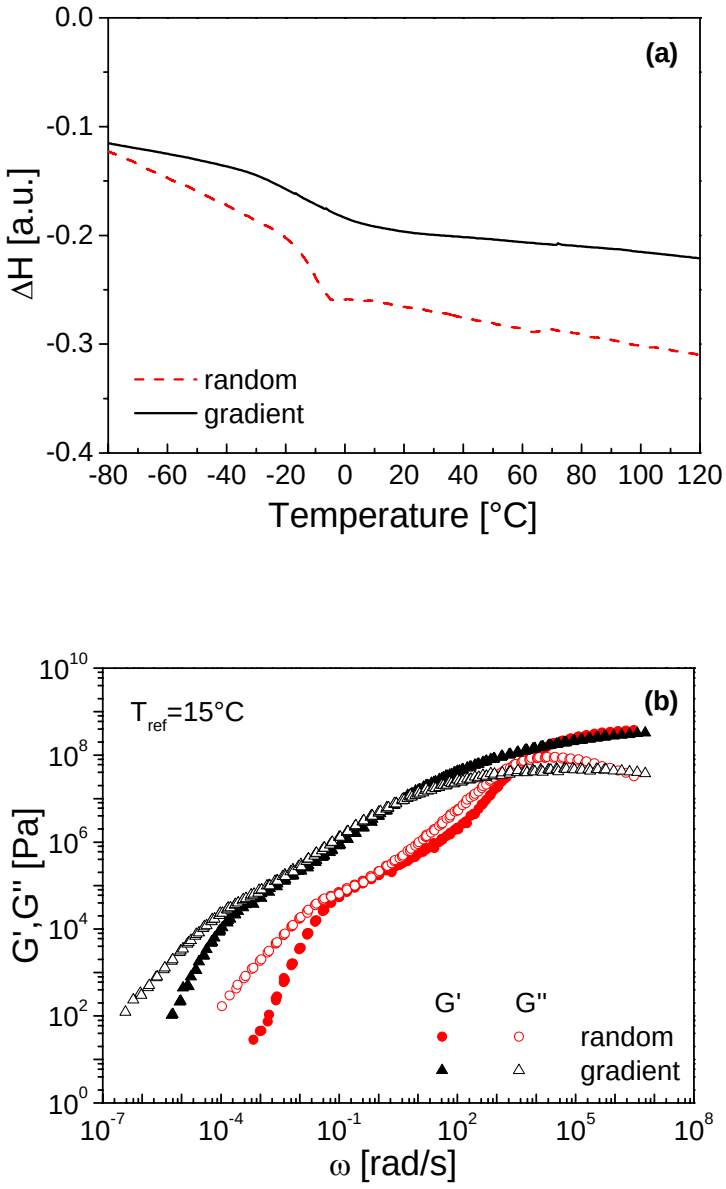

Figure 3.6. Comparisons between gradient IBA(47%)-*n*BA(53%) copolymer (broad T_g, M_n = 74 800 g/mol; WJ-02-45) and statistical IBA(44%)-*n*BA(56%) copolymer (T_g = -10.6 ºC, M_n = 53 000 g/mol; WJ-02-28).

Similar conclusions may be derived from the results of the DMA measurements illustrated in Figure 3.6(b). The master curve for the statistical copolymer shows the two distinct characteristic relaxation regions, as expected. The master curve

for the gradient copolymer, however, shows very broad distribution of relaxation processes, particularly in the segmental relaxation region.

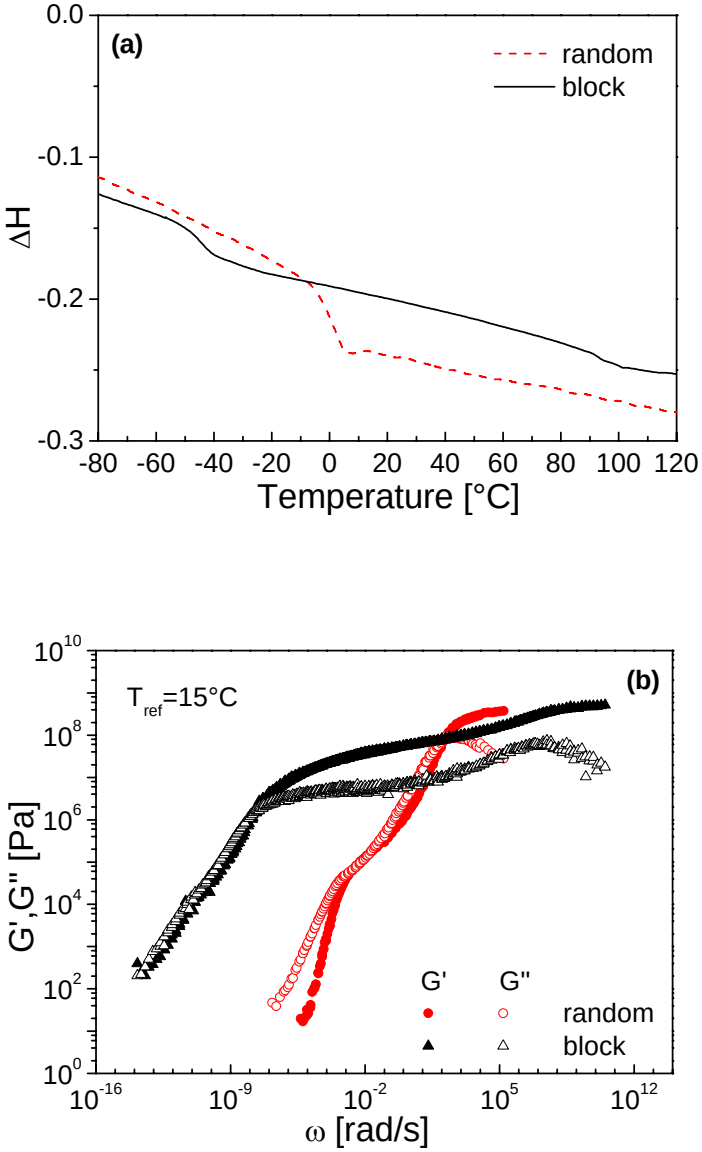

Figure 3.7. Comparisons of block IBA(54%)-*n*BA(46%) copolymer (T_g = -54 ºC, 94 ºC, M_n = 54 600 g/mol; WJ-02-230) and statistical IBA(54%)-*n*BA(46%) copolymer (T_g = 7 ºC, M_n = 69 000 g/mol; WJ-02-20).

It was previously reported that this broadening could be related to compositions' fluctuations in the studied copolymers [88-89]. A recent study of a similar system has shown that using experimental techniques such as photon correlation spectroscopy and dielectric spectroscopy the relaxation dynamic can be addressed in greater detail [90].

In Figure 3.7(a), the DSC thermographs of statistical and block copolymers with similar molecular weight and similar IBA/*n*BA composition are compared. While, the statistical copolymer has a single glass transition, the block copolymer shows two glass transition temperatures corresponding to the T_g's of each component indicating a micro-phase separation in the sample. In Figure 3.7(b) the frequency dependence of *G'* and *G"* of the same copolymers are compared. It is important to emphasize that in the case of the block copolymer, merely an attempt for constructing a master curve is shown, as the temperature dependence of the shift factors does not conform to the WLF equation. Nevertheless such an approach was shown to reveal important information for the morphology and order-disorder transitions in a number of block copolymer systems [91-93]. In our case, the block copolymer ''master curve'' provides additional evidences for the micro-phase separation in this sample. First of all the glass transitions of the two blocks are clearly distinguishable at low and high frequencies, respectively. Furthermore the behavior of the ''master curve'' in the very low frequency region, namely $G'(\omega)$ overlapping with $G''(\omega)$ and having a slope of ~0.5 may indicate the formation of a lamella structure as theoretically predicted [94].

In order to verify these findings, SAXS experiments were performed on the same pair of block and statistical copolymers. As expected the statistical copolymer has revealed a smooth scattered intensity distribution without any peaks. The block copolymer, however, showed a weak maximum, which may result from distance correlations between P*n*BA and PIBA domains. There are no other peaks in the spectra probably as result of the small contrast in the electronic densities of the two blocks. For this reason it is not possible to make any conclusions concerning

type of order or to identify any specific morphological forms. From the position of the maxima, however, a structural periodicity of = 20 nm can be assigned to the block copolymer sample.

3.2 Acrylate-based Block Copolymers as Thermoplastic Elastomers

Thermoplastic elastomers (TPEs) form an important class of materials combining elastomeric behavior with thermoplastic properties. Commonly these are A-B-A type triblock copolymers that combine a soft central block with glassy end blocks. These blocks should be immiscible and should phase separate with formation of thermoplastic microdomains, which act as physical cross-links for the soft matrix. One of the most common TPEs is the polystyrene–polybutadiene–polystyrene (SBS) triblock copolymer [95]. However, SBS suffers from two drawbacks. First, the unsaturated polybutadiene block is easily oxidized and is sensitive to UV degradation. Second, the upper service temperature is limited by T_g of the polystyrene block (ca. 100 ºC). Therefore, there is a continuous effort to replace polystyrene by thermoplastics with higher T_g and also substitute polybutadiene with more stable rubbery block [96].

Among the alternatives which have been considered are various fully acrylic TPEs based on combination of polyacrylates as soft blocks with different polymethacrylates as hard blocks synthesized by anionic [97] or controlled radical polymerization [86, 98-101] techniques. One of the advantages of acrylates is their versatility. For example, (meth)acrylic monomers cover a wide range of T_g from ca. -50 to +200 ºC. Furthermore, these polymers are not sensitive to UV and oxidation.

3.2.1 PMBL-PBA-PMBL linear triblock copolymers

In this section, the findings of our investigation into the morphology and thermomechanical properties of the synthesized PMBL-PBA-PMBL triblock copolymers containing a middle block of PBA and outer blocks of PMBL or random PMBL-PMMA are discussed.

Morphology

Due to the incompatibility between PBA and PMBL, the prepared triblock copolymers were expected to show strong phase separation. In order to gain insight on the effects of this phase separation and its resulting microstructures, SAXS analysis of thick films of the PMBL–PBA–PMBL triblock copolymers was performed. Typical results are presented in Figure 3.8. The triblock copolymers which did not undergo any additional thermal treatment were studied first. As shown in Figure 3.8(a), only the copolymer with a high PMBL content (B215-L120, 30.3 wt% PMBL) showed a well-ordered structure, consistent with hexagonally packed cylinders (three relatively sharp peaks at relative positions $s, \sqrt{3}s, \sqrt{7}s$). The copolymers with moderate PMBL content (19.3 and 12.6 wt% PMBL) did not exhibit well defined secondary peaks, indicating mainly short-range ordered. The SAXS experiments were then repeated after thermal annealing of the PMBL–PBA–PMBL samples at 150 ºC for 1 h in order to examine the effect of the annealing process on the morphology of the copolymer films. The comparison of Figure 3.8(b) with Figure 3.8(a) shows that the annealed films exhibited better ordering than the untreated samples, displaying at least three scattering peaks in each of the SAXS spectra. Furthermore, the ratios of the relative peak positions in all cases were $s, \sqrt{3}s, \sqrt{7}s$, i.e. consistent with a hexagonal lattice. A closer look at Figure 3.8 shows that for the same length of the PBA segment, an increase in PMBL block length leads to increase in the *d*-spacing. Similar cylindrical morphology was observed via SAXS for most PMBL–PBA–PMBL copolymers.

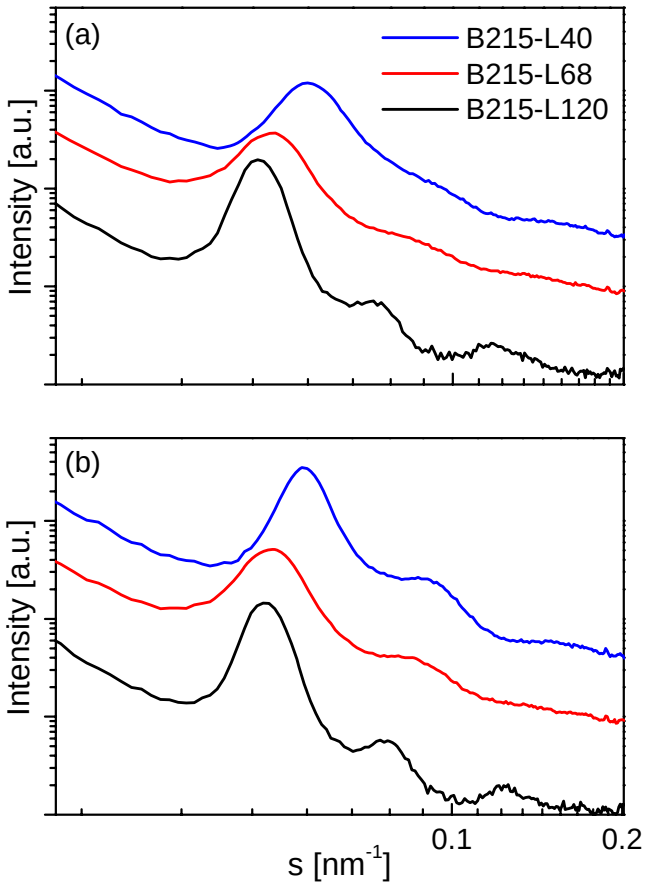

Figure 3.8. SAXS spectra of PMBL–PBA–PMBL triblock copolymers with constant PBA segments length and increasing PMBL length (a) before and (b) after annealing for 30 min at 150 ºC under nitrogen atmosphere.

The SAXS studies showed that PMBL–PBA–PMBL copolymers retain their phase separated morphology even when annealed at temperatures above the T_g of the hard PMBL component. Figure 3.9 compares the SAXS spectra of as prepared thick films of B215- L68 with those measured after annealing at 150 and 220 ºC respectively. The hexagonal morphology remained phase separated even after heating the copolymers to temperatures above the softening temperature of PMBL.

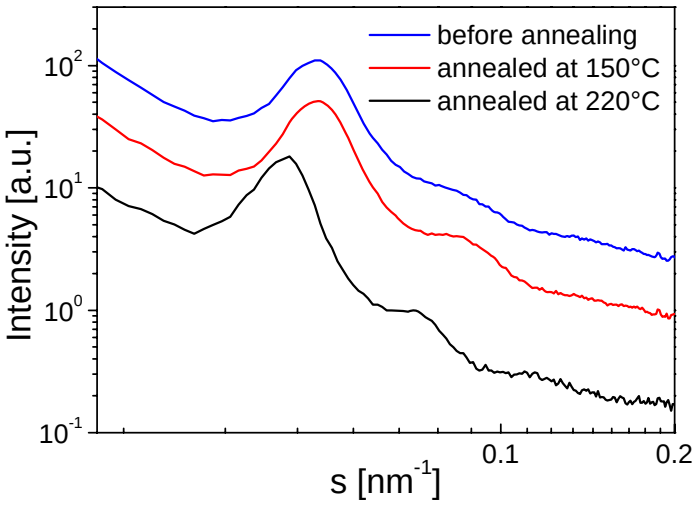

Figure 3.9. SAXS spectra of the B215-L68 before and after annealing at different temperatures.

Thermomechanical properties

Dynamic mechanical properties of the PMBL–PBA–PMBL linear triblock copolymers were characterized through the temperature dependencies of the real (*G'*) and the imaginary (*G"*) parts of the complex shear modulus. Typical results for series of copolymers with constant PBA content (DP = 215) and varying PMBL block lengths are shown in Figure 3.10 together with the respective DSC thermographs. Two distinct glass transition temperatures corresponding to the PBA (T_g ~ -50 ºC) and PMBL (T_g ~ 195 ºC) segments, respectively, were observed in both DMA and DSC data. This provides an additional evidence for the microphase separated morphology of the copolymers. However, the glass transition of PMBL becomes less obvious with decreasing PMBL content. With respect to the mechanical properties, all samples were glassy below the glass transition temperature of PBA, with storage modulus *G'* = 1 GPa. Above this glass transition, the copolymers become elastic and show a *G'* plateau extending up to the softening temperature of PMBL (~195 ºC). The height of the plateau strongly depends on the PMBL content. For example, the value of *G'* is

approximately 0.1 MPa for PMBL fraction around 12 wt% and up to ca. 10 MPa for PMBL content of 30 wt%. In this elastic state the PMBL blocks form glassy domains connecting the flexible PBA blocks. This is a typical situation for a thermoplastic elastomer in which the hard phase elements or glassy domains act as physical cross-links for the flexible component.

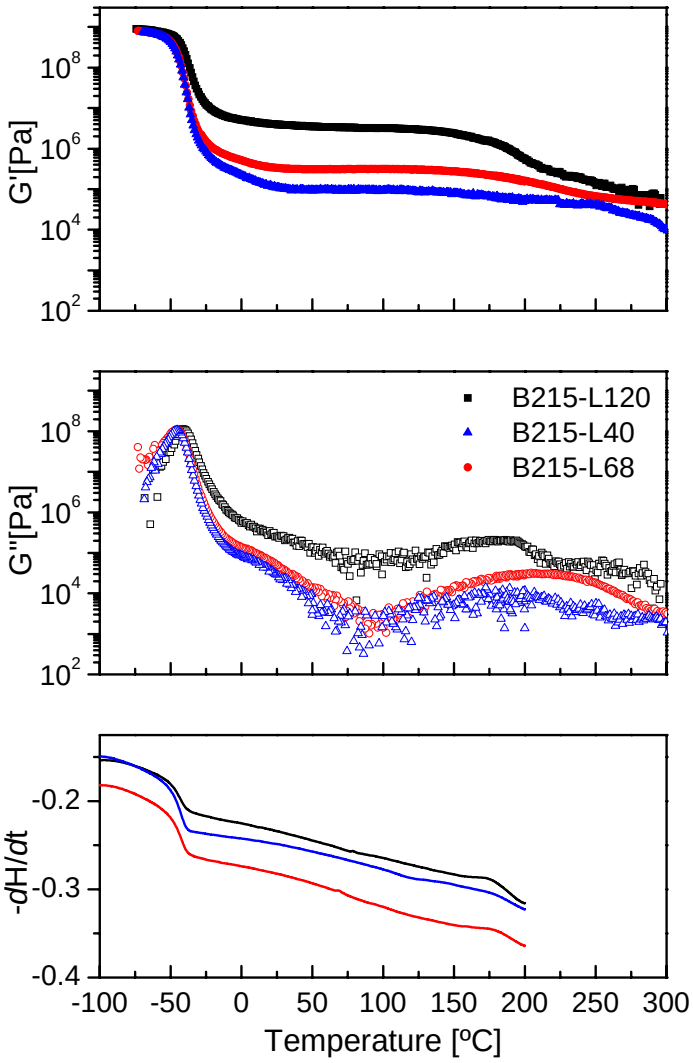

Figure 3.10. Thermo-mechanical (2 ºC/min) and DSC (10 ºC/min) analysis of PMBL–PBA–PMBL triblock copolymers.

The deep minimum of *G"* observed in this rubbery plateau region is related to the very big difference in the glass transition temperatures of the soft and hard components. The data for *G"* in the minimum are rather noisy due to profound elasticity of the copolymer, i.e. *G'*>>*G"* that results in a very small phase angle $\tan\delta = G''/G'$, that approaches the resolution limit of the rheometer. Finally, both storage and loss moduli decreased above the T_g of PMBL but the copolymer did not flow in the studied temperature range of up to 300 ºC.

Tensile properties

The tensile mechanical properties of the PMBL–PBA–PMBL linear triblock copolymers were investigated and typical results are shown in Figure 3.11(a). The materials showed elastic behavior largely influenced by their composition. An increase of the hard component (PMBL) content resulted in a significant increase of elastic modulus and ultimate tensile strength. The elongation at break, however, was relatively low i.e. up to 100% and not clearly related to copolymer composition. Annealing the samples for 1 h at 150 ºC did not help to improve the copolymer tensile properties, and elongation at break remained relatively low (see Figure 3.11(b)). This effect is most likely related to the brittleness of the hard PMBL blocks [102].

In order to improve the tensile properties of the PMBL based copolymers, a series of ABA type triblock copolymers were prepared in which the outer hard blocks were replaced with a random copolymer of PMBL and PMMA. The (PMBL-*r*-PMMA)–PBA–(PMBL-*r*-PMMA) triblock copolymers exhibit better tensile properties than their PMBL–PBA–PMBL counterparts.

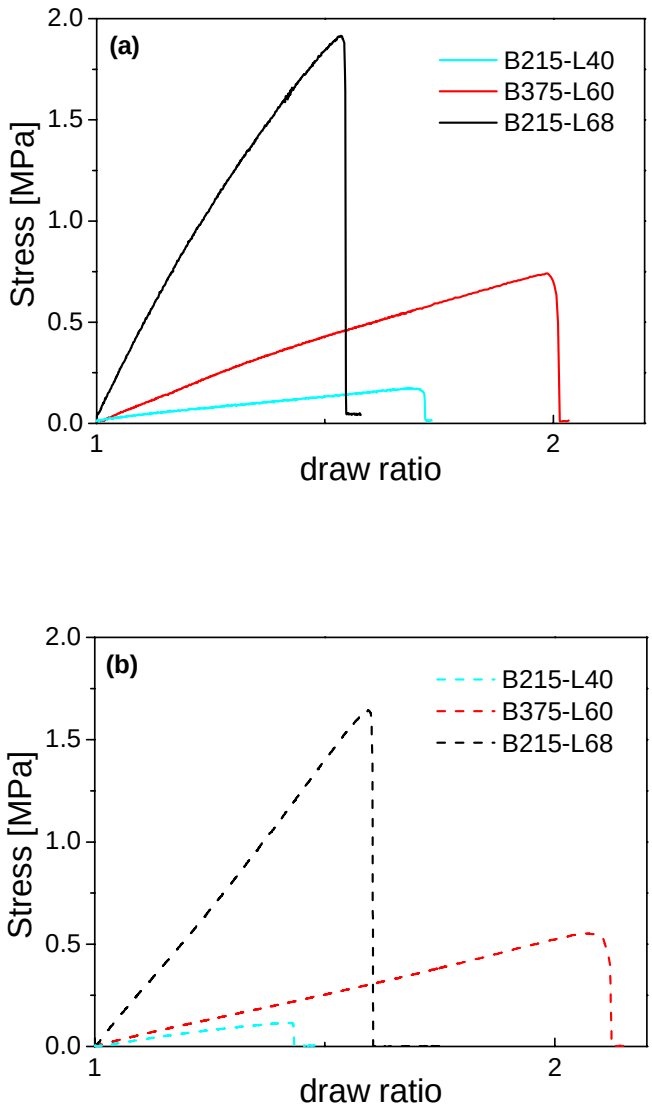

Figure 3.11. Tensile mechanical properties of PMBL–PBA–PMBL triblock copolymers with different compositions: (a) before and (b) after thermal annealing at 150 ºC for 1 h.

As shown in Figure 3.12, both elongation at break and ultimate tensile strength significantly increased up to values of ~200% and ~3.2 MPa, respectively. Nevertheless, the values of elongation at break are still significantly lower than

those of the pure PMMA–PBA–PMMA triblock copolymer, of which stress–strain curve is also shown in Figure 3.12.

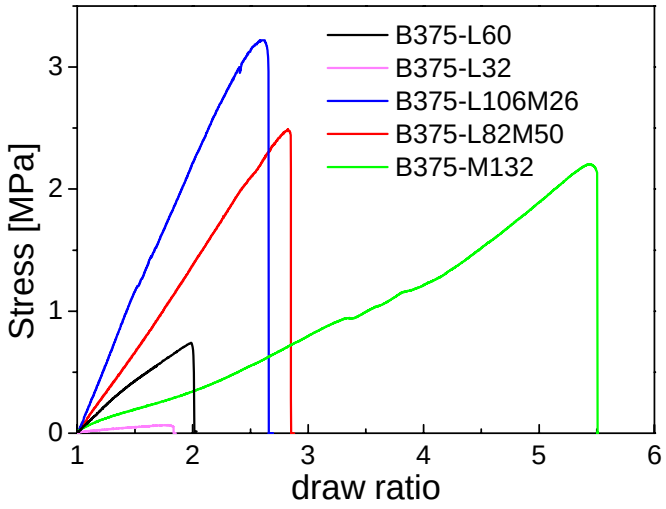

Figure 3.12. Tensile mechanical properties of (PMBL-*r*-PMMA)-PBA-(PMBL-*r*-PMMA) triblock copolymers compared to that of PMBL–PBA–PMBL.

Some limitations in the tensile properties of the PMBL–PBA–PMBL triblock copolymers may be related to incomplete chain extension, too short PMBL block, or the intrinsic brittleness of the PMBL.

While the tensile properties of the PMBL–PBA–PMBL and the (PMBL-*r*-PMMA)–PBA–(PMBL-*r*-PMMA) triblock copolymers are inferior to those of the PMMA–PBA–PMMA copolymer, they have significantly better thermal stability and retain their elastic properties up to very high working temperature of higher than 200 ºC. This is illustrated in Figure 3.13 that compares the temperature dependence of the shear moduli of B375-L82M50 and B375-M132. Both materials have similar molecular weights and hard block content. The copolymer with pure PMMA hard blocks shows a rubbery plateau that extends only to about 120 ºC. Furthermore, this material flowed at temperatures above 150 ºC. In contrast, the rubbery plateau of B375- L82M50 extends to more than 200 ºC and

no flow was observed up to 300 ºC. The same is true also for the copolymers having pure PMBL hard blocks, as illustrated in Figure 3.10. This effect is related to the very high glass transition temperature and high thermal stability [102] of PMBL that could make the PMBL based thermoplastic elastomers particularly suitable for high temperature applications.

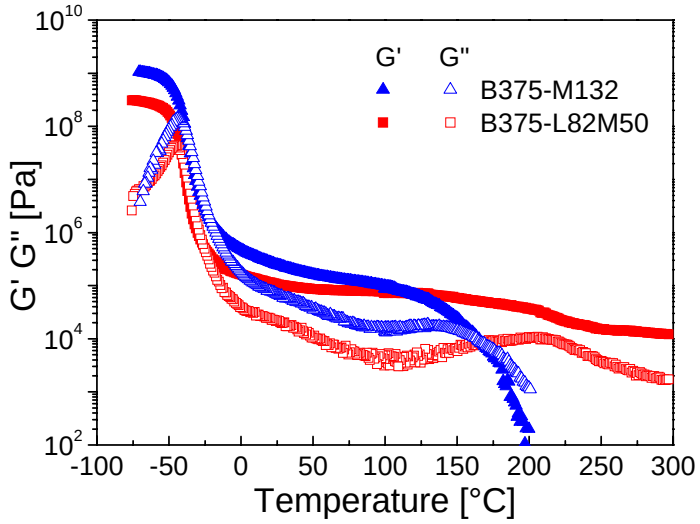

Figure 3.13. Comparison of the thermo-mechanical properties of (PMBL-*r*-PMMA)–PBA–(PMBL-*r*-PMMA) and PMMA–PBA–PMMA triblock copolymers.

3.2.2 PBA-PMBL multi-arm block copolymers

Recently, it was demonstrated that thermoplastic elastomers based on star block copolymers [100-101, 103-104] may exhibit improved properties in comparison with the linear A-B-A triblock copolymers. For example, multi-armed polystyrene-*b*-polyisobutylene (PS-*b*-PIB) star block copolymers have shown much lower sensitivity to diblock contamination and substantially better mechanical properties than their linear triblock counterparts [105]. This section delves further into the matter, and discusses how and to what extent the properties change with respect to the changes in the block copolymer architecture from an A-B-A triblock configuration, to that of 10-arm stars and eventually 20-arm stars.

Thermomechanical properties

Characterization of dynamic mechanical properties of the multi-arm stars PBA–PMBL block copolymers was accomplished through the temperature dependencies of the real (*G'*) and the imaginary (*G''*) parts of the complex shear modulus. Typical results for copolymers of constant PBA content and varying PMBL block lengths are shown in Figure 3.14(a). Two distinct glass transition temperatures corresponding to that of PBA (T_g ~ -50 ºC) and PMBL (T_g ~ 195 ºC) segments were observed in the DMA spectra. This provides evidence of a microphase-separated morphology of the copolymers. However, as can be seen in the figure, the glass transition of PMBL becomes less obvious with decreasing PMBL content. With respect to the mechanical properties, all samples were glassy below the glass transition temperature of PBA, with storage modulus *G'*~ 1 GPa. Above this glass transition, the copolymers become elastic and show a *G'* plateau extending up to the softening temperature of PMBL (~195 ºC). The height of the plateau strongly depends on the PMBL content. For example, in Figure 3.14(a) the value of *G'* at the rubber plateau region is approximately 0.1 MPa for copolymers of PMBL fraction of around 12.7 wt% (10B240-L46) and up to approximately 10 MPa for copolymers with PMBL content of 21.6 wt% (10B240-L86). In this elastic state the PMBL blocks form glassy domains connecting the flexible PBA blocks. This is a typical situation for thermoplastic elastomers in which the hard phase elements or glassy domains act as physical cross-links for the flexible component.

In Figure 3.14(b), a 10-arm star block copolymer 10B115-L30 is compared to an A-B-A triblock copolymer of the same PBA to PMBL composition ratio, the results of which were taken from a previous study. The two glass transition temperatures corresponding to that of PBA and PMBL were clearly indicated in both copolymers. A comparison of the rubbery plateau shows the 10-arm copolymer having improved strength over its triblock counterpart, demonstrating that the number of arms does have a significant effect on overall material strength.

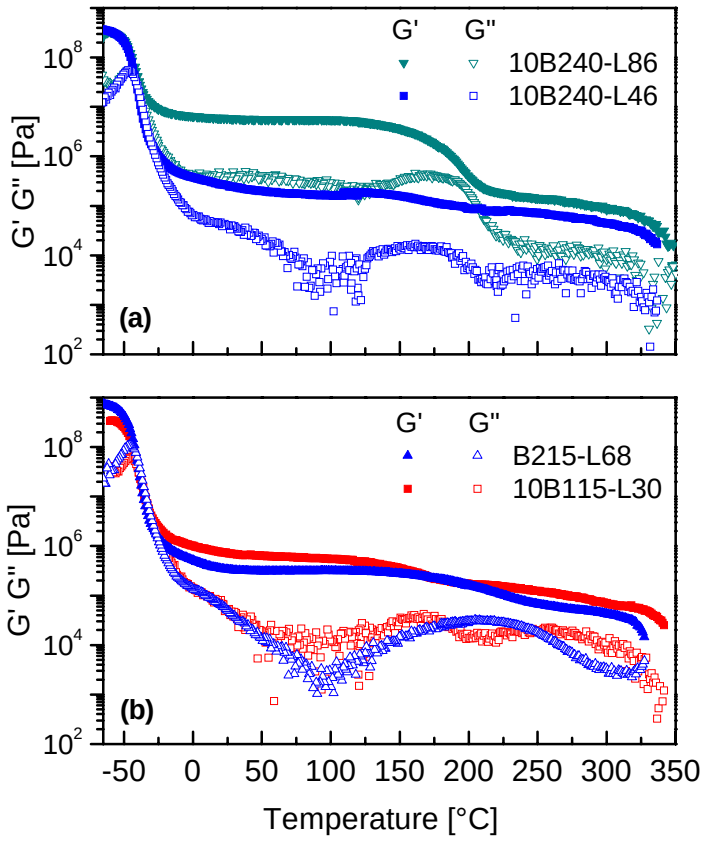

Figure 3.14. DMA spectra of the PBA-PMBL block copolymer (a) 10B240-L86, 10B240-L46, (b) B215-L68, 10B115-L30, (c) 10B115-L47, 20B115-L47.

As with their triblock counterparts, a deep minimum of *G"* can be observed in the rubbery plateau region of the DMA spectra. This is again related to the large difference in the glass transition temperatures of the soft and hard components. The data for *G"* in the minimum are also rather noisy due to profound elasticity of the copolymer, i.e. *G'>>G"* that results in a very small phase angle $\tan\delta = G''/G'$, that approaches the resolution limit of the equipment used. Finally, both storage and loss moduli begin to decrease above the T_g of PMBL but the copolymers did not flow in the studied temperature range of above 300 ºC.

Morphology

SAXS analysis of the 10 and 20-arm PBA-PMBL star copolymers was also performed. As the evidence from the DMA spectra have indicated, the thick films of these star copolymers were expected to show strong phase separation due to the strong incompatibility between the two phases. Scattering measurements were first made without additional thermal treatment to the samples. Then, in order to examine the effect of thermal treatment, the SAXS experiments were repeated after annealing the PBA-PMBL samples at 150°C. The results for 20BA115-MBL57 are presented in Figure 3.15.

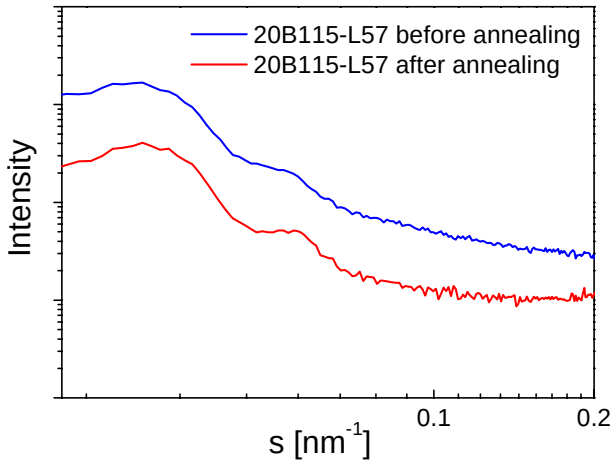

Figure 3.15. SAXS spectra of 20B115-L57 before and after annealing at 150°C for 60 min.

The comparison shows that the annealed films exhibit better ordering than the untreated samples, displaying two clear scattering peaks in each of the SAXS spectra. In this particular case for copolymer 20B115-L57 with PMBL content of 27.6 wt%, the ratios of the relative peak positions were *s, 2s,* consistent with a lamellar structure.

As demonstrated in the DMA spectra in Figure 3.14(a), an increase in material strength is observed as the length of the PMBL outer block was increased. This

was thought to have been attributed to the improved ordering of the material due to stronger phase separation. However, as the SAXS results of annealed samples in Figure 3.16 show, it was not simply an improved ordering which resulted in increased strength, but rather a change in the ordering itself with the increase in PMBL content.

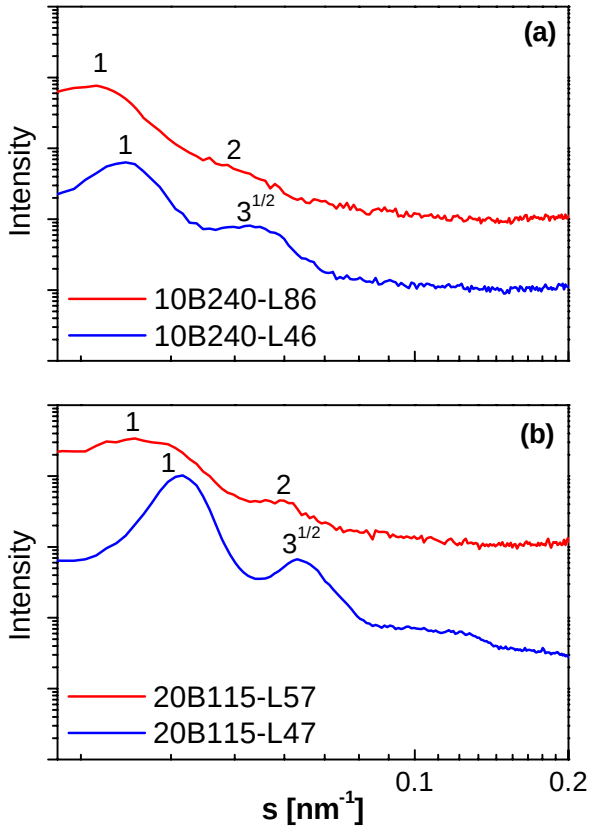

Figure 3.16. SAXS spectra after annealing at 150°C for 60 min for (a) 10B240-L86, 10B240-L46, and (b) 20B115-L57, 20B115-L47.

Copolymer 10B240-L46 in Figure 3.16(a) for example, having lower PMBL outer block length, appears at first glance to have a more ordered structure compared to its counterpart with higher outer block length, 10BA240-MBL86. But after determining the relative peak positions, 10BA240-MBL86 was shown to have a lamellar structure with scattering peaks occurring at relative positions *s, 2s,*

whereas 10BA240-MBL46 exhibited structures consistent with hexagonal-packed cylinders (two relatively sharp peaks at relative positions s , $\sqrt{3}s$). This change in ordering from hexagonal cylinders to lamellar may be the cause of the very large improvement in strength exhibited by copolymer 10B240-L86 in the DMA spectra (Figure 3.14(a)). Samples 20B115-L47 and 20B115-L57 also exhibited similar ordering changes, as shown in the Figure 3.16(b).

The different compositions of the 10-arm and 20-arm PBA-PMBL copolymers is shown to have an effect on the *d*-spacing in the micro-phase separated structures. As shown in the Table 3.2, the increase of PMBL block length leads to an increase in the *d*-spacing at the same length of the PBA segment. And demonstrated earlier in Figure 3.16, the SAXS results show that the multi-arm block copolymers with lower outer PMBL content revealing a micro phase separated morphology of cylindrical PMBL domains hexagonally arranged in the PBA matrix. Samples with higher PMBL content revealed a lamellar structure. At even higher molecular weight, in particular for samples 20B230-L96 and 20B750-L156, no clear indication of structure was revealed from the SAXS results. The number of arms did not seem to affect the *d*-spacing as shown in Table 3.2 when comparing for example, copolymers 10B115-L47 and 20B115-L47, both having the same PBA to PMBL ratio, but different number of arms.

Table 3.2

Compositions of the prepared PBA-PMBL star-like block copolymers, their phase separation spacing values and corresponding structure.

Sample	SAXS (before annealing)	SAXS (after annealing)	Structure
10BA115-MBL30	26.7 nm	25.3 nm	hexagonal cylinders
10BA115-MBL47	28.9 nm	28.5 nm	hexagonal cylinders
10BA240-MBL46	37.5 nm	36.7 nm	hexagonal cylinders
10BA240-MBL86	42.7 nm	42.1 nm	lamellar
20BA115-MBL47	28.9 nm	28.5 nm	hexagonal cylinders
20BA115-MBL57	35.7 nm	35.3 nm	lamellar
20BA230-MBL96	52.6 nm	49.6 nm	-
20BA750-MBL156	71.9 nm	73.3 nm	-

Tensile Properties

Tensile strength comparisons made between copolymers with varying PMBL contents demonstrate again that an increase in the PMBL block length results in a stronger material. However, in Figure 3.17(a) we observe that for copolymer 10B240-L86, elasticity is significantly reduced as a result of the higher PMBL content when compared to copolymer 10B240-L46 of lower PMBL content. This observation is due to the fact that the change in outer PMBL block lengths contributes to stronger physical cross-linking of the material, enhancing overall strength, however, sacrificing elasticity, and causing the material to become more brittle in the process.

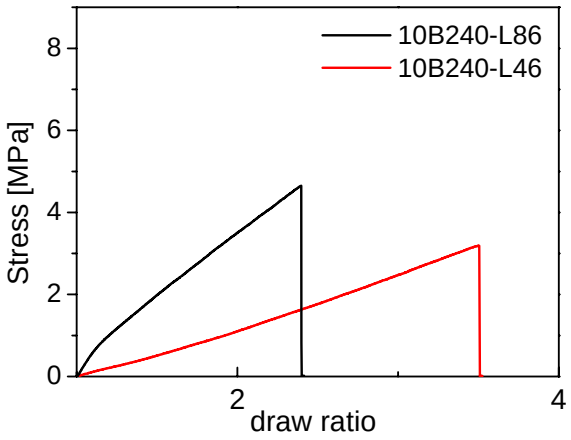

Figure 3.17. Tensile properties of copolymers 10B240-L86 and 10B240-L46.

3.2.3 PBA-PMMA multi-arm block copolymers

While thermoplastic elastomers containing PMBL have excellent thermal stability and retain their elastic properties up to a very high working temperature (more than 200 ºC), their intrinsic brittleness seriously limits their potential as thermoplastic elastomers. In this study, PMMA is used in place of PMBL in hopes of solving the brittleness issue. PMMA, though having improved elasticity, has a significantly lower glass transition temperature when compared to PMBL, making them unsuitable for high temperature applications, but nevertheless a possible candidate for use as hard blocks in thermoplastic elastomers.

Morphology

SAXS analysis of thick films of the star-like block copolymers illustrated that that the majority of the samples reveal an expected micro phase separated morphology of cylindrical PMMA domains hexagonally arranged in the PBA matrix (three relatively sharp peaks at relative positions s , $\sqrt{3}s, \sqrt{7}s$). The samples with shortest arm length and lower PMMA content, 10B115-M29 and 20B115-M38, did not reveal a clear structure. They exhibited a short-range ordering only, as indicated from the single broad peak observed in their SAXS spectra. The different compositions of the 10-arm and 20-arm PBA-PMMA copolymers also affect the *d*-spacing in the micro-phase separated structures. Table 3.3 shows the calculated results of the *d*-spacing obtained from AFM and SAXS data of the measured PBA-PMMA star block copolymers. As can be seen in Table 3.3, the increase of PMMA block length leads to an increase in the *d*-spacing at the same length of the PBA segment. Number of arms seems to have negligible influence on change in *d*-spacing.

In order to examine the effect of thermal treatment on the copolymer films morphology, the SAXS experiments were repeated after annealing the PBA-PMMA copolymer samples at 150 °C. The experiment showed that there was no lost of phase separation after annealing for 60 minutes and the annealed films

even exhibited better ordering than the untreated samples, displaying at least three scattering peaks in each of the SAXS spectra. The ratios of the relative peak positions in these cases remained unchanged, s , $\sqrt{3}s, \sqrt{7}s$, consistent with a hexagonal lattice. As an example the SAXS spectra of a thick film of 20B115-M60 measured before and after annealing are presented in Figure 3.18.

Table 3.3

Compositions of the prepared PBA-*b*-PMMA) star-like block copolymers and their phase separation spacing values.

Sample	Triblock composition	Spacing (nm)	
		AFM	SAXS
10B115-M29	$PBiBEA_{10}$-(PBA_{115}-$PMMA_{29}$)$_{10}$	-	22
10B115-M51	$PBiBEA_{10}$-(PBA_{115}-$PMMA_{51}$)$_{10}$	30	24
10B240-M54	$PBiBEA_{10}$-(PBA_{240}-$PMMA_{54}$)$_{10}$	59	30
10B240-M117	$PBiBEA_{10}$-(PBA_{240}-$PMMA_{117}$)$_{10}$	63	38
20B115-M38	$PBiBEA_{20}$-(PBA_{115}-$PMMA_{38}$)$_{20}$	-	23
20B115-M60	$PBiBEA_{20}$-(PBA_{115}-$PMMA_{60}$)$_{20}$	48	24
20B230-M59	$PBiBEA_{20}$-(PBA_{230}-$PMMA_{59}$)$_{20}$	61	33
20B230-M107	$PBiBEA_{20}$-(PBA_{230}-$PMMA_{107}$)$_{20}$	67	35
20B750-M180	$PBiBEA_{20}$-(PBA_{750}-$PMMA_{180}$)$_{20}$	100	63
20B750-M300	$PBiBEA_{20}$-(PBA_{750}-$PMMA_{300}$)$_{20}$	111	73

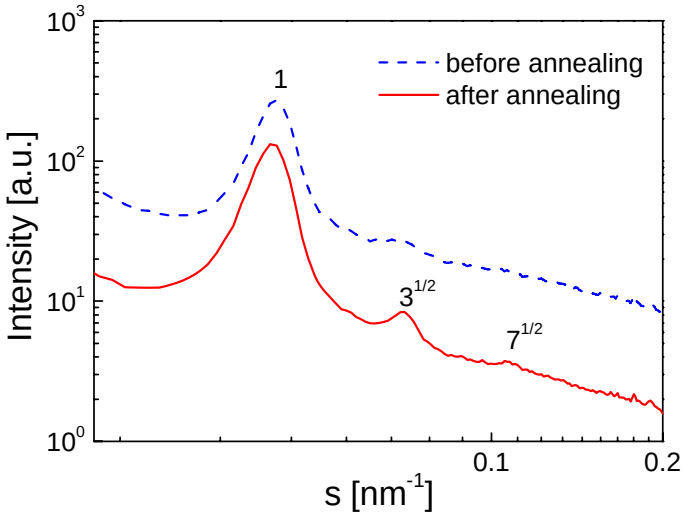

Figure 3.18. SAXS spectra of 20B115-M60 before and after annealing at 150°C for 60 minutes.

Thermomechanical Properties

Dynamic mechanical properties of the multi-arm stars PBA–PMMA block copolymers were characterized through the temperature dependencies of the real (*G'*) and the imaginary (*G''*) parts of the complex shear modulus. Typical results obtained for two 20-arm star block copolymers with different arm compositions (20B230-M59 and 20B230-M107) are shown in Figure 3.19(a).

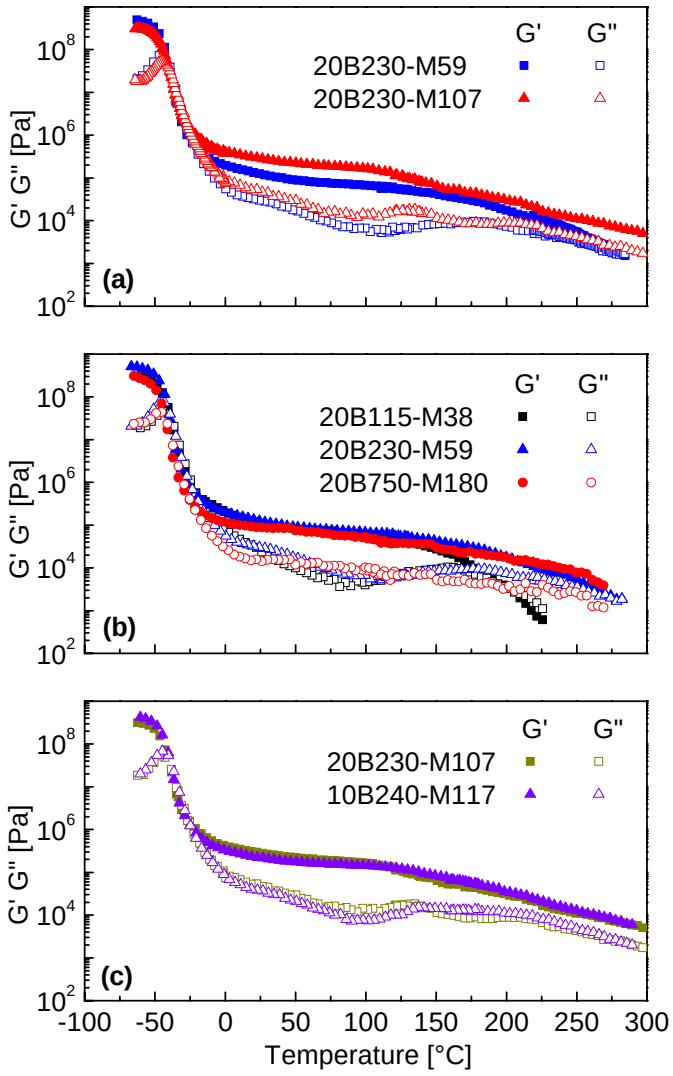

Figure 3.19. DMA spectra of the star PBA-PMMA block copolymer (a) 20B230-M59, 20B230-M107, (b) 20B115-M38, 20B230-M59, 20B750-M180 and, (c) 20B230-M107, 10B240-M117.

The existence of two distinct glass transitions corresponding to the PBA (T_g~50 ºC) and PMMA (T_g~130 ºC) segments is clearly displayed in both the DMA and DSC data. This constitutes a further evidence for the microphase-separated morphology of the copolymers. With respect to the mechanical properties, both samples were glassy below the glass transition temperature of PBA, with storage modulus *G'*~1 GPa. Above this glass transition, the copolymers became elastic and showed a rubbery plateau (*G'*<1 MPa) extending up to the softening temperature of PMMA (~130 ºC). In this elastic state, the PMMA blocks form glassy domains connecting the flexible PBA blocks. As can be expected, the degree of elasticity depends on the composition, i.e. the sample with lower PMMA content has a smaller *G'* value in the rubbery plateau region. The thermo-mechanical properties at higher temperatures also show dependence on the copolymer composition. While both materials retained their phase separated morphology and low modulus rubbery behaviour well above the PMMA glass transition, the copolymer 20B230-M59, with only a 16.7% PMMA content, eventually start flowing at a temperature of around 250°C. On the other hand, the copolymer 20B230-M107 did not flow in the entire temperature range studied, i.e. up to 300 ºC.

Figure 3.19(b) illustrates the effect of the overall molecular weight on the mechanical properties of the star copolymers by comparing the DMA spectra of 20B115-M38, 20B230-M59 and 20B750-M180, three materials that have similar compositions but significantly different M_w. As can be seen, the high molecular weight copolymers (20B230-M59 and 20B750-M180) retain their phase separated morphology and low modulus rubbery behaviour well above the PMMA glass transition. In contrast the low molecular weight 20B115-M38 starts flowing at temperature of 200°C. In spite of their very different molecular weights all three copolymers have very similar values of the storage modulus *G'* in the rubbery plateau region between the glass transition temperatures of the two components. This finding indicates that the copolymer composition and not the overall

molecular weight is the main factor that determines the elastic properties of these thermoplastic elastomer materials.

As discussed earlier, another important parameter that could influence the thermo-mechanical properties of the star-like copolymers is the number of arms. Figure 3.19(c) compares the DMA spectra of a 10 and 20 arm star copolymers with similar block lengths and compositions: 10B240-M117 and 20B230-M107. As can be seen the two materials show practically identical spectra which indicates that the number of arms have little influence on their mechanical properties. This finding is not that surprising taking into account that both materials have a rather large number of arms, i.e. 10 and 20 respectively. Indeed earlier studies of polystyrene-*b*-polyisobutylene [104] and polystyrene-*b*-polydiene [106] star like block-copolymers, have shown that the tensile properties of these materials reach a plateau in the N_{arm} = 5-10 range. Evidently the presence of such a plateau explains the similar mechanical properties of the 10 and 20 arm PBA-PMMA star block copolymers.

Tensile Properties

The tensile properties of the PBA-PMMA star-like block copolymers listed in Table 3 were also studied. Typical examples of the measured stress–strain dependencies are shown in Figure 3.20(a). As expected the composition has a major effect on the tensile properties of the PBA-PMMA star copolymers. We found that both the initial modulus (E) and the tensile strength (σ break) increase strongly with PMMA content, while the draw ratio at break seems to increase with the length of PBA segment and be reduced with increasing PMMA content. During the last several years it was demonstrated that thermoplastic elastomers based on star block copolymers [107-111] may exhibit superior properties as compared to the linear ABA triblock type TPEs. Furthermore it was also shown that the tensile properties of the star block copolymers improve with the number of arms until reaching saturation at the N_{arm} = 5-10. In an attempt to explore these effects in the case of PBA-PMMA based materials we have compared the newly

synthesized 10 and 20 arm 10B115-M51 and 20B115-M60 to the 3-arm star copolymer 3B164-M76 that we have studied recently [101] and to a linear PMMA-PBA-PMMA block copolymer prepared using ATRP by the Jerome group[112].

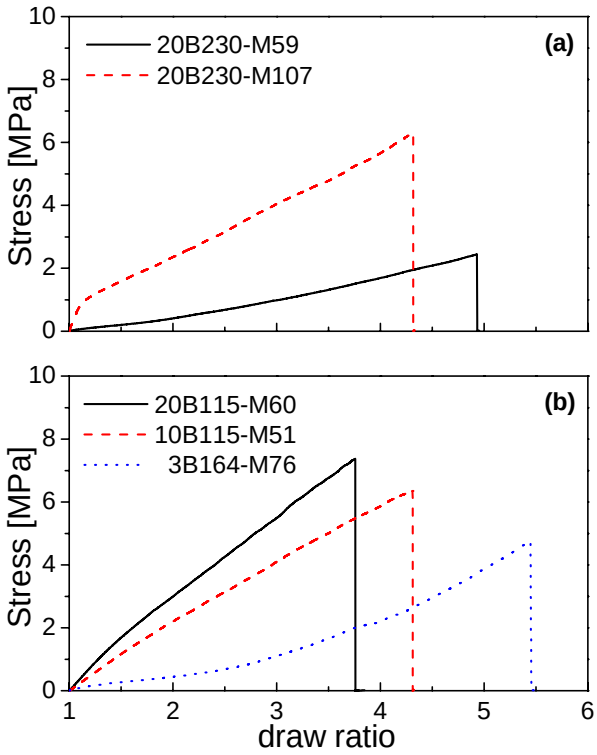

Figure 3.20. Tensile properties of copolymers (a) 20B230-M59, 20B230-M107, and (b) 20B115-M60, 10B115-M51, 3B164-M7.

Table 3.4

Ultimate tensile strength and maximum elongation at break of PBA-PMMA block copolymers with similar composition but varying numbers of arms.

Sample	M_n (g/mol)	PDI	PMMA content (wt %)	ultimate tensile strength σ (MPa)	maximum elongation at break λ (%)
linear ABA type copolymer	69,000	1.15	26	4.2	520
3-arm star B164-M76 block copolymer	85,800	1.19	26	4.8	545
10-arm B115-M51 copolymer	197,000	1.25	25.7	6.4	430
20-arm B115-M60 copolymer	412 000	1.36	28.9	7.4	375

As shown in Table 3.4 all four materials have practically the same polymer chain composition ratio. As the 3-arm star copolymer B164-M76 has the same overall composition and only slightly higher molecular weight as compared to the linear PMMA-PBA-PMMA, in Table 3.4 we compared the properties of these materials. While tensile strength and DMA results of the 10 and 20 arm star block copolymers suggest that the number of arms have little influence on their mechanical properties, an attempt was made to compare the tensile properties of these new samples to earlier studies performed on 3-arm star PBA-PMMA block copolymers as well as linear triblock PBA-PMMA copolymers. In the table below we compare the properties of 4 materials. As can be seen from the table, there is an increase in ultimate tensile strength with the increase in number of arms. Particularly, the ultimate tensile strength of the 10-arm 10B115-M51 is significantly better than that of the 3-arm copolymer. The improvement isn't as significant when comparing the 10-arm versus the 20-arm samples, which suggests a plateau or saturation point in the improvement of the tensile properties with respect to number of arms. The table also shows that for the star block copolymers, the improvement in ultimate tensile strength results in the draw ratio being sacrificed, as the maximum elongation of the thermoplastic elastomers is significantly reduced with the increase in number of arms and ultimate tensile strength.

3.3 Siloxane-based Linear Copolymers: Gradient or Block?

Gradient copolymers, with a controlled composition along the backbone but with a homogeneous composition among the chains, are a promising class of materials with tunable microstructures and physical properties. They can potentially be used as polymer blend compatibilizers, surfactants, and environment-sensitive materials, for example, materials for vibration and noise dampening. They also can serve as the building blocks for the synthesis of complex macromolecular architectures, such as polymer brushes, hyperbranched polymers, dendrimers, and hybrid organic-inorganic materials [113-114].

3.3.1 Fluorosiloxane-based Copolymers

Fluorosilicones are polymers consisting of fluorocarbon groups, which have the lowest known inter-molecular forces of all pendant groups, with the unique flexibility of the siloxane backbone. The first and still the most common commercial fluorosilicone is poly[methyl(trifluoropropyl)siloxane], PMTFPS. PMTFPS products are used in many applications where resistance to fuel, oils and hydrocarbon solvents is required. Examples are lubricants in bearings exposed to such materials and sealants and elastomers for automotive fuel systems. Fluorosilicone rubber shows good performance at extremely low temperatures down to -70 ºC which makes it unrivalled material for aerospace applications. Other applications include antifoams for organic liquids and in cosmetics and other skin use formulations where long-lasting oil and water repellency is desired, release agents for PDMS-based pressure-sensitive adhesives, and antifouling coatings and lubricants [21, 113]. Because fluorinated polysiloxanes are quite expensive, their copolymers which can be used as additives to other polymers, improving their properties, are of great interest.

Thermomechanical Properties

It has previously been reported that the tapering nature of gradient copolymers affect the T_g's of both component monomers. In the case of fluorosiloxane-based copolymers, the T_g's of the corresponding homopolymers PDMS and PMTFPS are -127 ºC and -70 ºC, respectively [115]. DSC results of the PDMS homopolymer, illustrated in Figure 3.21(a), shows a characteristic crystallization band at -88 ºC and two endothermic peaks at -48.3 and -36.4 ºC, which are typical for PDMS if the chain length exceeds M_n = 5000, which corresponds to approximately 20 D_3 (PDMS) units [116]. From the differential scanning calorimetry (DSC), these transitions are still present in block and spontaneous gradient copolymers (Figure 3.21(c) and (d)) in which the dimethylsiloxane block is sufficiently long, that is, more than approximately 5000, although, the crystallization band becomes broader and moves to higher temperatures. The enthalpy of crystallization depends on the M_w (length of the pure dimethylsiloxane block). There is only one broad melting transition which appears at temperature between the two peaks occurring in the PDMS homopolymer. Assuming the enthalpy of melting of the crystalline PDMS to be 61.2 J/g [116], a PDMS homopolymer having a total enthalpy of fusion of about 40 J/g is 60–65% crystalline (under the fast cooling regime applied here). The enthalpy of crystallization decreases to approximately 15 J/g for the block copolymer (Figure 3.21(c) (M_w of the D block is approximately 5000) and to 8.6 J/g for the gradient copolymer synthesized via spontaneous copolymerization (Figure 3.21(d))(M_w of the D block is approximately 2800). These enthalpy values correspond to approximately 24% and 14% of the crystalline character of the PDMS block, respectively. The ‘‘forced’’ gradient copolymer (Figure 3.21(e)), or the gradient copolymer synthesized via semi-batch method, does not reveal any crystallization because the PDMS block is too short.

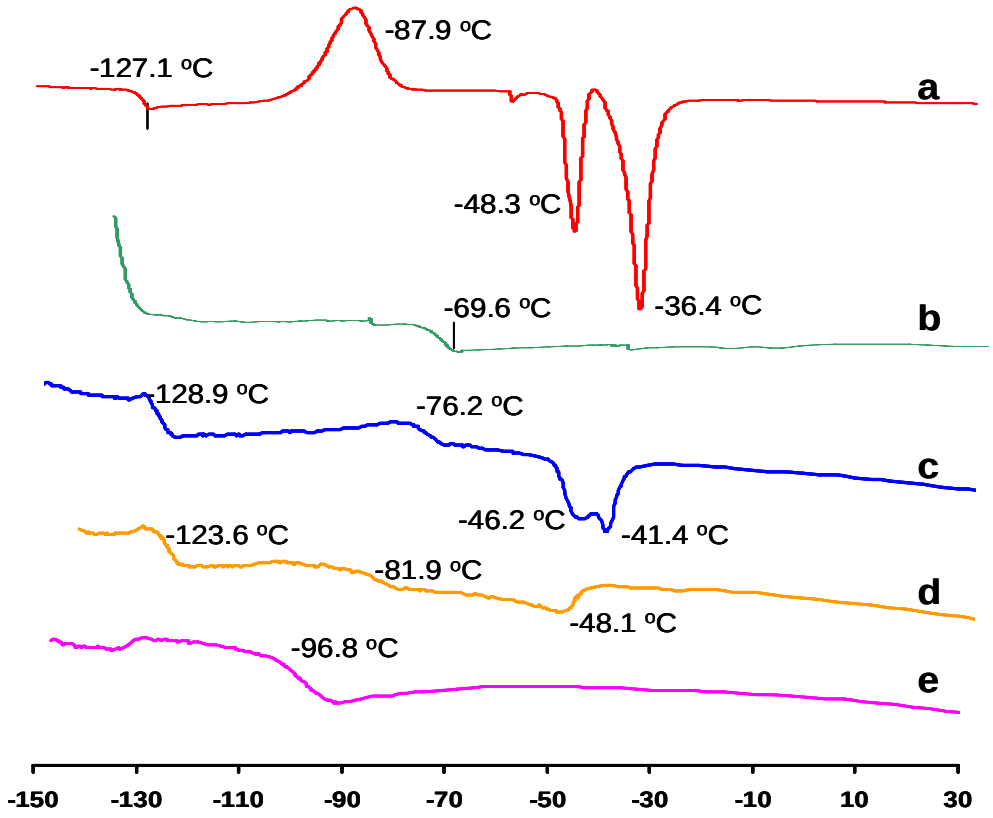

Figure 3.21. DSC of (a) PDMS homopolymer (M_n=17,400), (b) PMTFPS homopolymer (M_n=18,000), (c) PDMS-PMTFPS block copolymer (M_n=13,500, D:F=1:1), (d) spontaneous gradient copolymer (M_n=10,000, D:F=1:1), (e) gradient copolymer by semi-batch method (M_n=16,700, D:F=1:1).

The effect of increased compatibility of both microphases, due to the increased D content in the F-enriched segment, may also play a role. Glass transitions of both chain fragments in the gradient copolymer are moved toward each other (that is, T_g for the PDMS segment raises, whereas T_g for the PMTFPS segment decreases) and the melting of PDMS segment disappears, which indicates that gradient chain microstructure prevents crystallization of PDMS segments. These changes are also reflected in plots of shear modulus-temperature dependences showing that the modulus *G'* for the gradient copolymer is by about one order of magnitude lower than that for the block copolymer as it is discussed in the next paragraph.

Dynamic mechanical analysis for the copolymers in Figure 3.21(a), (b) and (c) were performed for the evaluation of their properties under shear deformation in a broad temperature range. Temperature sweep tests were conducted during both heating and cooling of the samples. The results are summarized in Figure 3.22. In the case of the block copolymer (Figure 3.22(a)), the glass transition of the PDMS block is clearly indicated in both cooling and heating curves by the drop in *G'* and the maximum in *G"* at low temperatures around -130 ºC. The softening related to this transition is considerable and involves a drop of the real part of the shear modulus by almost one order of magnitude. The glass transition of the PMTFPS block is not clearly visible as it is covered by the crystallization of PDMS which takes place in the same temperature region. Remarkably strong recrystallization of the PDMS on heating is observed despite the fact that cooling was done rather slowly at 2 K/min. This process is manifested by the strong increase of *G'* in the heating curve at temperatures of around -80 ºC. At even higher temperatures (above -50 ºC) the melting of the crystalline PDMS leads to a strong drop in the shear moduli. The temperature dependences of the *G'* and *G"* of the spontaneous gradient copolymer (Figure 3.22(b)) differ significantly from those of the block copolymer. Although the glass transitions of the two components are still well pronounced, the crystallization of the PDMS is prevented by the gradient chain structure of these copolymers. Furthermore, in the temperature range between the two T_g's, the storage modulus *G'* of the gradient copolymer is significantly lower than that of the block copolymer. Finally, the spectra of the copolymer prepared by semi-batch method (Figure 3.22(c)) reveals ‘‘pure gradient type’’ features, that is, single glass transition around -97 ºC (between the T_g's of the PDMS and PMTFPS) which is roughly at the some position as that of the statistical (random) copolymer, but is much broader as a result of the pure gradient structure.

It is important to emphasize at this point that the DMA data fit very well to DSC results despite the fact that different cooling/heating rates (2 K/min in the case of DMA and 10 K/min in the case of DSC) were used in the experiments.

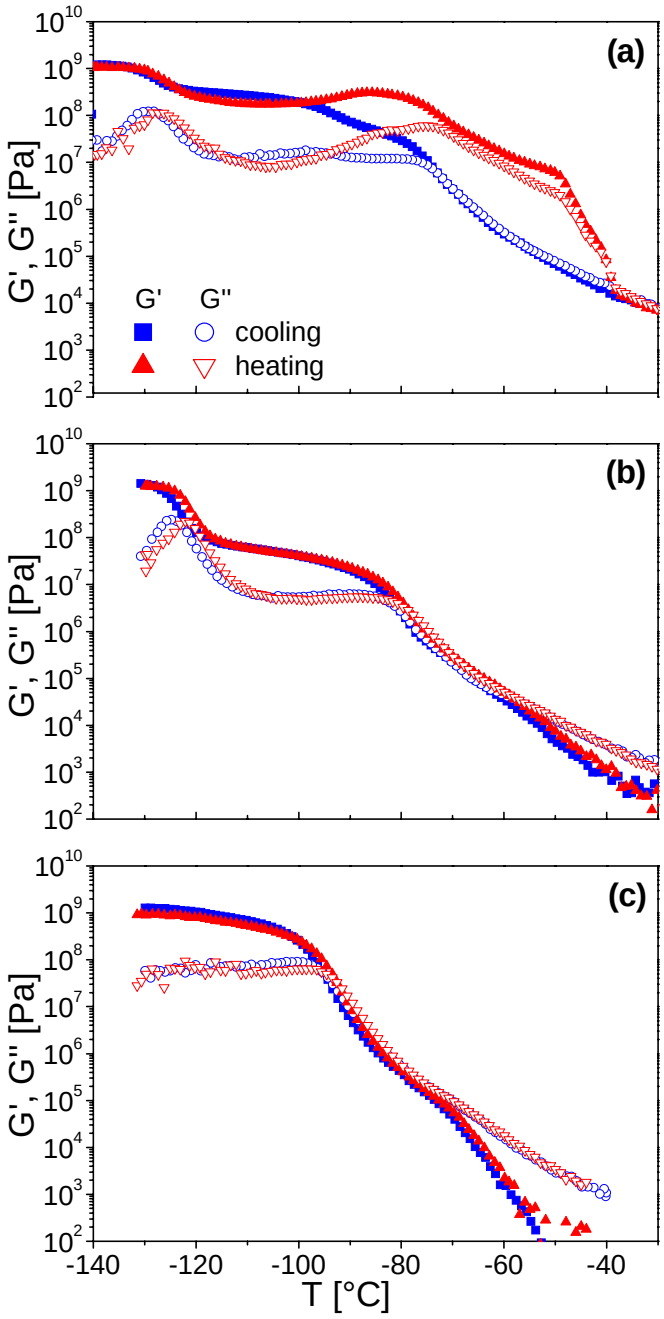

Figure 3.22. Temperature dependence of the shear and loss moduli of (a) PDMS-PMTFPS block copolymer (M_n = 13,500, D:F = 1:1), (b) spontaneous gradient copolymer (M_n = 10,000, D:F = 1:1) and (c) gradient copolymer by semi-batch method (M_n = 16,700, D:F = 1:1).

Morphology

As described above, both the DSC and DMA results have indicated a phase separation in the block and the spontaneous gradient copolymers. To explore this effect in more details and examine the type of the formed microstructures we have performed temperature dependent SAXS experiments. The results summarized in Figure 3.23 in the form of scattered intensity versus the scattering vector q, show a strong phase separation and ordering in both block and spontaneous gradient copolymers at all temperatures. Nevertheless, we again have significant differences between these two types of materials. In the case of the block copolymers (Figure 3.23(a)), several peeks are observed at relative positions $1:3^{1/2}:4^{1/2}:7^{1/2}:9^{1/2}$ which may indicate a hexagonal arrangement of cylinders, although the peak intensity does not precisely correspond to this structure, because the $3^{1/2}$ reflection has suppressed intensity. For the gradient copolymer obtained by simultaneous copolymerization (Figure 3.23(b)) two peaks were observed at relative positions 1:2 which suggest a lamellar structure. On the other hand, the gradient copolymer D-F, obtained by semi-batch method showed only one weak and broad peak corresponding to a characteristic correlation length of approximately 11 nm. This peak disappears after heating to $T > -40$ ºC.

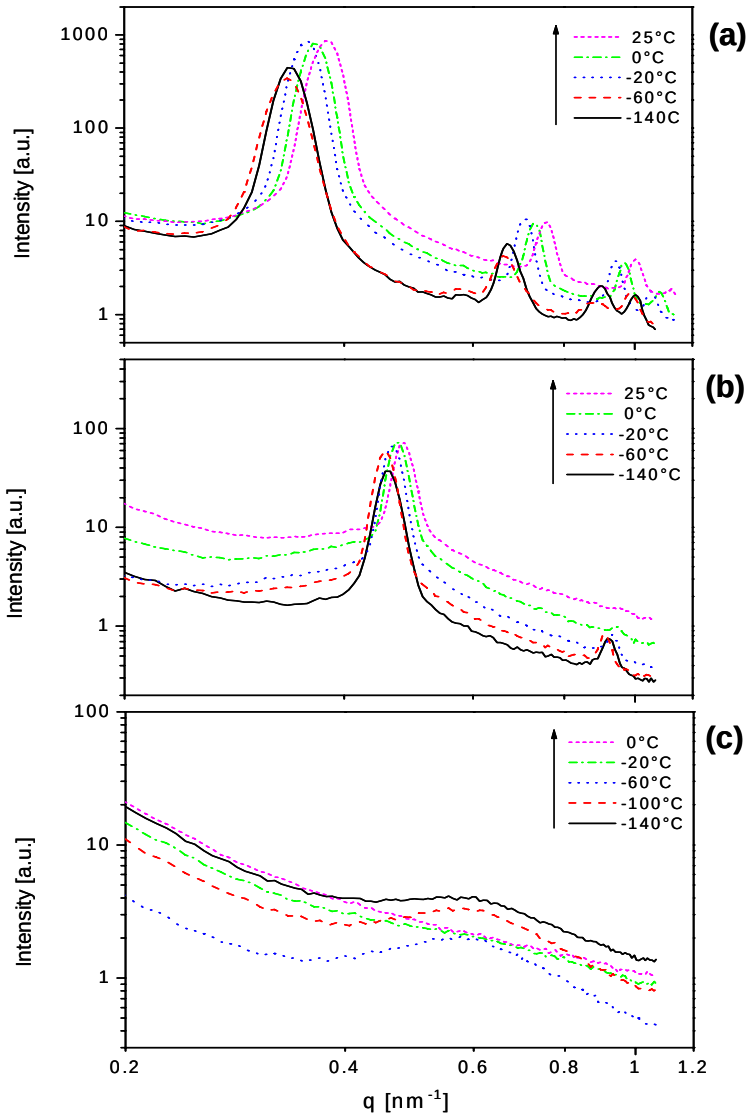

Figure 3.23. SAXS spectrum of the (a) PDMS-PMTFPS block copolymer (M_n = 13,500, D:F = 1:1), (b) spontaneous gradient copolymer (M_n = 10,000, D:F = 1:1) and (c) gradient copolymer by semi-batch method (M_n = 16,700, D:F = 1:1).

Dependance on Molecular Weight

To better understand the effects of the size and composition of the gradient copolymers on their thermomechanical properties, we have studied three-segment gradient copolymers with larger molecular weights prepared by simultaneous and semi-batch methods. The DMA and SAXS spectra of these materials are shown in

Figures 3.24 and 3.25, respectively. As can be seen in Figure 3.24(a), the copolymer obtained by simultaneous copolymerization (M_n = 44,000, M_w/M_n = 1.15) exhibited crystallization on heating, starting at about -90 ºC. Interestingly, there is an indication for weak crystallization on cooling as well at about -100 ºC. The second T_g at about -70 ºC is also visible on both heating and cooling curves. Furthermore, the sample is not flowing in the entire range studied that is, up to 20 ºC. All these effects, which were not observed for the lower molecular weight sample prepared in similar way (Figure 3.22(b)), indicate the presence of relatively large PDMS segments as in a block copolymer.

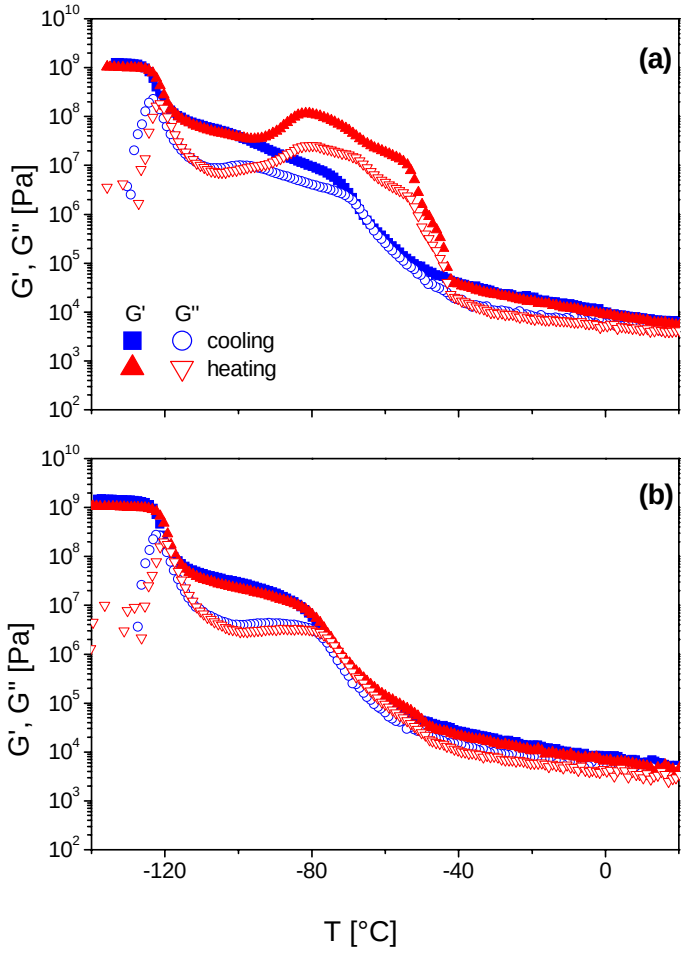

Figure 3.24. Temperature dependence of the shear and loss moduli of (a) spontaneous gradient copolymer D-F-D (M_n = 44,000, F:D = 1:1) and (b) gradient copolymer D-F-D obtained by the semi-batch method (M_n = 45,800, F:D = 1:1).

The SAXS spectra of the high molecular weight spontaneous gradient copolymer, which is shown on Figure 3.25(a), reveal four well defined peaks (as in the case of the block copolymer in Figure 3.23(a)) indicating again a very strong phase separation. Nevertheless, in contrast to the block copolymer that showed a hexagonal microstructure, here the positions of the scattering peaks are observed at q values of 1:2:3.4 indicating a lamellar structure. This is consistent with what was found for the similarly prepared gradient copolymer with lower molecular weight (Figure 3.23(b)).

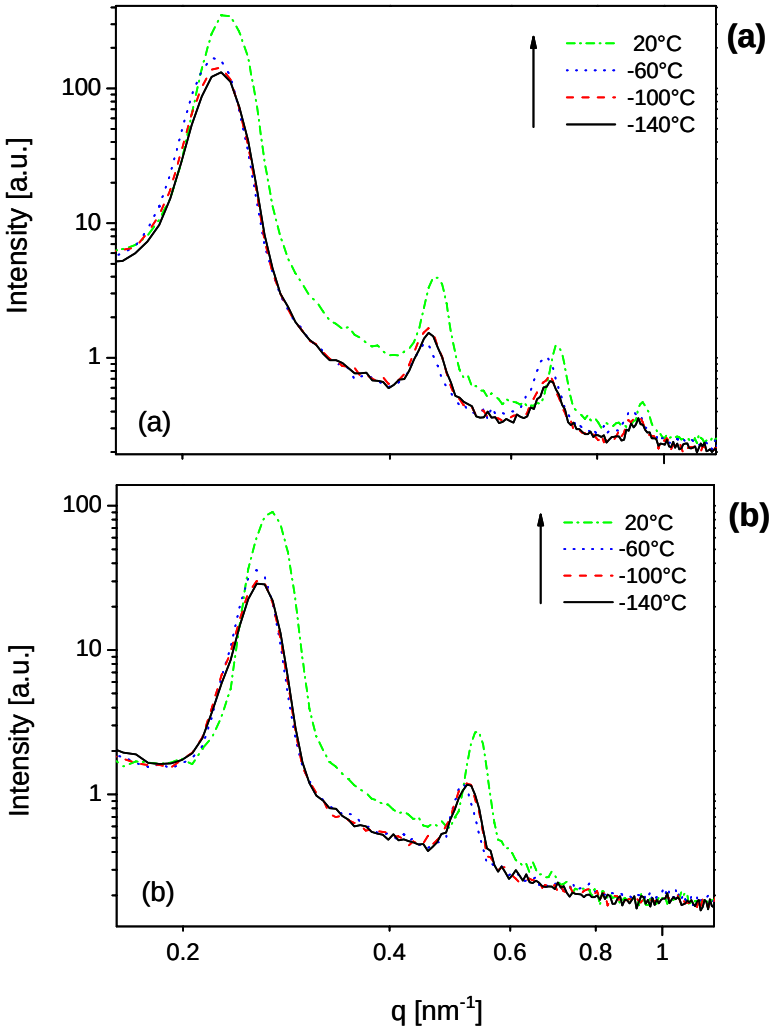

Figure 3.25. SAXS spectra of (a) spontaneous gradient copolymer D-F-D (M = 44,000, F:D = 1:1) and (b) gradient copolymer D-F-D obtained by the semi-batch method (M = 45,800, F:D = 1:1).

The high molecular weight gradient copolymer D-F-D obtained by the semi-batch method (M_n = 45,800, M_w/M_n = 1.15) also shows properties significantly different from those of its lower M_w counterpart (M_n = 16,000, D:F = 1:1). For example, the temperature dependences of *G'* and *G"* of this material shown on Figure 3.24(b) clearly reveal two T_g's, which was not the case for the low M_w copolymer (Figure 3.22(c)). Furthermore, the sample is not flowing in the entire range studied, that is, up to 20 ºC although the low molecular one was flowing above about -70 ºC. The observed differences in the mechanical properties are strongly related to the different microstructures of the two materials as manifested by their SAXS spectra. Although we were not able to identify a clear phase separation for the lower molecular weight copolymer (Figure3.23(c)), a lamella type microstructure was clearly observed for the high molecular weight material at all temperatures (Figure 3.25(b)). The presence of only two scattering peaks however shows that the effect is still weaker than those observed for the spontaneous gradient copolymer with similarly high molecular weight (Figure 3.25(a)).

Thus, the thermomechanical properties and the microstructure formation in these materials depend strongly on the molecular weight of the copolymers and on the lengths of the uniform block at the chain ends.

3.3.2 Vinylsiloxane-based Copolymers

The precise synthesis of polysiloxanes having vinyl groups attached to the polymer chain has the potential to open new routes to a wide class of functional siloxane copolymers with controlled chain structure, as the vinyl group at silicon is a known versatile precursor that can be easily modified by chemical transformations giving rise to a variety of side functionalized polysiloxanes. It can be converted into many useful functional groups by various kinds of addition reactions [117], such as hydrosilylation [82, 118-120], thiolene addition [116, 121-123], hydroboration [124], epoxidation [125-126], and others [127-128].

The apparent rate constants and reactivity ratios were estimated by computer simulation to be $r_{D_3} \approx 0.011$, $r_{V_3} \approx 49.3$. As a result of so much difference in reactivity rates, simultaneous polymerization is predicted to lead to copolymers of blocky structure containing a narrow intermediate fragment with gradient distribution of siloxane units. Polymers having more uniform distribution of the vinyl groups would be expected from the semi-batch process, by adding V_3 at a controlled rate to the polymerization of less reactive D_3.

The T_g's of the corresponding homopolymers, i.e., PDMS and PMVS are very close to each other, -127 °C and -131.8 °C, respectively (Figure 3.26). Thus, the differences related to the change in microstructure are hardly visible. PDMS homopolymer shows a characteristic crystallization band at -88 °C and two endothermic peaks at -48.3 and -36.4 °C, which are typical for PDMS if the chain length exceeds M_n=10000 [129]. These transitions are still present in block and spontaneous gradient copolymers if M_n>15000 in which the dimethylsiloxane block is sufficiently long. The crystallization band becomes broader and moves to higher temperatures and the enthalpy of transition depends on the M_n (size of the homogeneous dimethylsiloxane chain segment). There is only one broad melting transition which appears at temperature between the two peaks occurring in the

PDMS homopolymer. Assuming the enthalpy of melting of the crystalline PDMS to be 61.2 J/g, the PDMS homopolymer shown in Figure 3.26(A) having a total enthalpy of fusion of about 40 J/g is 60-65% crystalline (under the fast cooling regime applied here). The degree of crystallinity decreases to around 15 J/g for the block copolymer (Figure 3.26(C)) and to 8.6 J/g for the spontaneous gradient copolymer (Figure 3.26(D)). These enthalpy values correspond to approximately 24% and 14% of the crystalline character of the PDMS block, respectively. Of course the degree of crystallinity varies with the length of pure dimethylsiloxane block in the copolymer. Semi-batch gradient copolymer (Figure 3.26(E)) does not reveal the crystallization probably because the PDMS block is too short (the weight of the PDMS block estimated from monomer conversion is 10000 in the semi-batch gradient copolymer). The effect of increased compatibility of both microphases, due to the increased D content in the V-enriched segment, may also play a role.

The rate of temperature change in the DSC measurements also appears to have an effect on crystallization and microstructural behaviors exhibited by the copolymers. This is demonstrated in Figure 3.27 (b) and (c) with the block copolymer as well as in Figure 3.28 (b) and (c) with the spontaneous copolymer. The figures illustrate the results of DSC measurements performed at rates of temperature change of 2 K/min and 10 K/min. From these results, we can clearly see that the glass transition temperature is generally unaffected by the different cooling and heating rates. This melting points of the copolymers were also unaffected by the different rates of temperature change. However, when we take a look at the crystallization temperatures, we are able to see that at different cooling and heating rates, the recrystallization process can take place not only at different temperature points upon cooling, but could also in fact take place upon heating.

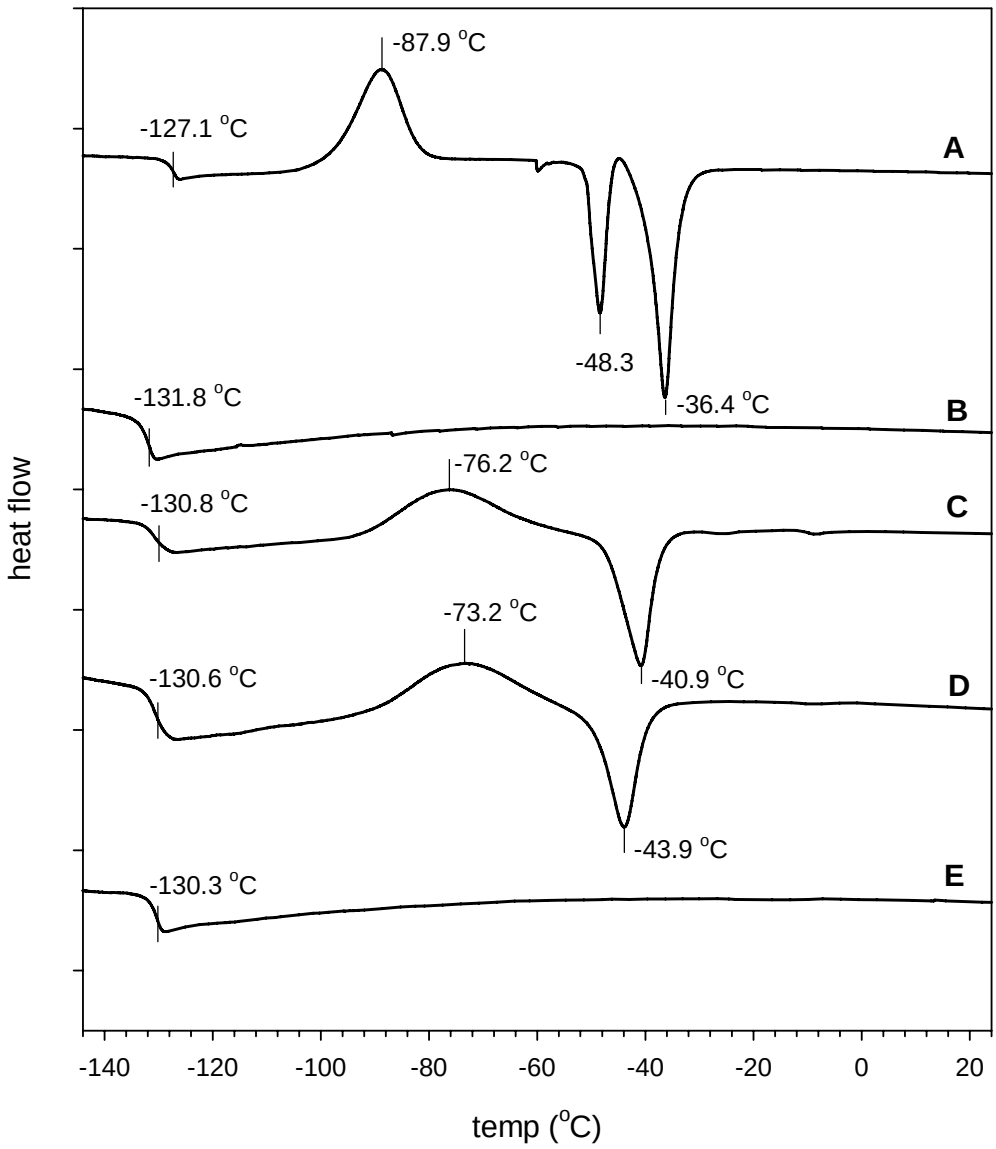

Figure 3.26. DSC of (A) PDMS homopolymer (M_n=17,400), (B) PMVS homopolymer (M_n=14,500), (C) PDMS-PMVS block copolymer (M_n=24,000, D:V=1:1), (D) spontaneous gradient copolymer (M_n=35,500, D:V=1:1), (E) gradient copolymer by semi-batch method (M_n=25,700, D:V=0.8:1).

To further analyze the different behaviors between the gradient and block copolymers of PDMS-PMVS, dynamic mechanical analysis measurements were

conducted on the block copolymer and both the gradient copolymers to study their properties under shear deformation in a broad temperature range.

The samples were put through temperature sweep tests which were conducted first during the cooling of the samples, then followed by heating. The results for the block copolymer, the spontaneous gradient copolymer, and the semi-batch gradient copolymer are displayed in Figures 3.27(a), 3.28(a) and 3.29(a) respectively. In the case of the block copolymer in Figure 3.27(a), the glass transition temperature at around -130 °C is clearly indicated in both cooling and heating curves by the drop in *G'* and the maximum in *G"*. This data is also supported by the results obtained in the DSC measurements in Figure 3.27(b) and (c). The DMA results for the block copolymer also show crystallization occurring upon cooling at about -90 °C and melting upon heating at about -40 °C. This behavior is also supported by the DSC data, but only the measurement performed at a rate of temperature change of 2 K/min (Figure 3.27(b)). Interestingly, the DSC measurements taken at a higher rate of temperature change of 10deg/min showed crystallization occurring upon heating. In the case of the spontaneous gradient copolymer which was obtained by simultaneous copolymerization, the glass transition at around -130 °C also shows up in both DSC and DMA measurements (Figure 3.28). The DMA results further indicate crystallization upon heating occurring in the spontaneous gradient copolymer, beginning at around -80 °C and melting at approximately -45 °C. If we look at Figures 3.28(b) and (c), this strong recrystallization behavior upon heating is supported by the DSC measurements performed at a slower rate of temperature change of 2 deg/min but is not observed at the rate of 10 K/min. As for the semi-batch gradient copolymer, the glass transition at around -130 °C shows up in both DSC and DMA data as expected. However, for this type of gradient copolymer which was obtained by semi-batch method, the DSC as well as DMA results show no indication of crystallization or melting.

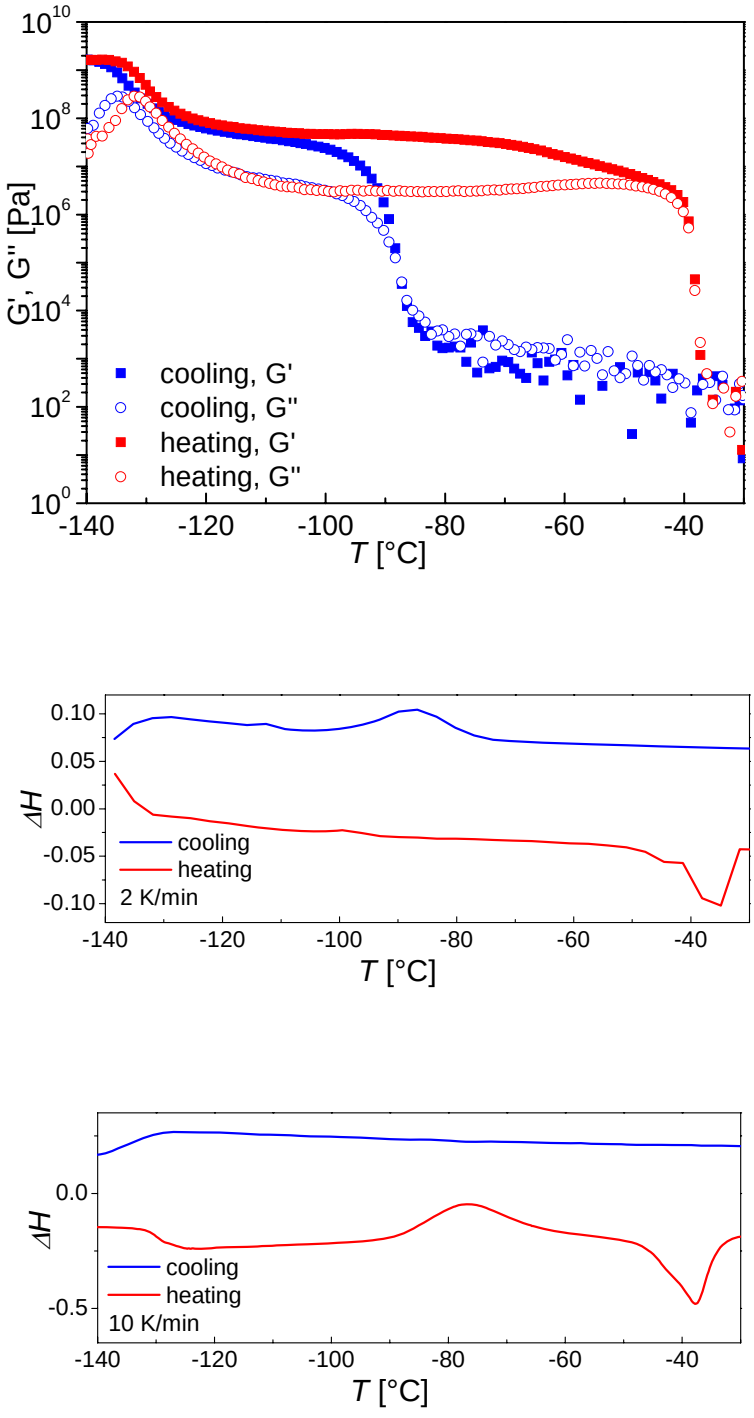

Figure 3.27. PDMS-PMVS block copolymer (M_n=24,000, D:V=1:1), (a) Temperature dependence curves of the shear and loss moduli (b) DSC measurement at 2 K/min (c) 10K/min.

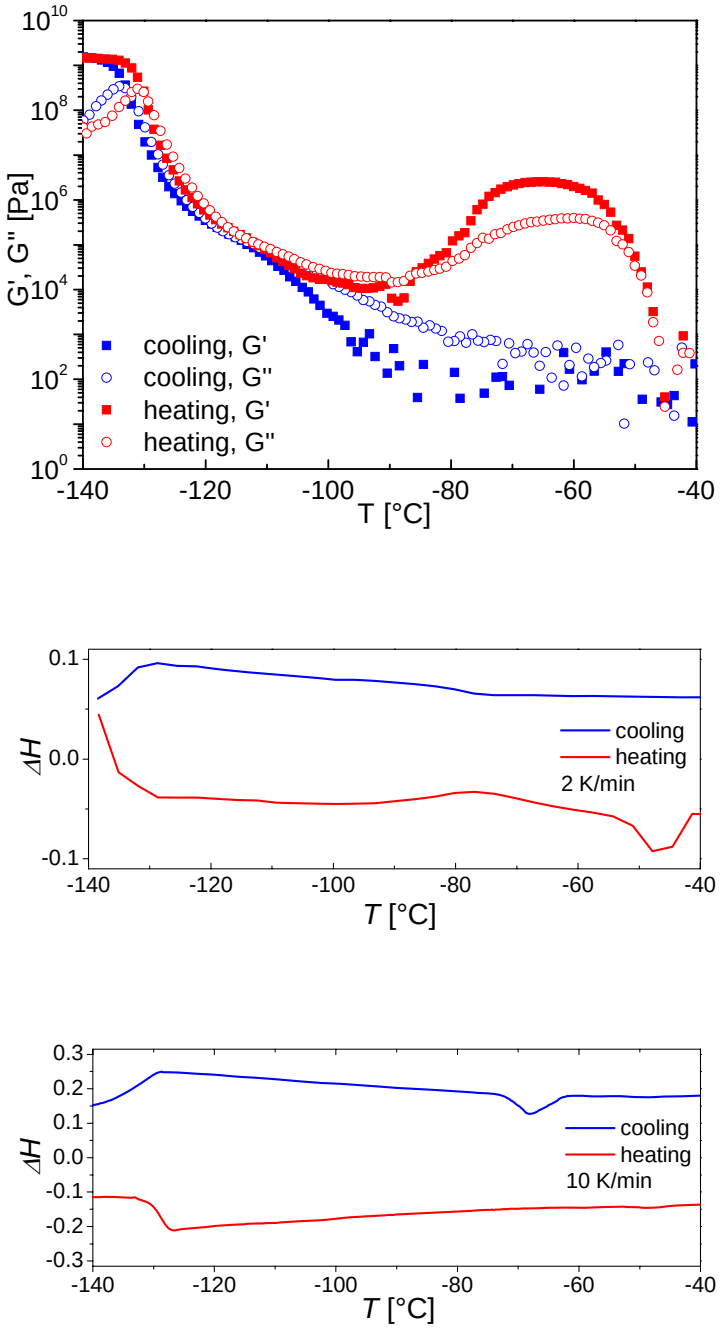

Figure 3.28. Spontaneous gradient copolymer (M_n=35,500, D:V=1:1), (a) Temperature dependence curves of the shear and loss moduli (b) DSC measurement at 2 K/min (c) 10K/min.

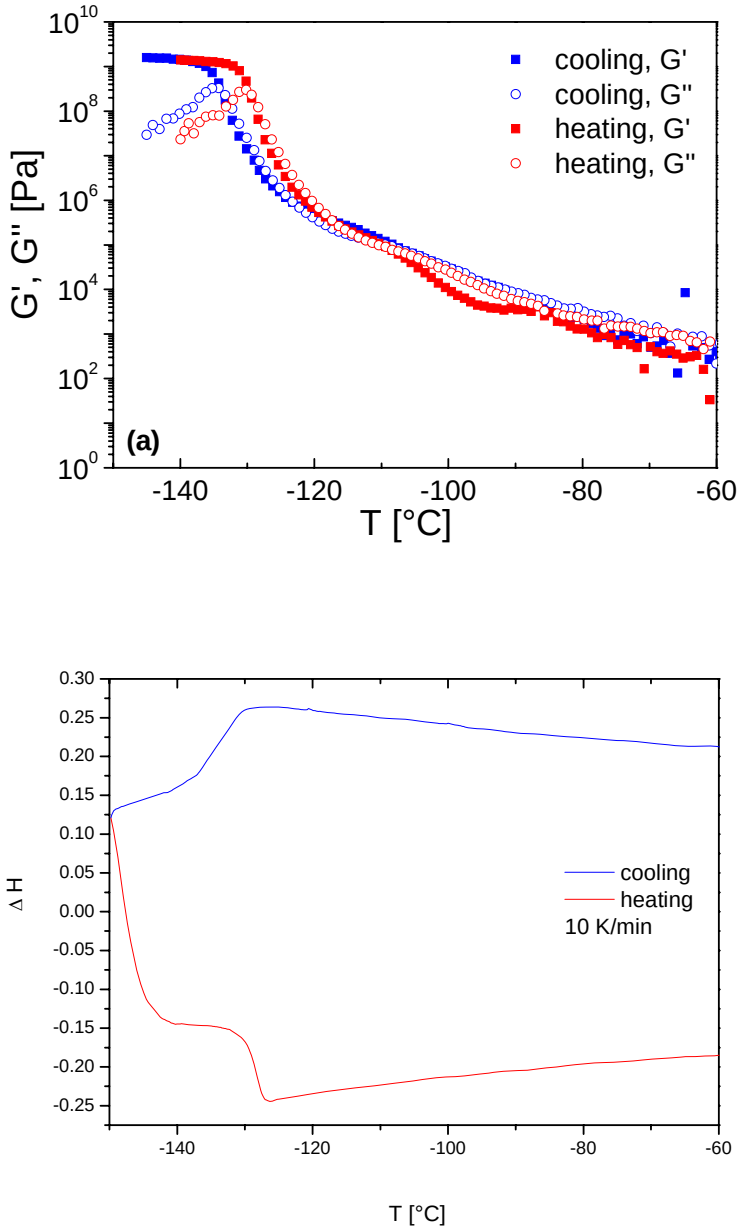

Figure 3.29. Gradient copolymer prepared using semi-batch method (M_n=25,700, D:V=1:1). (a) Temperature dependence curves of the shear and loss moduli (b) DSC measurement at 10 K/min.

From the data gathered by the DSC and DMA measurements, it can be concluded that DSC measurements taken at cooling and heating rates of 2 K/min fit well with the DMA measurements performed. And it should also be emphasized that DSC measurements taken at a faster cooling and heating rate of 10 K/min showed conflicting results when compared to the results from the DMA measurements.

Morphology

In order to further examine the microstructure formation in block and gradient copolymers we performed temperature dependent SAXS experiments on samples. The results are summarized in Figure 3.30 in the form of scattered intensity vs. the scattering vector q. The results show significant differences between these two copolymer materials. In the case of the block copolymer, peaks are observed at -60°C and -100°C at the relative positions 1:2 which suggest a lamellar structure. For the spontaneous gradient copolymer, two peaks were also observed at the same temperatures, but at relative positions 1:3. However, the secondary peak obtained from the spontaneous gradient copolymer was weaker and broader when compared to the block copolymer. And in the case of both copolymers, the structures seemed to have been lost when either cooled down to 140°C or when heated back to room temperature.

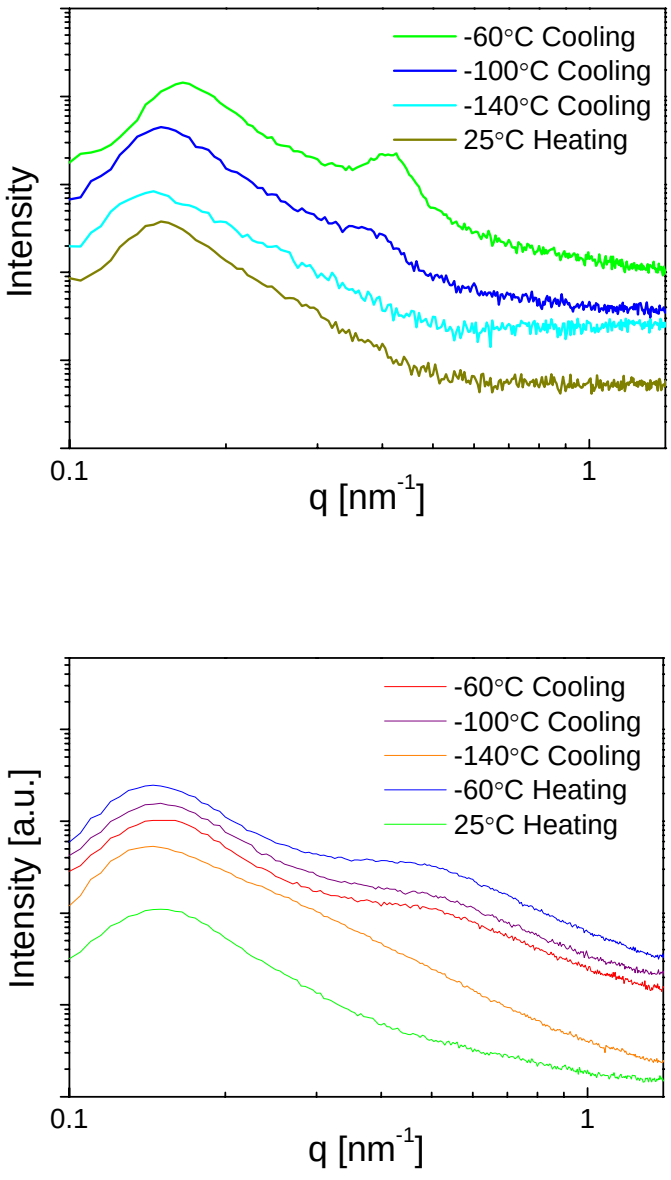

Figure 3.30. SAXS spectrum of (a) PDMS-PMVS block copolymer (M_n=24,000, D:V=1:1); and of (b) PDMS-PMVS spontaneous gradient copolymer (M_n=35,500, D:V=1:1).

4 Conclusion

The main focus of the studies discussed in this volume was to explore specific systems which have not been studied before in hopes of having a better understanding of structure-property relations in complex copolymer systems. And from these various different studies which were done, it is clear that molecular properties such as chain length, chain stiffness, degree of branching, molecular architecture, and the number of charge groups, are of great significance, and perhaps even more so than the detailed chemical make-up of polymers, in determining their physical characteristics. This was well-demonstrated with the different physical properties exhibited by the statistical, block and gradient copolymers. All three types of these copolymers, even when built with the same type and number of units, have completely different properties as a result of their different architectures. The studies revealed that a deeper understanding of this relationship between the molecular architecture and the physical characteristics is vital for aiding in the design of new materials with more useful properties, as constantly advancing technologies demand new, high performance and more specialized materials with highly specialized functions. And it is this deeper understanding of the structure-property relations that would undoubtedly be one of the key factors contributing to the continuing rapid growth in the field of polymer science.

Bibliography

1. Flory, P.J., *Fundamental Principles of Condensation Polymerization.* Chemical Reviews, 1946. **39**(1): p. 137-197.
2. Leibler, L., *Nanostructured plastics: Joys of self-assembling.* Progress in Polymer Science, 2005. **30**(8-9): p. 898-914.
3. Choi, H.S. and N. Yui, *Design of rapidly assembling supramolecular systems responsive to synchronized stimuli.* Progress in Polymer Science, 2006. **31**(2): p. 121-144.
4. Frechet, J.M.J., *Functional polymers: from plastic electronics to polymer-assisted therapeutics.* Progress in Polymer Science, 2005. **30**(8-9): p. 844-857.
5. Higgins, J.S., M. Tambasco, and J.E.G. Lipson, *Polymer blends; stretching what we can learn through the combination of experiment and theory.* Progress in Polymer Science, 2005. **30**(8-9): p. 832-843.
6. Khandare, J. and T. Minko, *Polymer-drug conjugates: Progress in polymeric prodrugs.* Progress in Polymer Science, 2006. **31**(4): p. 359-397.
7. Macosko, C.W., H.K. Jeon, and T.R. Hoye, *Reactions at polymer-polymer interfaces for blend compatibilization.* Progress in Polymer Science, 2005. **30**(8-9): p. 939-947.
8. Meijer, H.E.H. and L.E. Govaert, *Mechanical performance of polymer systems: The relation between structure and properties.* Progress in Polymer Science, 2005. **30**(8-9): p. 915-938.
9. Sukhorukov, G., A. Fery, and H. Mohwald, *Intelligent micro- and nanocapsules.* Progress in Polymer Science, 2005. **30**(8-9): p. 885-897.
10. Matsen, M.W. and F.S. Bates, *Origins of complex self-assembly in block copolymers.* Macromolecules, 1996. **29**(23): p. 7641-7644.
11. Helfand, E. and Z.R. Wasserman, *Block Co-Polymer Theory .6. Cylindrical Domains.* Macromolecules, 1980. **13**(4): p. 994-998.
12. Semenov, A.N., *Contribution to the Theory of Microphase Layering in Block-Copolymer Melts.* Zhurnal Eksperimentalnoi I Teoreticheskoi Fiziki, 1985. **88**(4): p. 1242-1256.
13. Ohta, T. and K. Kawasaki, *Equilibrium Morphology of Block Copolymer Melts.* Macromolecules, 1986. **19**(10): p. 2621-2632.
14. Ohta, T. and K. Kawasaki, *Comment on the Free-Energy Functional of Block Copolymer Melts in the Strong Segregation Limit.* Macromolecules, 1990. **23**(8): p. 2413-2414.
15. Hong, K.M. and J. Noolandi, *Theory of Inhomogeneous Multicomponent Polymer Systems.* Macromolecules, 1981. **14**(3): p. 727-736.
16. Muthukumar, M., *Fluctuation Effects in the Density-Functional Theory of Order-Disorder Transitions in Block-Copolymers.* Macromolecules, 1993. **26**(19): p. 5259-5261.
17. Matsen, M.W. and M. Schick, *Lamellar Phase of a Symmetrical Triblock Copolymer.* Macromolecules, 1994. **27**(1): p. 187-192.
18. Olmsted, P.D. and S.T. Milner, *Strong-Segregation Theory of Bicontinuous Phases in Block-Copolymers.* Physical Review Letters, 1994. **72**(6): p. 936-939.

19. Morkved, T.L., et al., *Mesoscopic Self-Assembly of Gold Islands an Diblock-Copolymer Films.* Applied Physics Letters, 1994. **64**(4): p. 422-424.
20. Archibald, D.D. and S. Mann, *Template Mineralization of Self-Assembled Anisotropic Lipid Microstructures.* Nature, 1993. **364**(6436): p. 430-433.
21. Matyjaszewski, K., et al., *Gradient copolymers by atom transfer radical copolymerization.* Journal of Physical Organic Chemistry, 2000. **13**(12): p. 775-786.
22. Aksimentiev, A. and R. Holyst, *Phase behavior of gradient copolymers.* Journal of Chemical Physics, 1999. **111**(5): p. 2329-2339.
23. Pakula, T. and K. Matyjaszewski, *Copolymers with controlled distribution of comonomers along the chain .1. Structure, thermodynamics and dynamic properties of gradient copolymers. Computer simulation.* Macromolecular Theory and Simulations, 1996. **5**(5): p. 987-1006.
24. Shull, K.R., *Interfacial activity of gradient copolymers.* Macromolecules, 2002. **35**(22): p. 8631-8639.
25. Kim, J., et al., *Polymer blend compatibilization by gradient copolymer addition during melt processing: Stabilization of dispersed phase to static coarsening.* Macromolecules, 2005. **38**(4): p. 1037-1040.
26. Matyjaszewski, K. and D. Greszta, *Thermal properties of gradient copolymers and their compatibilizing ability.* Abstracts of Papers of the American Chemical Society, 1997. **213**: p. 330-POLY.
27. Kim, J., et al., *Uniquely broad glass transition temperatures of gradient copolymers relative to random and block copolymers containing repulsive comonomers.* Macromolecules, 2006. **39**(18): p. 6152-6160.
28. Jakubowski, W., et al., *Comparison of thermomechanical properties of statistical, gradient and block copolymers of isobornyl acrylate and n-butyl acrylate with various acrylate homopolymers.* Polymer, 2008. **49**(6): p. 1567-1578.
29. Berry, G.C., *Translational Frictional Constant of Comb-Branched Polymers.* Journal of Polymer Science Part a-2-Polymer Physics, 1968. **6**(8pa2): p. 1551-&.
30. Graessley, W.W., *Some Phenomenological Consequences of the Doi-Edwards Theory of Viscoelasticity.* Journal of Polymer Science Part B-Polymer Physics, 1980. **18**(1): p. 27-34.
31. Williams, M.L., R.F. Landel, and J.D. Ferry, *Mechanical Properties of Substances of High Molecular Weight .19. The Temperature Dependence of Relaxation Mechanisms in Amorphous Polymers and Other Glass-Forming Liquids.* Journal of the American Chemical Society, 1955. **77**(14): p. 3701-3707.
32. Angell, C.A., *Formation of Glasses from Liquids and Biopolymers.* Science, 1995. **267**(5206): p. 1924-1935.
33. Stillinger, F.H., *A Topographic View of Supercooled Liquids and Glass-Formation.* Science, 1995. **267**(5206): p. 1935-1939.
34. Sokolov, A.P., *Why the glass transition is still interesting.* Science, 1996. **273**(5282): p. 1675-1676.
35. Grest, G.S., et al., *Density of States and the Velocity Auto-Correlation Function Derived from Quench Studies.* Journal of Chemical Physics, 1981. **74**(6): p. 3532-3534.

36. Bendler, J.T., J.J. Fontanella, and M.F. Shlesinger, *A new Vogel-like law: Ionic conductivity, dielectric relaxation, and viscosity near the glass transition.* Physical Review Letters, 2001. **8719**(19): p. -.
37. Pakula, T., *Collective dynamics in simple supercooled and polymer liquids.* Journal of Molecular Liquids, 2000. **86**(1-3): p. 109-121.
38. Doolittle, A.K., *Studies in Newtonian Flow .2. The Dependence of the Viscosity of Liquids on Free-Space.* Journal of Applied Physics, 1951. **22**(12): p. 1471-1475.
39. Fulcher, G.S., *Analysis of recent measurements of the viscosity of glasses. II.* Journal of the American Ceramic Society, 1925. **8**(12): p. 789-794.
40. Fulcher, G.S., *Analysis of recent measurements of the viscosity of glasses.* Journal of the American Ceramic Society, 1925. **8**(6): p. 339-355.
41. Tammann, G. and W. Hesse, *The dependancy of viscosity on temperature in hypothermic liquids.* Zeitschrift Fur Anorganische Und Allgemeine Chemie, 1926. **156**(4): p. -.
42. Naoki, M., H. Endou, and K. Matsumoto, *Pressure Effects on Dielectric-Relaxation of Supercooled Ortho-Terphenyl.* Journal of Physical Chemistry, 1987. **91**(15): p. 4169-4174.
43. Ferrer, M.L., et al., *Supercooled liquids and the glass transition: Temperature as the control variable.* Journal of Chemical Physics, 1998. **109**(18): p. 8010-8015.
44. Tolle, A., et al., *Fast relaxation in a fragile liquid under pressure.* Physical Review Letters, 1998. **80**(11): p. 2374-2377.
45. Mpoukouvalas, K., et al., *Pressure-enhanced dynamic heterogeneity in block copolymers of poly(methyl vinyl ether) and poly(isobutyl vinyl ether).* Physical Review E, 2005. **72**(1): p. -.
46. Roland, C.M., et al., *Volume and temperature as control parameters for the dielectric a relaxation of polymers and molecular glass formers.* Philosophical Magazine, 2004. **84**(13-16): p. 1573-1581.
47. Floudas, G., K. Mpoukouvalas, and P. Papadopoulos, *The role of temperature and density on the glass-transition dynamics of glass formers.* Journal of Chemical Physics, 2006. **124**(7): p. -.
48. Dreyfus, C., et al., *Temperature and pressure study of Brillouin transverse modes in the organic glass-forming liquid orthoterphenyl.* Physical Review E, 2003. **68**(1): p. -.
49. Casalini, R. and C.M. Roland, *Thermodynamical scaling of the glass transition dynamics.* Physical Review E, 2004. **69**(6): p. -.
50. Alba-Simionesco, C., et al., *Scaling out the density dependence of the a relaxation in glass-forming polymers.* Europhysics Letters, 2004. **68**(1): p. 58-64.
51. Tarjus, G., et al., *Disentangling density and temperature effects in the viscous slowing down of glassforming liquids.* Journal of Chemical Physics, 2004. **120**(13): p. 6135-6141.
52. Roland, C.M. and R. Casalini, *Comment on: "Disentangling density and temperature effects in the viscous slowing down of glass forming liquids" [J. Chem. Phys. 120, 6135 (2004)].* Journal of Chemical Physics, 2004. **121**(22): p. 11503-11504.
53. Bragg, W.L., *The diffraction of short electromagnetic waves through a crystal.* Zeitschrift Fur Anorganische Chemie, 1914. **90**(2/3): p. 153-168.

54. Matyjaszewski, K., *Macromolecular engineering: From rational design through precise macromolecular synthesis and processing to targeted macroscopic material properties.* Progress in Polymer Science, 2005. **30**(8-9): p. 858-875.
55. Coessens, V., et al., *Functionalization of polymers prepared by ATRP using radical addition reactions.* Macromolecular Rapid Communications, 2000. **21**(2): p. 103-109.
56. Matyjaszewski, K., et al., *Molecular brushes with variable composition and topology by ATRP: Synthesis and properties.* Abstracts of Papers of the American Chemical Society, 2006. **231**: p. -.
57. Patten, T.E. and K. Matyjaszewski, *Atom transfer radical polymerization and the synthesis of polymeric materials.* Advanced Materials, 1998. **10**(12): p. 901-+.
58. Wong, H.F. and G.D. Brown, *beta-methoxy-gamma-methylene-alpha,beta-unsaturated-gamma-butyrolactones from Artabotrys hexapetalus.* Phytochemistry, 2002. **59**(1): p. 99-104.
59. Vuckovic, I., et al., *Phytochemical investigation of Anthemis cotula.* Journal of the Serbian Chemical Society, 2006. **71**(2): p. 127-133.
60. Trendafilova, A., et al., *Sesquiterpene lactones from Achillea collina J. Becker ex Reichenb.* Phytochemistry, 2006. **67**(8): p. 764-770.
61. Williams, C.K. and M.A. Hillmyer, *Polymers from renewable resources: A perspective for a special issue of polymer reviews.* Polymer Reviews, 2008. **48**(1): p. 1-10.
62. Akkapeddi, M.K., *Poly(Alpha-Methylene-Gamma-Butyrolactone) Synthesis, Configurational Structure, and Properties.* Macromolecules, 1979. **12**(4): p. 546-551.
63. Sheiko, S.S., B.S. Sumerlin, and K. Matyjaszewski, *Cylindrical molecular brushes: Synthesis, characterization, and properties.* Progress in Polymer Science, 2008. **33**(7): p. 759-785.
64. Neugebauer, D., et al., *Densely-grafted and double-grafted PEO brushes via ATRP. A route to soft elastomers.* Macromolecules, 2003. **36**(18): p. 6746-6755.
65. Sheiko, S.S., et al., *Single molecule rod-globule phase transition for brush molecules at a flat interface.* Macromolecules, 2001. **34**(23): p. 8354-8360.
66. Sheiko, S.S., et al., *Adsorption-induced scission of carbon-carbon bonds.* Nature, 2006. **440**(7081): p. 191-194.
67. Qin, S.H., et al., *Synthesis and visualization of densely grafted molecular brushes with crystallizable poly(octadecyl methacrylate) block segments.* Macromolecules, 2003. **36**(3): p. 605-612.
68. Greszta, D. and K. Matyjaszewski, *Mechanism of controlled/"living" radical polymerization of styrene in the presence of nitroxyl radicals. Kinetics and simulations.* Macromolecules, 1996. **29**(24): p. 7661-7670.
69. Greszta, D. and K. Matyjaszewski, *Living radical polymerization: Kinetic results - Comments.* Macromolecules, 1996. **29**(15): p. 5239-5240.
70. Greszta, D. and K. Matyjaszewski, *Gradient copolymers - A new class of materials.* Abstracts of Papers of the American Chemical Society, 1996. **211**: p. 85-Poly.

71. Arehart, S.V., D. Greszta, and K. Matyjaszewski, *Gradient copolymers of styrene and n-butyl acrylate through atom transfer radical polymerization.* Abstracts of Papers of the American Chemical Society, 1997. **213**: p. 329-POLY.
72. Matyjaszewski, K. and J.H. Xia, *Atom transfer radical polymerization.* Chemical Reviews, 2001. **101**(9): p. 2921-2990.
73. Ishizu, K. and A. Ichimura, *Synthesis of cyclic diblock copolymers by interfacial condensation.* Polymer, 1998. **39**(25): p. 6555-6558.
74. Yu, G.E., et al., *Association and surface properties of tapered statistical copolymers of ethylene oxide and butylene oxide in water.* Journal of the Chemical Society-Faraday Transactions, 1997. **93**(18): p. 3383-3390.
75. Okabe, S., et al., *Small-angle neutron scattering study on block and gradient copolymer aqueous solutions.* Polymer, 2006. **47**(21): p. 7572-7579.
76. Chojnowski, J., et al., *Controlled synthesis of vinylmethylsiloxane-dimethylsiloxane gradient, block and alternate copolymers by anionic ROP of cyclotrisiloxanes.* Polymer, 2002. **43**(7): p. 1993-2001.
77. Chojnowski, J., et al., *Synthesis of branched polysiloxanes with controlled branching and functionalization by anionic ring-opening polymerization.* Macromolecules, 2003. **36**(11): p. 3890-3897.
78. Cypryk, M., et al., *Modifications of siloxane polymers.* Polimery, 2007. **52**(7-8): p. 496-502.
79. Cazacu, M., et al., *Heterogeneous catalyzed copolymerization of octamethylcyclotetrasiloxane with 1,3,5,7-tetravinyl-1,3,5,7-tetramethylcyclotetrasiloxane.* Journal of Macromolecular Science-Pure and Applied Chemistry, 1996. **A33**(1): p. 65-76.
80. Ziemelis, M.J. and J.C. Saam, *Sequence Distribution in Poly(Dimethylsiloxane-Co-Methylvinylsiloxanes).* Macromolecules, 1989. **22**(5): p. 2111-2116.
81. Teng, C.J., W.P. Weber, and G.P. Cai, *Anionic and cationic ring-opening polymerization of 2,2,4,4,6,6-hexamethyl-8,8-divinylcyclotetrasiloxane.* Macromolecules, 2003. **36**(14): p. 5126-5130.
82. Cai, G.P. and W.P. Weber, *Synthesis and chemical modification of poly(divinylsiloxane).* Polymer, 2002. **43**(6): p. 1753-1759.
83. Herczynska, L., et al., *Synthesis of microsequential methylvinylsiloxane-dimethylsiloxane copolymers by nonequilibrium copolymerization.* Journal of Polymer Science Part a-Polymer Chemistry, 1998. **36**(1): p. 137-145.
84. Blochowiak, M., et al., *Thermodynamics and rheology of cycloolefin copolymers.* Journal of Chemical Physics, 2006. **124**(13): p. -.
85. Zhang, Y., et al., *Structure and properties of poly(butyl acrylate-block-sulfone-block-butyl acrylate) triblock copolymers prepared by ATRP.* Macromolecular Chemistry and Physics, 2005. **206**(1): p. 33-42.
86. Matyjaszewski, K., et al., *Simple and effective one-pot synthesis of (meth)acrylic block copolymers through atom transfer radical polymerization.* Journal of Polymer Science Part a-Polymer Chemistry, 2000. **38**(11): p. 2023-2031.
87. Kim, S. and J.M. Torkelson, *Self-referencing fluorescence-based oxygen sensor with temperature-independent response: Novel pressure-sensitive paint based on polydimethylsiloxane films.* Abstracts of Papers of the American Chemical Society, 2003. **226**: p. U107-U107.

88. Karatasos, K., et al., *Composition fluctuation effects on dielectric normal-mode relaxation in diblock copolymers .2. Disordered state in proximity to the ODT and ordered state.* Macromolecules, 1996. **29**(4): p. 1326-1336.
89. Kumar, S.K., et al., *Concentration fluctuation induced dynamic heterogeneities in polymer blends.* Journal of Chemical Physics, 1996. **105**(9): p. 3777-3788.
90. Alvarez, F., et al., *Segmental Dynamics in Bulk Poly(Isobornyl Methacrylate) and Its Random Copolymer with Poly(Methyl Methacrylate) near T-G.* Macromolecules, 1995. **28**(19): p. 6488-6493.
91. Floudas, G., R. Ulrich, and U. Wiesner, *Microphase separation in poly(isoprene-b-ethylene oxide) diblock copolymer melts. I. Phase state and kinetics of the order-to-order transitions.* Journal of Chemical Physics, 1999. **110**(1): p. 652-663.
92. Floudas, G., et al., *Microphase separation in star block copolymers of styrene and isoprene. Theory, experiment, and simulation.* Macromolecules, 1996. **29**(11): p. 4142-4154.
93. Hodrokoukes, P., et al., *Microphase separation in normal and inverse tapered block copolymers of polystyrene and polyisoprene. 1. Phase state.* Macromolecules, 2001. **34**(3): p. 650-657.
94. Rubinstein, M. and S.P. Obukhov, *Power-Law-Like Stress-Relaxation of Block Copolymers - Disentanglement Regimes.* Macromolecules, 1993. **26**(7): p. 1740-1750.
95. Abreu, F.O.M.S., M.M.C. Forte, and S.A. Liberman, *SBS and SEBS block copolymers as impact modifiers for polypropylene compounds.* Journal of Applied Polymer Science, 2005. **95**(2): p. 254-263.
96. El Sheemy, H., *Thermoplastic elastomers and mineral oils.* Kautschuk Gummi Kunststoffe, 1999. **52**(9): p. 586-587.
97. Tong, J.D., et al., *Synthesis and bulk properties of poly(methyl methacrylate)-b-poly(isooctyl acrylate)-b-poly(methyl methacrylate).* Polymer, 2000. **41**(12): p. 4617-4624.
98. Moineau, G., et al., *Controlled radical polymerization of (meth)acrylates by ATRP with NiBr2(PPh3)(2) as catalyst.* Macromolecules, 1999. **32**(1): p. 27-35.
99. Braunecker, W.A. and K. Matyjaszewski, *Controlled/living radical polymerization: Features, developments, and perspectives.* Progress in Polymer Science, 2007. **32**(1): p. 93-146.
100. Dufour, B., et al., *Polar three-arm star block copolymer thermoplastic elastomers based on polyacrylonitrile.* Macromolecules, 2008. **41**(7): p. 2451-2458.
101. Dufour, B., et al., *PBA-PMMA 3-arm star block copolymer thermoplastic elastomers.* Macromolecular Chemistry and Physics, 2008. **209**(16): p. 1686-1693.
102. Mosnacek, J., et al., *Synthesis, morphology and mechanical properties of linear triblock copolymers based on poly(alpha-methylene-gamma-butyrolactone).* Polymer, 2009. **50**(9): p. 2087-2094.
103. Shim, J.S. and J.P. Kennedy, *New polyisobutylene stars part XXI - Novel thermoplastic elastomers. III. Synthesis, characterization, and properties of star-block copolymers of poly(indene-b-isobutylene) arms emanating from cyclosiloxane cores.* Journal of Polymer Science Part a-Polymer Chemistry, 2000. **38**(2): p. 279-290.

104. Shim, J.S. and J.P. Kennedy, *New polyisobutylene stars part XIX - Novel thermoplastic elastomers. II. Properties of star-block copolymers of PSt-b-PIB arms emanating from cyclosiloxane cores.* Journal of Polymer Science Part a-Polymer Chemistry, 1999. **37**(6): p. 815-824.
105. Huckstadt, H., V. Abetz, and R. Stadler, *Synthesis of a polystyrene-arm-polybutadiene-arm-poly(methyl methacrylate) triarm star copolymer.* Macromolecular Rapid Communications, 1996. **17**(8): p. 599-606.
106. Puskas, J.E., et al., *The effect of hard and soft segment composition and molecular architecture on the morphology and mechanical properties of polystyrene-polyisobutylene thermoplastic elastomeric block copolymers.* European Polymer Journal, 2003. **39**(10): p. 2041-2049.
107. Storey, R.F., B.J. Chrisholm, and K.R. Choate, *Synthesis and characterization of multi-arm star-branched polyisobutylenes.* Journal of Polymer Science, Part A: Polymer Chemistry, 1994. **34**: p. 2003-2017.
108. Storey, R.F. and K.A. Shoemake, *Effect of reaction conditions on synthesis and properties of multiarm star-branched polyisobutylenes.* Journal of Polymer Science, Part A: Polymer Chemistry, 1998. **36**: p. 471-483.
109. Shim, J.S., et al., *Novel thermoplastic elastomers. I. Synthesis and characterization of star-block copolymers of PSt-b-PIB arms emanating from cyclosiloxane cores.* Journal of Polymer Science, Part A: Polymer Chemistry, 1998. **36**(17): p. 2997-3012.
110. Shim, J.S. and J.P. Kennedy, *Novel thermoplastic elastomers. II. Properties of star-block copolymers of PSt-b-PIB arms emanating from cyclosiloxane cores.* Journal of Polymer Science, Part A: Polymer Chemistry, 1999. **37**(6): p. 815-824.
111. Shim, J.S. and J.P. Kennedy, *Novel thermoplastic elastomers. III. Synthesis, characterization, and properties of star-block copolymers of poly(indene-b-isobutylene) arms emanating from cyclosiloxane cores.* Journal of Polymer Science, Part A: Polymer Chemistry, 2000. **38**(2): p. 279-290.
112. Tong, J.D., et al., *Synthesis, Morphology, and Mechanical Properties of Poly(methyl methacrylate)-b-poly(n-butyl acrylate)-b-poly(methyl methacrylate) Triblocks. Ligated Anionic Polymerization vs Atom Transfer Radical Polymerization.* Macromolecules, 2000. **33**(2): p. 470-479.
113. Borner, H.G., et al., *Synthesis of molecular brushes with gradient in grafting density by atom transfer polymerization.* Macromolecules, 2002. **35**(9): p. 3387-3394.
114. Chojnowski, J., et al., *Controlled synthesis of all siloxane-functionalized architectures by ring-opening polymerization.* Synthesis and Properties of Silicones and Silicone-Modified Materials, 2003. **838**: p. 12-25.
115. Kelen, T. and F. Tudos, *Analysis of Linear Methods for Determining Copolymerization Reactivity Ratios .1. New Improved Linear Graphic Method.* Journal of Macromolecular Science-Chemistry, 1975. **A 9**(1): p. 1-27.
116. Herczynska, L., et al., *Modification of polysiloxanes by free-radical addition of pyridylthiols to the vinyl groups of the polymer.* European Polymer Journal, 1999. **35**(6): p. 1115-1122.

117. Boutevin, B., F. Guida-Pietrasanta, and A. Ratsimihety, *Synthesis of photocrosslinkable fluorinated polydimethylsiloxanes: Direct introduction of acrylic pendant groups via hydrosilylation.* Journal of Polymer Science Part a-Polymer Chemistry, 2000. **38**(20): p. 3722-3728.
118. Hempenius, M.A., R.G.H. Lammertink, and G.J. Vancso, *Side-chain liquid-crystalline polysiloxanes via anionic polymerization: (n-undecyloxy)arenecarboxylic acid mesogens linked to poly(dimethylsiloxane-co-methylvinylsiloxane).* Macromolecules, 1997. **30**(2): p. 266-272.
119. Paulasaari, J.K. and W.P. Weber, *Preparation and orthogonal polymerizations of 1-hydrido-1-vinyldimethylsiloxy-3,3,5,5-tetramethylcyclotrisiloxane.* Macromolecules, 1999. **32**(16): p. 5217-5221.
120. Vadala, M.L., et al., *Block copolysiloxanes and their complexation with cobalt nanoparticles.* Polymer, 2004. **45**(22): p. 7449-7461.
121. Abdellah, L., B. Boutevin, and B. Youssef, *Synthesis and Applications of Photolinkable Poly(Dimethylsiloxanes) .2. Synthesis of Polysiloxane with Urethane Acrylate Groups.* European Polymer Journal, 1991. **27**(8): p. 821-825.
122. RozgaWijas, K., et al., *Controlled synthesis of siloxane copolymers having an organosulfur group by polymerization of cyclotrisiloxanes with mixed units.* Macromolecules, 1996. **29**(8): p. 2711-2720.
123. Scibiorek, M., N.K. Gladkova, and J. Chojnowski, *Controlled synthesis of amphiphilic siloxane-siloxane block copolymers with carboxyl functions.* Polymer Bulletin, 2000. **44**(4): p. 377-384.
124. Brunner, A.R., et al., *Synthesis and ceramic conversion reactions of pinacolborane- amd diethylborazine-modified poly(vinylsiloxane)s. The development of a processable single-source polymeric precursor to boron-modified silicon carbide.* Chemistry of Materials, 2000. **12**(9): p. 2770-2780.
125. Bauer, J., N. Husing, and G. Kickelbick, *Synthesis of new types of polysiloxane based surfactants.* Chemical Communications, 2001(01): p. 137-138.
126. Bauer, J., N. Husing, and G. Kickelbick, *Preparation of functional block copolymers based on a polysiloxane backbone by anionic ring-opening polymerization.* Journal of Polymer Science Part a-Polymer Chemistry, 2002. **40**(10): p. 1539-1551.
127. Ganicz, T., et al., *A novel organometallic route to phenylethenyl-modified polysiloxanes.* Journal of Materials Chemistry, 2005. **15**(5): p. 611-619.
128. Gupta, S.K. and W.P. Weber, *Ruthenium-catalyzed chemical modification of poly(vinylmethylsiloxane) with 9-acetylphenanthrene.* Macromolecules, 2002. **35**(9): p. 3369-3373.
129. Wang, B.Y. and S. Krause, *Properties of Dimethylsiloxane Microphases in Phase-Separated Dimethylsiloxane Block Copolymers.* Macromolecules, 1987. **20**(9): p. 2201-2208.

List of Figures

List of Tables